Fast Surgical Simulation to Improve Mitral Valve Repair

Fast Surgical Simulation to Improve Mitral Valve Repair

A dissertation presented
by

Neil Arturo Tenenholtz

to
The School of Engineering and Applied Sciences
in partial fulfillment of the requirements
for the degree of
Doctor of Philosophy
in the subject of

Engineering Sciences

Harvard University
Cambridge, Massachusetts
May 2014

Thesis Advisor

Robert D. Howe

Author

Neil Arturo Tenenholtz

Fast Surgical Simulation to Improve Mitral Valve Repair

Abstract

Mitral valve repair, the preferred method of treating mitral regurgitation, is a demanding surgical procedure consisting of the resection and approximation of valve tissue. Operating on an arrested heart, the clinician is forced to predict closed valve shape and the effect of surgical modifications. The valve's complex morphology makes this a difficult task, and as a result, the procedure is underperformed by less experienced surgeons in lieu of the simpler, less effective valve replacement.

This thesis details the use of fast, computer-based simulation to ease this predictive task and facilitate valve repair. A computational model is first developed and optimized for speed of execution. Valve closure is simulated with sub-millimeter accuracy in less than one second, more than an order of magnitude faster than previous results. An intuitive surgical planning system is then constructed. To maximize ease of use, a haptic device, leveraging the models greater than three kilohertz update rate, serves as the primary means user interaction.

This interactive system was then used to assess and improve the ability of senior medical students in predicting closed valve shape. After initial studies revealed a success rate equivalent to random chance, far below that of the surgeons evaluated, simulator-based instruction was provided to investigate its efficacy as a pedagogical tool. More so than a leading surgical textbook, this alternative educational methodology was shown to result in improved user performance in both a virtual setting and ex-vivo porcine model.

Finally, through repeated simulation, the robustness of mitral valve repair in the treatment of ischemic mitral regurgitation was investigated. The existing standard of care was shown to exhibit a heightened response to small changes in cardiac geometry, thus explaining the common recurrence of regurgitation. A novel surgical technique was therefore assessed and optimized for reduced sensitivity to these variations.

Contents

Acknowledgments

While this thesis may bear my name, it represents the contributions of many. From my mentors who guided me, to the clinicians who were patient enough to teach a mechanical engineer cardiac surgery, to my colleagues, family, and friends who inspired and supported me, your contributions to this work, while largely unacknowledged, were crucial to its completion. I owe you a great deal of gratitude as this truly would not have been possible without you.

Firstly, I would like to thank my advisor, Professor Robert Howe. The flexibility he afforded me in pursuing my academic interests has enabled me to grow as both a researcher and educator. While allowing me to mold my own path, Professor Howe has always been available to provide wisdom and guidance, even when half a world away. I would also like to acknowledge the contributions of Professor Hanspeter Pfister, not only for his support and assistance in the development of this work, but also for being a wonderful mentor as I learned to teach computer science.

Additionally, I am truly indebted to Dr. Pedro del Nido and the talented clinicians at Boston Children's Hospital, including Drs. Assunta Fabozzo, Eric Feins, and Nikolay Vasilyev. In addition to sharing his clinical expertise, Dr. del Nido welcomed me into his research group, where I was exposed to some of the groundbreaking work they perform. I am blessed to have been granted this unique opportunity and thankful for their assistance with my research.

I would also like to express my sincere gratitude to all members, past and present, of the Harvard BioRobotics Lab, including Laura Brattain, Leif Jentoft, Paul Loschak, Qian Wan, Alperen Degirmenci, Molly Finn, Frank Hammond, Yaroslav Tenzer, Mohsen Delvand, Ray Yeow, Samuel Kesner, and Shelten Yuen. Your companionship and diverse competencies have made the long hours in lab all the more productive and pleasant. Peter Hammer, Douglas Perrin, and Robert Schneider deserve a special thanks. Pete's initial

efforts in simulating mass-spring models of the mitral valve motivated much of this work, and his insights and assistance with the data collection process have been invaluable. All the while, Doug's and Rob's companionship, wisdom, and counsel have made navigating the rigors of graduate school that much easier.

To my friends and family, thank you for tolerating the late nights, paper deadlines, and other oddities associated with the graduate student lifestyle. Your support and encouragement have been instrumental in managing the highs and lows of this journey. And Monica, I am unable to enumerate, nevermind thank you enough, for all you have done for me. The patience and understanding you exhibited surpasses anything I could have imagined. I am truly lucky to have you in my life.

Last but certainly not least, Mom, you have been my role model for as long as I can remember. Everything I have today has been made possible through your endless dedication, devotion, and support; this work is as much yours as it is mine. I can only hope you're as proud of me as I am to be your son.

Dedicated to my friends and family, whose unwavering loyalty and support I truly cherish.

Chapter 1

Introduction

Computational modeling of the mitral valve is a mature field of study. However, algorithmic complexity and insufficient processing capabilities have previously limited its application to a laboratory setting. This work details the construction and evaluation of a methodology for rapidly simulating valve closure and explores new applications enabled by this model. To best convey the intricacies of this work, a brief description of valve function and pathology is first provided.

1.1 Cardiac Function

The human heart is the primary organ responsible for ensuring the adequate flow of blood in the body. Divided into four chambers via its internal structure, the heart serves as two pulsatile pumps operating synchronously and in parallel. The left heart, consisting of the left atrium and left ventricle, is responsible for distributing oxygenated blood from the lungs to the the body (systemic circulation). Separated from the left heart via the interatrial and interventricular septa, the right heart delivers deoxygenated blood to the lungs for reoxygenation, after which it returns to the left heart (pulmonary circulation).

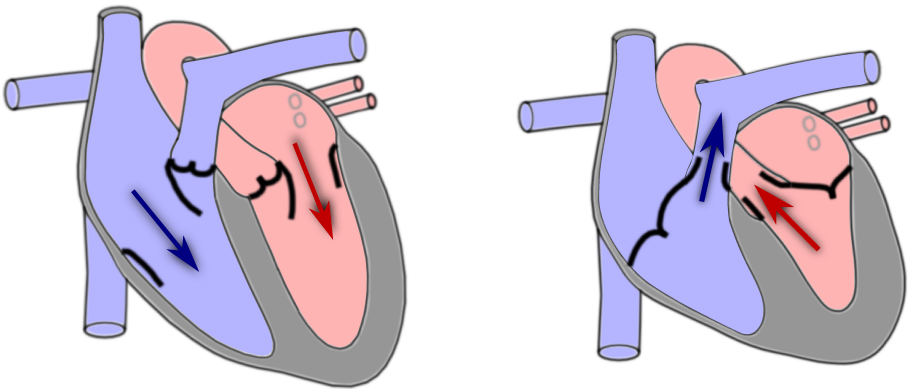

Figure 1.1: The human heart drives the flow of blood throughout the body through ventricular contraction. The left heart circulates oxygenated blood to the body (pink), while the right heart, operating synchronously, forces deoxygenated blood to the lungs (blue). (Images courtesy of Peter Hammer, PhD)

Both the left and right heart induce this flow in a similar manner.

Through the heart's contractile motion, pressure gradients arise which produce the desired blood flow. Blood is first collected in the atrium and is forced through the open atrioventricular valve into the ventricle via upstream pressure and atrial contraction (atrial systole). Upon ventricular contraction (ventricular systole), the atrioventricular valves passively close due to the induced pressure gradient. Therefore, the blood instead passes through the outflow tract, before which it must travel through the semilunar outflow valves. As the ventricles relax to collect blood in the subsequent cardiac cycle, the semilunar valves passively close with the resulting pressure drop to best maintain arterial pressure downstream (Figure 1.1).

1.2 Mitral Anatomy

The mitral valve, the focus of this work, is the atrioventricular valve of the left heart. Named after a bishop's miter for its appearance, the valve and its subvalvular apparatus consist of two membranous leaflets, a fibrous annulus, the tendinous chordae

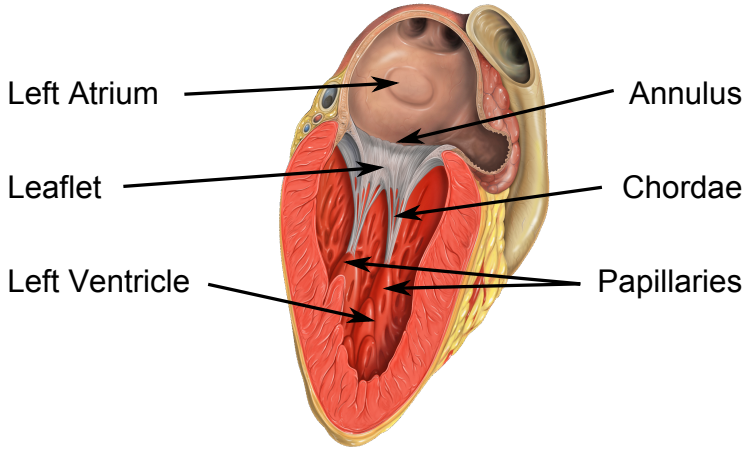

Figure 1.2: Consisting of the mitral annulus, leaflets, chordae tendineae, and papillary muscles, the mitral valve and its subvalvular apparatus are key to ensuring proper function of the left heart. The valve regulates the unidirectional flow of blood, permitting the filling of the left ventricle via the left atrium but preventing undesireable backflow. (Image courtesy of Patrick J. Lynch, medical illustrator and C. Carl Jaffe, MD, cardiologist)

tendineae, and the contractile papillary muscles (Figure 1.2). Largely irregular in shape, the anterior and posterior leaflets typically meet at the commissures to form a continuous piece of tissue. While the anterior leaflet is similar in area to the posterior leaflet, their shapes differ greatly. The anterior leaflet is significantly taller than the posterior leaflet, whereas the posterior leaflet is longer circumferentially. Additionally, while the anterior leaflet consists of a single lobe, the posterior leaflet is readily identifiable via its three scallops. To assist in identification, the anterolateral-most scallop of the posterior leaflet is labeled P1 with the medial and posteromedial scallops referred to as P2 and P3 respectively. Opposite these scallops, corresponding regions on the anterior leaflet, despite lacking the geometric distinctions of the posterior leaflet, are classified as A1 through A3. The two commissures are similarly classified by their anatomic location, known as the anterolateral and posteromedial commisure respectively (Figure 1.3) [21].

The leaflets themselves are thin, typically less than 3 mm in thickness [100]. Embedded between their external layers of endothelial cells is a preferentially oriented network

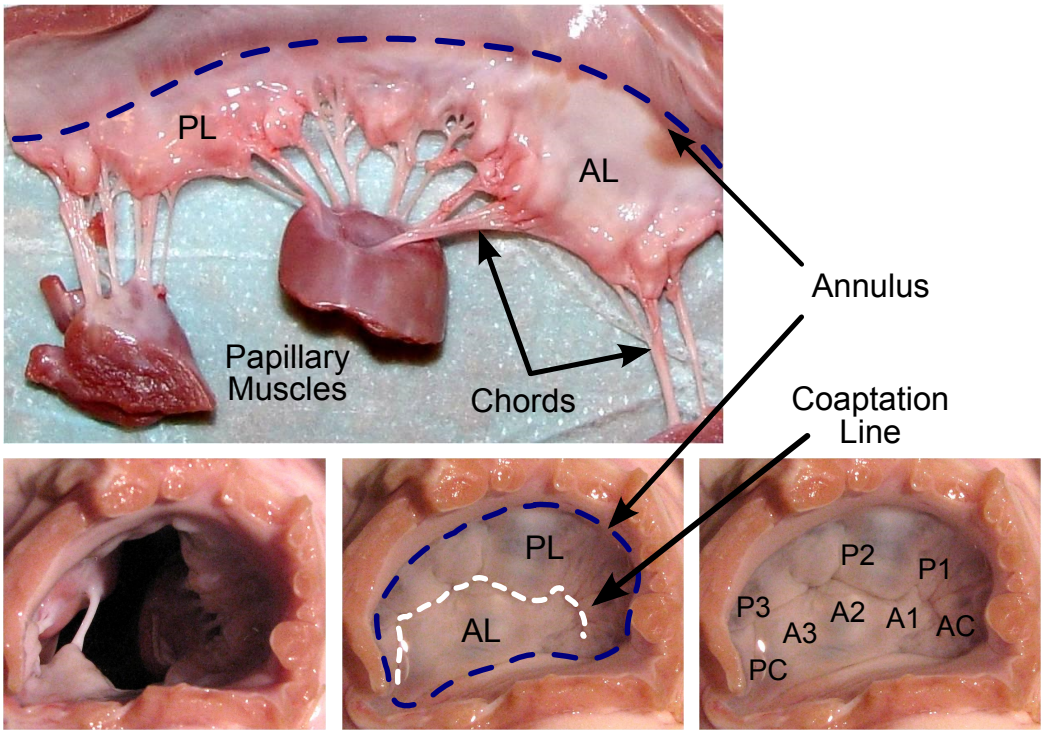

Figure 1.3: The anatomy of the mitral valve and its subvalvular apparatus is complex. (*Top*) The chordae tendineae insert into the anterior leaflet (AL) and posterior leaflet (PL) via a complex branching pattern to relieve stress. (*Bottom Left*) Even with the left atrium excised, visibility of the left ventricle is poor. (*Bottom Center*) When the left ventricle is artificially pressurized with saline, the valve closes and the archetypal "smile" of a closed, healthy valve is visible. (*Bottom Right*) The various leaflet scallops are labeled A1-A3, P1-P3, the posteromedial commissure (PC), and the anterolateral commissure (AC) to aid in referencing leaflet geometry. (Images from dissection of porcine heart, courtesy of Peter Hammer, PhD)

of collagen fibers [84, 99]. Crimped in an unstressed state, the fibers permit a region of high distensibility. However, once the fibers straighten, the tissue stiffness increases dramatically, resulting in highly nonlinear behavior. While the orientation of the fibers is complex, it is largely circumferential, thereby imparting tissue anisotropy with the circumferential direction exhibiting roughly 3x greater stiffness and significantly less distensibility [41, 83].

At their most superior point, the leaflets are embedded into the cardiac wall via a fibrous ring known as the mitral annulus, which separates the left atrium from the left ventricle and forms a 120° angle with the aortic valve. Kidney-shaped with a saddle-like

three dimensional profile, the annulus in a healthy adult typically ranges from 28 to 36 mm in the anterolateral-posteromedial dimension and is roughly 25% smaller in the anteroposterior dimension. Along its flatter anterior portion, the annulus passes through the left and right fibrous trigones, important cardiac landmarks that provide structural support and are also the lowest points on the saddle [21].

Inferiorly, the leaflets attach to the chordae tendineae (Figure 1.4). Tendinous in nature, the chordae are significantly stiffer than leaflet tissue when taut but exert little resistance when in an unstressed state [68, 86]. Their attachment to the leaflets is complex, with large amounts of branching prior to insertion. Commonly classified by insertion site, the chordae are referred to as marginal, intermediary, or basal. The marginal chordae, also known as primary chordae, are most numerous. Attached to the free edge of the leaflets, they are the thinnest of the three, often less than 1 mm in diameter. Attached superiorly on the ventricular side of the leaflets are the intermediary or secondary chordae, which tend to be thicker and fewer in number. Finally, the basal or tertiary chordae insert at the annulus or base of the leaflet and are the thickest and least numerous of the three [21]. Variations in chordae count, insertion, and origination are common [70].

On the distal end, the chordae originate from the papillary muscles. Contractile tissue which inserts into the ventricular wall, the papillaries are typically less than 5 cm in height and are bunched in two groups located below the commissures. Thus, similar to the commissures, they are referred to by their anatomical location, i.e. anterolateral and posteromedial. Each site, situated approximately two thirds of the annular-apical distance down from the annulus, contains multiple papillary heads. In humans, there is often little variation in this structure. However, in porcine and other mammalian hearts, the variability can be substantial.

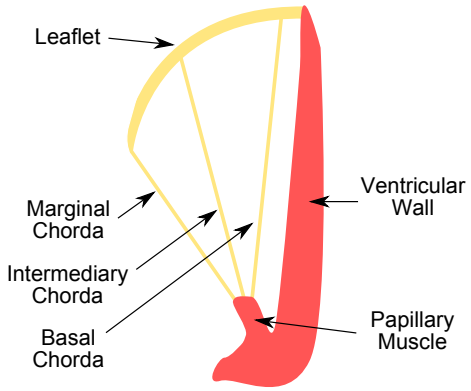

Figure 1.4: The chordae, serving as the suspension system of the valve, are classified by their insertion into the leaflets. While the marginal chordae attach to the free edge of the leaflets, the intermediary chordae insert into the ventricular side of the leaflets, regulating their curvature. The insertions of the basal chordae are superior to those of both the marginal and intermediary chordae, attaching to the base of the leaflet or annulus.

1.3 Mitral Physiology

Coordinated activity and anatomically proportionate sizing of these various components are necessary for proper valve closure. Upon ventricular systole, the atrioventricular pressure gradient and flow entrainment force the leaflets upwards towards the left atrium. This motion is restricted via the marginal chordae, which restrict the maximum travel of the leaflets' free edge. The papillary muscles assist in this task by contracting to remove excess slack and preventing leaflet prolapse into the atrium. The annulus also contracts, shrinking in area by approximately 25% [91], to reduce the mitral orifice and assist in valve closure. The result in a healthy mitral valve is a complete seal formed by the mitral leaflets that prevents backflow across the valve.

Robustness is provided via an area of leaflet contact known as the surface of coaptation. Roughly 7-9 mm in height, this area of overlap safeguards against cardiac dilation, ensuring a complete seal will still be formed in the presence of small increases in annular size. Looking down on the valve from the left atrium, the anterior leaflet is disproportionately responsible for valve closure, extending across 75% of the valve orifice

while the posterior leaflet covers the remaining 25% [21].

With an expected lifespan of over two billion cycles, minimizing stress within the heart and maximizing cardiac efficiency is vital. The intermediary and basal chordae assist in this process. By limiting the extent to which the medial areas of leaflets can extend into the left atrium, the intermediary chordae reduce leaflet curvature and thereby decrease leaflet strain while simultaneously reducing fatigue by partially bearing the pressure load. Additionally, the resultant decrease in ventricular volume increases cardiac output, lessening the effort exerted by the ventricular wall. The basal chordae restrict the motion of the coapted anterior leaflet, pulling it away from the outflow tract and easing the ejection of blood. Animal studies as well as clinical studies in humans have also demonstrated their importance in preserving ventricular shape, with ventricular dilatation more prone to occur in their absence [38].

1.4 Mitral Pathophysiology

Because systemic circulation must traverse more distant regions of the body, substantially greater pressures are found in the left heart than in the right. While the left ventricle normally reaches pressures of up to 140 mmHg (20 kPa), the right ventricle typically remains below 30 mmHg (4 kPa) in a healthy adult [63]. This increased load makes the left heart more susceptible to valvular disease. With the mitral valve experiencing the greatest pressure gradients, it also suffers from the greatest incidence of disease [115].

Mitral regurgitation, also known as mitral insufficiency, is a common pathology, occurring in significant amounts in 2% of the population [58]. Characterized by an incomplete seal formed by the mitral leaflets in systole, undesirable backflow occurs across the valve (Figure 1.5). This reduces cardiac output and efficiency, placing greater strain on the heart as it attempts to compensate. To counteract the decreased output volume, the

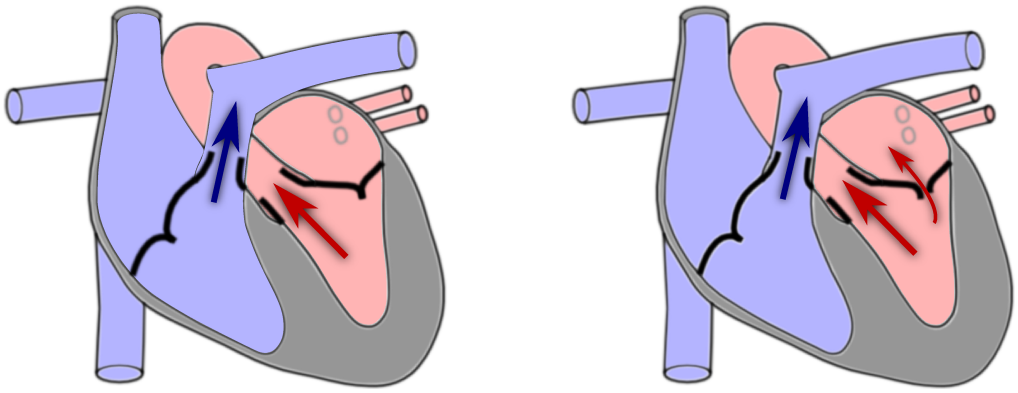

Figure 1.5: Unlike in a healthy mitral valve (left), a regurgitant valve forms an incomplete seal, permitting undesirable backflow (right). (Images courtesy of Peter Hammer, PhD)

ventricle will often dilate to increase its stroke volume. This dilation increases the size of the mitral orifice, further reducing leaflet coaptation and increasing the regurgitant volume. Creating a downward spiral, this can result in contractile dysfunction and eventually heart failure if left untreated.

Mitral regurgitation can be caused by a variety of pathologies. To aid in classification, Carpentier has proposed a pathophysiologic triad: first identifying the underlying cause of the disease (etiology), then determining the resulting anatomical malformations (lesions), and finally characterizing the physiological change in valve behavior (dysfunction) [20]. Classifying by etiology, the vast majority of cases in the western world can be attributed to degenerative valve disease and instances of functional mitral regurgitation [55].

1.4.1 Degenerative Valve Disease

Degenerative pathologies are characterized by their morphological changes to valve tissue which inhibit normal valve function. Although the lesions and therefore dysfunction may vary based on the precise etiology, these conditions are often considered together as the underlying cause of valve dysfunction can be directly attributed to abnormal valvular tissue. Within this designation, the most common pathologies are Barlow's disease, Marfan's

syndrome, and fibroelastic deficiency [5].

Barlow's disease is the most common of the three, observed in 4-5% of the general population. Largely affecting the heart, the patients present with a normal physical appearance. However, the mitral valve is strongly affected, exhibiting strong annular dilation; excess, highly thickened leaflet tissue, and grossly irregular chordae. As a result, the zone of coaptation is found closer to the plane of the mitral annulus, and the excess tissue results in the leaflets billowing into the left atrium [21].

Unlike Barlow's disease, patients with Marfan's syndrome are known to exhibit noticeable physical manifestations in the skeletal, ocular, and cardiovascular systems, including a tall stature with long arms and toes, visual impairment, and aortic root dilatation. Additionally, 80% of patients develop mitral regurgitation. Similar to Barlow's disease however, the valve often possesses a highly dilated annulus as well abnormally large, thickened leaflets, albeit with lesser thickening than Barlow's patients. The chordae demonstrate pronounced thinning, frequent elongation, and at times rupture. As a result, both normal and excess leaflet motion are common [21].

Fibroelastic deficiency, the second most common degenerative valve disease, presents quite differently than Barlow's disease and Marfan's syndrome. Not only do the patients tend to be older and, unlike those suffering from Marfan's syndrome, show no outwardly observable malformations, the disease progresses over a shorter period of time with treatment often required much sooner after diagnosis [5]. Additionally, mild annular dilatation as well as thinning, rather than an excess or thickening, of leaflet tissue is observed. This thinning extends to the chordae as well and often leads to elongation or rupture, resulting in leaflet segments with insufficient chordal support that prolapse into the left atrium.

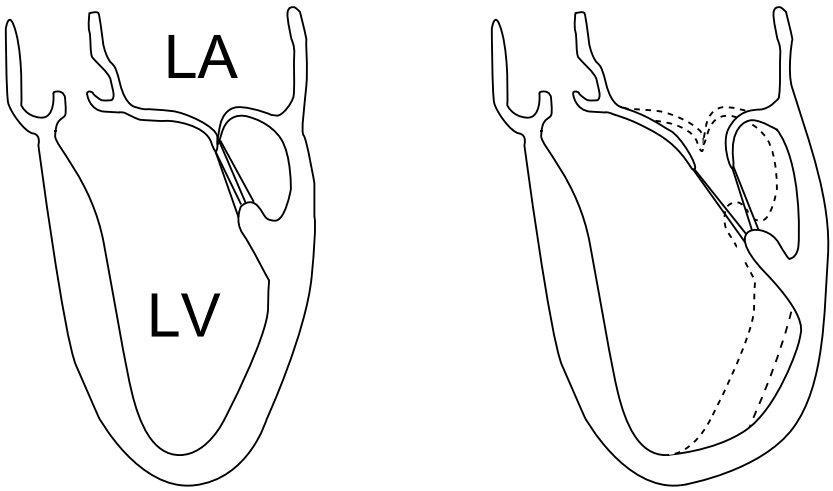

Figure 1.6: Dilatation of the left ventricle (LV), often due to a previous myocardial infarction or dilated cardiomyopathy, can produce regurgitation in an otherwise healthy valve. This change in ventricular shape displaces the nearby papillary muscle and produces corresponding dilatation in the mitral annulus, limiting leaflet mobility in a larger mitral orifice. The result is an incompetent valve despite the absence of a primary valvular pathology.

1.4.2 Functional Mitral Regurgitation

Unlike degenerative patholgies, functional mitral regurgitation is defined as valve incompetence despite the presence of a healthy valve. In these cases, valve dysfunction is a secondary effect of cardiac disease elsewhere in the heart. This pathology is commonly associated with conditions of the left ventricle, such as a previous myocardial infarction (heart attack). The ischemia and damage to the myocardium result in reduced ventricular contractility, which can produce annular dilatation and displace the nearby papillary muscle both laterally and apically (Figure 1.6). With the length of the choardae remaining unchanged, this shift restricts leaflet mobility in systole, preventing leaflet coaptation. The enlarged annulus serves to exacerbate this problem. As a result, moderate or severe ischemic mitral regurgitation has been reported to occur in 12% of those examined within 30 days of a myocardiac infarction, with mild regurgitation found in an additional 38% [18].

1.5 Treatment of Mitral Pathologies

Mitral regurgitation historically has been treated via a variety of means, including medical therapy, percutaneous intervention, valve replacement, and valve repair. While the ultimate goal would be to completely restore valve function and thereby eliminate the undesireable backflow, valve repair is the only method that strives to achieve this objective with the remaining techniques aiming to artificially reduce or eliminate regurgitation through alternate means. Despite these efforts, modern standards of care indicate valve replacement and repair are the only proven curative treatments [19].

Medical therapy, consisting largely of the noninvasive administration of vasodilators and beta-blockers, is now understood to be best used in a limited fashion. By lessening the aortic pressure, vasodilators are used to reduce the resistance in the outflow track, thereby decreasing the regurgitant volume and limiting afterload. This treatment is sometimes complemented by beta-blockers, which are prescribed to further limit afterload. However, such methods are typically ineffective in treating chronic, severe mitral regurgitation. Instead, they are used to stabilize the patient prior to surgery or to mitigate ventricular dysfunction in patients suffering from functional mitral regurgitation, including those where surgery is inappropriate due to high surgical risk [12, 77].

More recently, it has been proposed that high-risk patients could be treated percutaneously. The most clinically advanced device is the MitraClip. Introduced into the femoral vein, a catheter enters the right atrium via the inferior vena cava, proceeds through the atrial septum into the left atrium, and bends down into the left ventricle. At the distal end of the catheter, a V-shaped clip (MitraClip) opens, encompasses portions of the A2 and P2 leaflet, and then closes, performing edge-to-edge leaflet plication and creating a dual-orifice valve. By decreasing the area of the mitral orifice, the clip facilitates mitral sufficiency. Although the device has a strong intraoperative safety record, high rates of

reoperation have been required when compared to open surgery [34, 82].

1.5.1 Valve Replacement

In contrast to percutaneous intervention, valve replacement is a highly invasive procedure with greater history and widespread use. Requiring surgical access to the native valve tissue, the heart is arrested using cardioplegia, and the patient is placed on cardiopulmonary bypass to provide oxygenated blood to the body. The mitral valve is then replaced with either a bio- or mechanical prosthesis, each with their own benefits and pitfalls, to compensate for the incomplete seal at systole.

A mechanical prosthesis is an engineered device that is functionally equivalent yet geometrically quite distinct from the mitral valve (Figures 1.7(a), 1.7(b), and 1.7(c)). Highly durable materials are chosen, such as titanium and carbon, resulting in devices that commonly outlive the patient. However, because of the exposure of foreign materials to the blood, a lifelong prescription of anticoagulants is required and must be carefully monitored to prevent the formation of clots which impede device function, lessen the chance of thromboembolism, and minimize the risk of hemorrhage [116].

Conversely, bioprostheses (Figure 1.7(d)) obviate this issue by avoiding the use of exposed artificial materials. Instead, they are constructed with chemically treated tissue, most commonly bovine or porcine but homografts are also feasible [1], which eliminates the need for anticoagulants. This material tradeoff significantly impairs valve durability, with bioprostheses having a typical lifespan to 10-15 years, after which the valve must be excised and replaced with a new prosthesis.

Regardless of the type of prosthesis chosen, which is largely determined via the patient's age, health, and lifestyle, implantation is nearly identical; an appropriately sized prosthesis is affixed to the mitral annulus, and the valve apparatus is largely preserved and

(a) (b)

(c) (d)

Figure 1.7: Valve prostheses appear in a variety of geometries, often eschewing form for function by permitting only the unidirectional flow of blood across their surface. Mechanical prostheses such as the (a) Starr-Edwards, (b) Medtronic Hall, and (c) On-X are extremely durable but require a strict anticoagulation regimen, whereas bioprostheses such as the (d) Carpentier-Edwards Duraflex sacrifice durability for fewer short-term complications.

displaced whenever possible as excising the chordae has been shown to subsequently impair left ventricular function [27, 98].

1.5.2 Valve Repair

Like valve replacement, valve repair is highly invasive, requiring cardiac cessation and cardiopulmonary bypass. However, instead of replacing the incompetent valve, valve repair restores leaflet coaptation through a series of tissue resections and approximations. As a result, the procedure is highly patient-specific, much more so than valve replacement. When formulating a repair plan, the surgeon has access to a variety of surgical techniques that modify all of the valvular structures, including the mitral annulus, the leaflets, the

chordae tendineae, and the papillary muscles.

With annular dilation common in regurgitant valves across a variety of pathologies, restoring the mitral orifice to physiological dimensions is crucial. Thus, one of the most common techniques in valve repair, one that is performed in nearly all procedures [36], is the mitral annuloplasty. By suturing an appropriately sized ring to the mitral annulus, the orifice is reduced to the desired size, facilitating leaflet coaptation. Although functionally all rings achieve this goal, large variations in ring shape and flexibility exist to match surgeon preference and treat specific pathologies (Figure 1.8). While some rings are flexible and conform to natural annular dynamics, others are rigid and restrict the annulus to a static pose. Additionally, some rings are complete (i.e., extend around the entirety of the annulus) and possess a 3-dimensional shape, whereas other are partial and/or planar.

In cases of degenerative valve disease where excess leaflet tissue is present, tissue is often excised to reduce leaflet size. Depending on the amount and location of the tissue being removed, the shape of the resection can vary. Triangular or, if more tissue must be resected, quadrangular resections are commonly used (Figure 1.9). Because the quandrangular resection extends to the annulus, annular plication, the cinching of the annulus, is often necessary to relieve localized strain. However, when this is insufficient, thin triangular excisions are made parallel to the annulus and the leaflets are stretched to supplement or replace plication [21].

A variety of methods have also been developed to correct for lesions of the subvalvular apparatus. The simplest of these techniques is chordal resection, which can be performed to rid the valve of tethering, calcified, or ruptured chordae. Conversely, the implantation of synthetic neochordae using Goretex suture is also used to compensate for chordal rupture as well as chordal elongation. The difficulties of accurately determining neochordae length can be avoided by instead performing chordal transplantation, the trans-

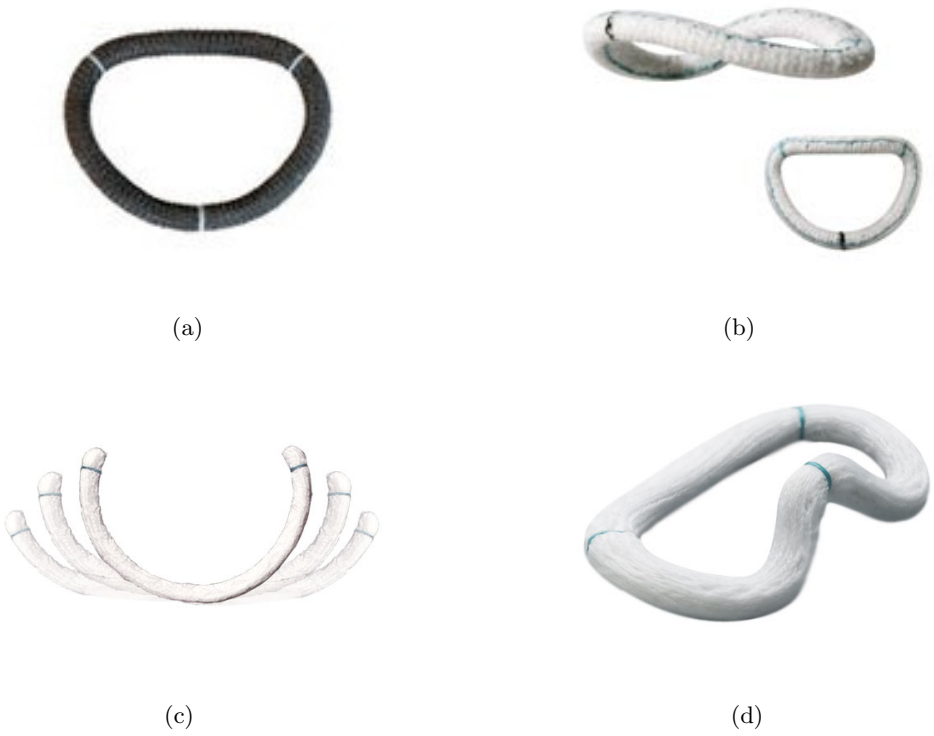

(a) (b)

(c) (d)

Figure 1.8: Annuloplasty rings, while all providing similar functionality, come in a variety of shapes and degrees of rigidity. (a) The Soren Sovering is a flexible, planar, complete band that covers the entire annulus. (b) The St. Jude Medical Rigid Saddle, while also complete, possesses a rigid structure and a 3-dimensional saddle shape. (c) The Cosgrove-Edwards Annuloplasty System is a flexible, partial band that less aggressively modifies annular shape. (d) Finally, the Edwards GeoForm is a complete, rigid ring with a unique 3-dimensional profile that reduces the posteromedial dimension and is designed for patients with restricted motion of the posterior leaflet.

fer of chordae from one leaflet to another. While introducing its own complexities, both techniques have been effectively used clinically. Finally, the effective length of the chordae can also be altered by either modifying their attachment to the papillary head or by modifying the papillary heads themselves. The latter has been performed by splitting a papillary head and adjusting the relative heights of the halves as well as by the more experimental papillary muscle approximation and papillary muscle sling [21, 52, 130].

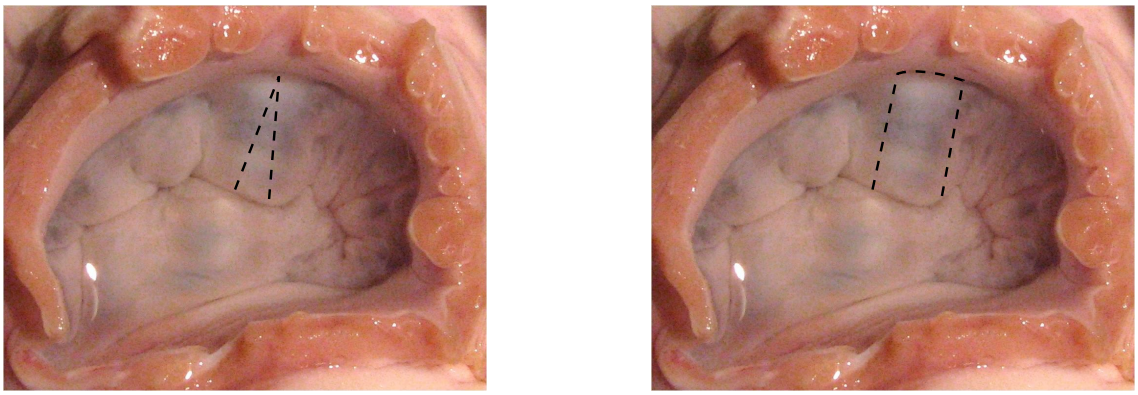

(a) (b)

Figure 1.9: Leaflet resection is a common technique in degenerative mitral valve disease. For smaller amounts of excess tissue, (a) a more limited triangular resection is possible. When larger amounts of tissue must be excised, (b) the more aggressive quandrangular resection is performed.

1.5.3 Comparison of Valve Repair and Replacement

Because valve repair and replacement are the only established curative treatments for mitral regurgitation, many studies have been conducted comparing their efficacy as well as post-operative patient quality of life. For degenerative pathologies, the results conclusively favor the use of repair in lieu of replacement with significant increases in patient survival [3,31,57,87]. While the results are less definitive for those suffering from functional mitral regurgitation, largely because of the poor prognosis regardless of treatment, recent studies suggest repair again provides improve patient longevity [37, 119]. Repair also provides improved quality of life as a durable repair requires no continued treatment, whereas a mechanical prosthesis requires anticoagulation therapy and a bioprosthesis necessitates re-replacement every 10-15 years. As a result, the American College of Cardiology, the American Heart Association, the European Society of Cardiology, and the European Association for Cardio-Thoracic Surgery all recommend valve repair whenever feasible [12, 117].

However, valve repair is also far more difficult to perform. Because of the poor

resolution of preoperative imaging relative the the size of the valvular structures, the surgeon must identify valvular lesions and formulate the complex repair plan intraoperatively. Cardiopulmonary bypass, while necessary, exacerbates these challenges. With the heart arrested for the procedure, the surgeon is unable to directly verify the success of a repair. Instead, the effects of the various repair techniques as well as the closed valve shape must be predicted via intraoperative analysis of the valve and past experience. While the prediction can be aided by the insufflation of the incontractile left ventricle with saline to induce valve closure and approximate the valve's systolic shape, the "saline test" can be time-consuming and requires care to avoid introducing air into the coronary arteries [6, 21]. This process of identification of lesions, formulation and implementation of repair plan, and verification of repair success must be performed in an efficient and timely manner though, as prolonged exposure to cardiopulmonary bypass has been shown to significantly increase the risk of cognitive impairment as well as stroke [14, 89, 108].

As a result, valve repair is highly underperformed. Nationally, the rate of valve repair falls between 40% and 60% with the remainder receiving a simpler and less time-consuming valve replacement [11]. However, it has been suggested that repair rates should exceed 90% or greater, levels that are achieved by top surgeons [2, 4, 22]. One significant cause of this discrepancy is surgical experience. It has been shown, both in the US and abroad, that surgical volume is a key predictor of the rate of valve repair, with higher volume surgeons repairing valves at a significantly greater rate (Figure 1.10) [4, 11].

1.6 Computer-Based Simulation of the Mitral Valve

Because of the complex nature of valve physiology and repair, computer-based simulation has been used to study valve function and treatment. By adapting the detailed finite element models initially designed for the analysis of bridges, buildings, and airplanes,

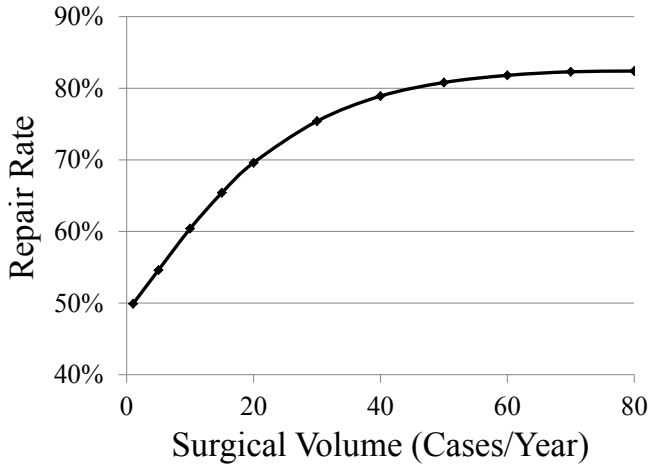

Figure 1.10: The rate of valve repair is a function of surgical volume. While the repair rate is low for low-volume surgeons, it rapidly increases as surgical volume increases and stabilizes at a load of roughly 50 cases per year [11].

it is possible to not only predict the valve's shape in systole, but also the behavior of blood in the heart [72,122]. However, commonly used by those with advanced engineering degrees, such tools are far too involved to be accessible to surgical community. Furthermore, the existing surgical workflow requires far shorter simulation times than current models provide. This complexity has made existing valve simulation methodologies impractical in a clinical setting and thus limited their impact.

1.7 Thesis Contributions

With the aim of making valve simulation available to a surgical audience, this work details the design and application of a simplified yet accurate model of the mitral valve. Rather than implementing a complex finite element model, inspiration is drawn from the modeling of cloth by the video game industry, permitting speeds far beyond what was previously feasible. Integrated into an interactive haptic surgical simulation platform for valve repair, a complex multithreaded structure and greater than 1 kHz update rate was

required to provide a seamless user experience. The result is an environment in which the user is able to directly interact with the valve model and assess the quality of a repair plan.

This technology is then leveraged to further the state-of-the-art in surgical education via the assessment and instruction of repair-related cognitive skills. Tests conducted using the system provide the first quantitative means of evaluating a user's ability to predict closed valve shape. Additionally, by providing interactive instruction, the system also presents the first economical, nonoperative method to improve these skills.

Finally, the fast simulation model is used to investigate the poor survival rates of those suffering from ischemic mitral regurgitation. With minimal time required to simulate valve closure, in-depth measurements of procedural robustness and response to continued ventricular dilatation are provided, representing the most rigorous comparison of these techniques and their modes of failure.

1.8 Thesis Overview

This thesis describes the development of an interactive simulation platform for mitral valve repair and its applicability surgical training and disease treatment.

Chapter 2 details the structure of this model and the complexities of integrating it into an interactive platform. The effects of model resolution on speed of simulation are characterized, and it is shown that an update rate of greater than 2 kHz is achievable with valve closure simulated in less than 1 second. The system is then validated using high resolution microCT of artificially inflated ex-vivo porcine specimens. Despite using a computationally simpler model in lieu of a more complex finite element model, sub-millimeter accuracy is demonstrated across a variety of hearts and surgical modifications.

Chapter 3 investigates the benefits of such an interactive platform on surgical education, focusing on the prediction of closed valve shape. One of the most challenging

aspects of valve repair, it is shown that the system can be used to differentiate between users of differing skill levels. It is then demonstrated that this predictive ability can then be improved via interactive training. Additionally, these improvements are confirmed in an ex-vivo tissue model.

Chapter 4 presents the benefits of fast simulation in assessing ischemic mitral regurgitation and evaluating methods of treatment. By perturbing valve geometry, the sensitivity of regurgitant orifice area is computed through repeated simulation. A novel surgical technique is then optimized for robustness to variation.

Chapter 5 discusses the implications of this work on the future of mitral valve repair. Demonstrating the benefits of fast surgical simulation on anisotropic, stiff tissue, the techniques and concepts demonstrated in this thesis can be extended to different surgical techniques as well as the automated design of repair plans. Further improvements to this research are also outlined.

Chapter 2

Fast, Interactive Simulation of Mitral Valve Repair

2.1 Background

Due to the aforementioned complexity of valve dynamics and valve repair, the simulation community has developed a variety of models for predicting and analyzing valve behavior. Kunzelman was one of the early pioneers in the field, characterizing mitral valve anatomy in both porcine and human hearts [68, 70] and creating the first finite element model of the mitral valve using idealized geometry derived from these measurements [69]. This spurred interest in simulation of valve pathology and repair. While Kunzelman and colleagues studied the effects of altered leaflet collagen concentration and traditional repair techniques [66, 67, 73, 74, 96], Votta, in conjunction with Alfieri (widely known for his eponymous Alfieri Stitch), investigated more experimental techniques [79, 123, 124].

However, because these models use a generic model of valve anatomy, meaningful assesment of their accuracy is not possible. This motivated the development of patient-specific models, which could subsequently be compared with imaged patient data. By

segmenting the leaflets from transesophogeal echocardiography, Burlina created a patient-specific model of the valvular apparatus, computed closed valve shape using energy minimization techniques, and compared the results across a variety of mechanical tissue models [15–17,106]. Rather than segment the leaflets, a computationally intensive task, Ionasec and Voigt segment key valve landmarks, which when combined with a geometric prior, produce a valve model for simluation [54,120]. However, such model fitting can result in large geometric error and even larger simulation error. To improve simulation accuracy, Kanik shows that an inverse finite element model can be used to optimize leaflet properties and chordae length to best fit the imaged data [61, 62]. These improved valve models led to a second generation of simulated valve procedures, with results that could be quantiatively compared to an imaged ground truth [80, 107].

Building on the gains from patient-specific leaflet geometry, the simulation community moved toward improving simulation fidelity by developing more detailed models including dynamic blood flow and ventricular contraction. Some of the earliest fluid-structure interaction models, which simultaneously solve for the motion of the tissue and blood, were developed by Peskin in the 1970's and 1980's [94, 95]. More recently improved by Griffith, Ma, Kunzelman, and many others [44, 45, 71, 78], these models are computationally expensive due to the added cost of the fluid flow problem. Rather than model flow, Wenk has created an augmented valve model that includes a anatomically accurate, contractile ventricle, permitting improved simulation of ventricular disease and treatment [128, 129].

Despite these advances in valve simulation, model sensitivity to the chordae and their generic description in these models have limited improvements in simulation accuracy [49, 80]. Thus, Wang and Hammer have both developed models with patient-specific chordal geometry. In [126], Wang segments the annulus, leaflets, chordae, and papillary muscles from multi-slice CT volumes to generate a personalized valve model, which was then

simulated to closure with an anisotropic, hyperelastic finite element model. Conversely, using an anisotropic mass-spring model, Hammer simulates ex-vivo porcine specimens with similarly individualized geometric models generated from microCT [49]. By providing an accurate sub-valvular apparatus, the authors are able to significantly reduce model error, highlighting the importance of the chordae.

Although these models furthered the state of the art with regards to simulation accuracy, valve modeling remains largely inaccessible to the clinical audience due to the complexity and time required to simulate valve closure. The tools used are highly specialized and often require advanced, domain-specific expertise. Arnoldi attempted to simplify the process with a graphical user interface, but the system described is non-interactive, does not permit the planning of valve repair, and demands a computing cluster to execute the simulation, a technological burden that most hospitals will be unable to satisfy [7]. The computational requirements of interactivity have challenged others as well. Although simulation times vary by model, Sprouse reports times between 5 minutes and 24 hours, depending on mesh resolution [106]; Mansi presents 10 minute simulations at 0.3 frames per second [80]; and Hammer, whose model is optimized for computational speed and efficiency, reduces the time required to less than 30 seconds, which while an improvement, is still too slow for interactivity [50].

The system described in this chapter overcomes these limitations, detailing the construction and validation of an *interactive* surgical simulation platform for mitral valve repair (Figure 2.1). This is achieved through the use of a mass-spring model, similar to that described in [50], that is highly optimized for computational efficiency. The fast mechanical model, operating at 3 kHz and simulating valve closure in less than one second, enables the integration of a Geomagic Touch haptic device (3D Systems, Rock Hill, South Carolina, USA) for user interaction with the valve model. With the haptic device, users can then

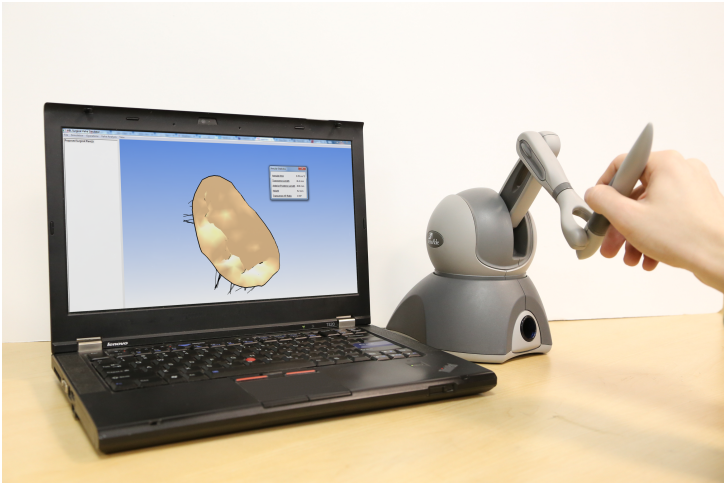

Figure 2.1: The surgical simulation platform consists of an off-the-shelf PC on which the simulation runs and a haptic interface for interacting with the valve model.

analyze and manipulate the valve and perform virtual surgery with ease. Finally, the system is validated by comparing the simulated closed valve shape to that observed in excised porcine hearts that have been artificially pressurized.

2.2 Methods

2.2.1 Overview

The platform described in this work is the result of an interdisciplinary effort with tools and techniques drawn from image processing, deformable modeling, video-game physics, and haptic interfaces (Figure 2.2). A 3D image of the mitral valve is first acquired, segmented, and meshed. Serving as input to a mechanical modeling unit, the valve model is then deformed by both internal tissue forces and external forces resulting from valve pressurization and user interaction. The current, simulated valve state is visually and haptically rendered to the user in real-time, enabling virtual surgery and the rapid, iterative development of a patient-specific surgical plan.

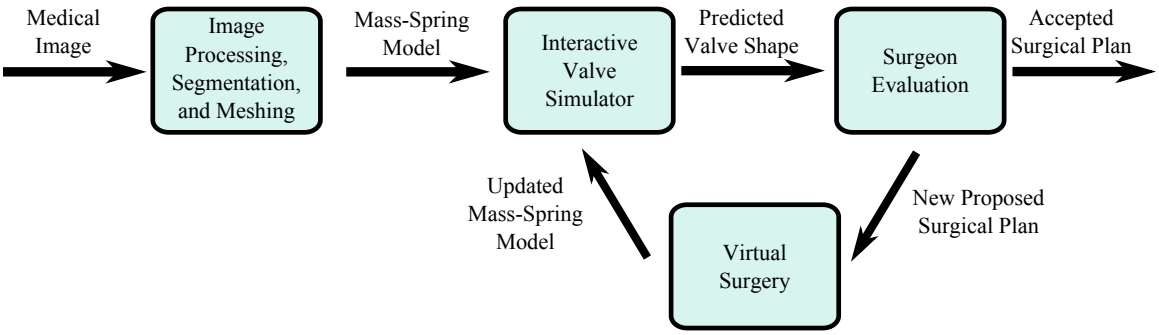

Figure 2.2: A system diagram of the interactive simulation platform described in this work.

2.2.2 Valve Model Generation

Previous efforts in segmenting the mitral valve have largely focused on 3D ultrasound (3DUS) because of its widespread use and low cost. This has led to the development of semi-automated algorithms for extracting leaflet and annular geometry [16, 102, 103]. However, due to 3D ultrasound's noisy nature and poor resolution relative to the subvalvular apparatus, methods for extracting the chordae tendineae are not yet available. Given their importance to simulation accuracy, high-resolution computed tomography (MicroCAT II, Siemens) was used, much like in [50], for its improved noise characteristics and resolution (100 μm isotropic voxel size), better isolating simulation error from geometric modeling error (see Figure 2.3 for a comparison of typical image quality).

The MicroCAT II possesses a small bore and 5.4 cm transaxial field of view, necessitating the excision of cardiac specimens. Thus, freshly excised hearts of 25-40 kg Yorkshire pigs were used in this study. The mitral valve was pressurized using air introduced into the left ventricle via the aorta. Air pressure was controlled and measured using a regulator and pressure transducer. Transvalvular pressure was set to the maximum each valve could withstand without leakage and remained above 70 mmHg in all specimens. To prevent undesired transients, the coronary arteries were ligated and sealed using cyanoacrylate. Images were then acquired of both the unpressurized and pressurized valve to generate a valve model.

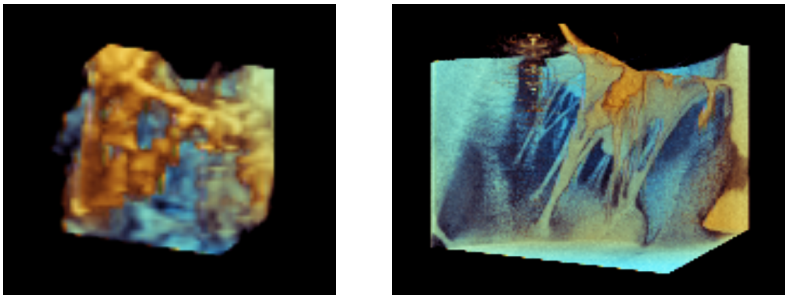

(a) (b)

Figure 2.3: While 3DUS is a clinical imaging modality, its images provide (a) poor resolution and high noise making segmentation of valve geometry challenging. Conversely, microCT provides images of (b) significantly improved quality and clarity. Therefore, in this work microCT is used to best assess the accuracy of the mechanical model.

Using a combination of custom and open-source software (3DSlicer and Meshlab), the valve structure and subvalvular apparatus were segmented from the previously mentioned volumetric images. Unstressed leaflet geometry and chordal attachments were acquired from the unpressurized images, while pressurized annular shape, displaced papillary locations, and chordal lengths were acquired from the pressurized image. A lower resolution leaflet mesh was then developed through a combination of downsampling and edge relaxation techniques [93]. This resolution was determined experimentally to balance modeling accuracy and the performance requiements of the haptic device.

2.2.3 Simulation of Valve Closure

Commonly used in videogames to simulate cloth, mass-spring models are known for their computational efficiency. While in the engineering community finite element models are the standard for mechanical membrane simulations, in the context of valve simulation, they are are an order of magnitude slower than their mass-spring counterparts and provide a limited improvement in accuracy [50]. Therefore, to achieve the 1 kHz update rate required for smooth haptic interaction, a mass-spring approximation of a finite element model

was implemented. Nodal masses were computed using Equation (2.1), whereas physically accurate spring stiffnesses were calculated using Equation (2.2), a method first described by van Gelder [118],

$$m_{n_i} = \frac{\rho t}{3} \sum_{T_j \in N(n_i)} \text{area}\,(T_j) \tag{2.1}$$

$$k_{e_i} = \frac{Et}{\ell_0^2} \sum_{T_j \in N(e_i)} \text{area}\,(T_j) \tag{2.2}$$

where ρ is the tissue density of $1060 \frac{kg}{mm^3}$; t, the tissue thickness, is assigned to be a uniform 1 mm; T_j are the triangles sharing the specified node in Equation (2.1) or edge in Equation (2.2); E, the modulus of elasticity, is configuration dependent (see below); and ℓ_0, the natural length of edge e_i, is determined from the unpressurized mesh.

To further decrease computational complexity, a nonlinear Fung-elastic constitutive law was approximated using a computationally simpler bilinear model (Figure 2.4). Below a critical strain, the tissue is highly distensible and is modeled with an elastic modulus that is significantly more pliable than that found in the post-transition region. To account for tissue anisotropy, these pre- and post-transitional properties are a function of spring orientation in the unpressurized valve. Modeled in an orthotropic manner with increased stiffness in the cirumferential direction, location-specific tissue stiffnesses are interpolated using a trigonometric weighting scheme (Equation (2.3)) as described by Hammer [50]. With spring stiffness varying linearly with the elastic modulus (Equation (2.2)), the result is the bilinear force law described in Equation (2.4).

$$E(\theta) = \sqrt{(E_c \cos\theta)^2 + (E_r \sin\theta)^2} \tag{2.3}$$

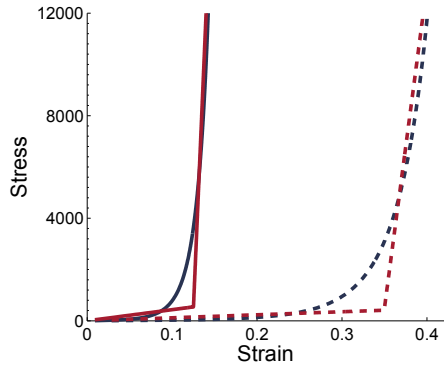

Figure 2.4: The complex nonlinear constitutive law (navy) is replaced by a computationally simpler bilinear approximation (crimson) to increase speed of simulation. The tissue is assumed to be orthotropic with the radial direction (dashed) exhibiting greater distensibility than the circumferential direction (solid). Edge stiffnesses are computed using a weighted average based on their orientation.

$$\vec{f}(\vec{e_i}) = \begin{cases} k_{pre} \cdot (|\vec{e_i}| - \ell_0) \dfrac{\vec{e_i}}{|\vec{e_i}|} & : |\vec{e_i}| \leq (1+\lambda) \cdot \ell_0 \\ \left(k_{pre}\lambda\ell_0 + k_{post} \cdot (|\vec{e_i}| - (1+\lambda) \cdot \ell_0) \right) \dfrac{\vec{e_i}}{|\vec{e_i}|} & : |\vec{e_i}| > (1+\lambda) \cdot \ell_0 \end{cases} \tag{2.4}$$

In addition to the forces generated via leaflet deformation, the forces generated by the chordae tendineae, papillary muscles, and mitral annulus must also be considered. Due to their string-like nature, the chordae are treated as uniaxial rods of a 1 mm diameter supporting only tension. They provide significantly greater resistance to elongation than leaflet tissue with an elastic modulus of 40 MPa. Finally, the mitral annulus and papillary muscles are treated as fixed boundary conditions due to their anchoring in the cardiac skeleton and musculature. A summary of model parameters is found in Table 2.1.

Valve closure is induced via a static load applied to each face of the mesh. With a magnitude equal to peak systolic pressure and a direction normal to each face, the load is evenly divided amongst each face's nodes. Simple to compute, this approximation lies in stark contrast to the complex and computationally expensive fluid-structure interaction models, which would be infeasible in an interactive environment.

Parameter	Value
Tissue Density	$1060 \frac{\text{kg}}{\text{mm}^3}$
Leaflet Thickness	1 mm
Elastic Modulus (circumferential, pre-transition)	11 kPa
Elastic Modulus (circumferential, post-transition)	2.3 MPa
Transitional Strain (circumferential)	13%
Elastic Modulus (radial, pre-transition)	3.3 kPa
Elastic Modulus (radial, post-transition)	760 kPa
Transitional Strain (radial)	33%
Diameter (chordae)	1 mm
Elastic Modulus (chordae)	40 MPa

Table 2.1: Model parameters are derived from ex-vivo testing of porcine specimens and fit to the selected computational model.

Regardless of implementation, valve pressurization results in leaflet collisions that must be resolved. The naïve pairwise solution would be $\mathcal{O}(N^2)$, which is intractable in an interactive setting for even coarse meshes. Therefore, as is customary, a two-phase approach is taken. First, potential collisions are rapidly pared using a cache-friendly variant of the sweep and prune algorithm [8]. Exploiting temporal coherence, the algorithm's performance improves as more items remain stationary. Remaining collision candidates are then inspected, and a C^1 continuous penalty force is applied to the colliding faces.

After the forces due to tissue deformation, pressurization, self-collision, and user-tissue interaction (detailed later in this work) are computed, a small fictitious damping force is added to ensure numerical stability. The model is then stepped forward using a symplectic Euler integrator, which was chosen for its combination of speed and stability.

2.2.4 User Interface

Written using OpenGL and wxWidgets for cross-platform support, the user interface is designed for ease of use, which has been demonstrated in preliminary studies [112]. Key to this is the integration of a haptic device. While the 1 kHz update rate required for smooth, stable haptic interaction severely limits model complexity, previous work has shown that more comprehensive models which include secondary and tertiary effects at the cost of long simulation times are too involved for clinical use. Therefore, given the goal of this work is to develop an interactive tool for practicing surgeons, the richer input space and more intuitive feedback afforded by the Geomagic Touch make this a worthy design tradeoff provided sufficient simulation accuracy can be maintained.

Not only does the haptic device's 3-dimensional positioning facilitate accurate movements in the virtual world, the force feedback permits the user to feel and manipulate the valve tissue (Figure 2.5). By pressing a button on the haptic stylus, the user can grasp a valve leaflet at the desired location. This action engages a stiff spring-damper coupling between the virtual position of the haptic stylus and the desired tissue region. Such a technique allows for precise grasping and has been demonstrated to be more stable than a direct position-based coupling [24]. The computed force is then applied to the valve mesh and, after scaling and aligning to the user's perspective, the haptic stylus as well.

The ability to haptically interact with the model in real-time extends the surgical workflow into the virtual environment. Much like is performed in the operating room, the surgeon can use the haptic device to pull the free edge of the leaflet towards the atrium, examining for abnormal leaflet mobility caused by chordal malformations. Moving beyond what is feasible clinically, the user can also visually inspect the height of leaflet coaptation, an important metric of repair quality, by pulling apart the two leaflets in the pressurized valve model. While such data is commonly acquired intraoperatively, it typically requires

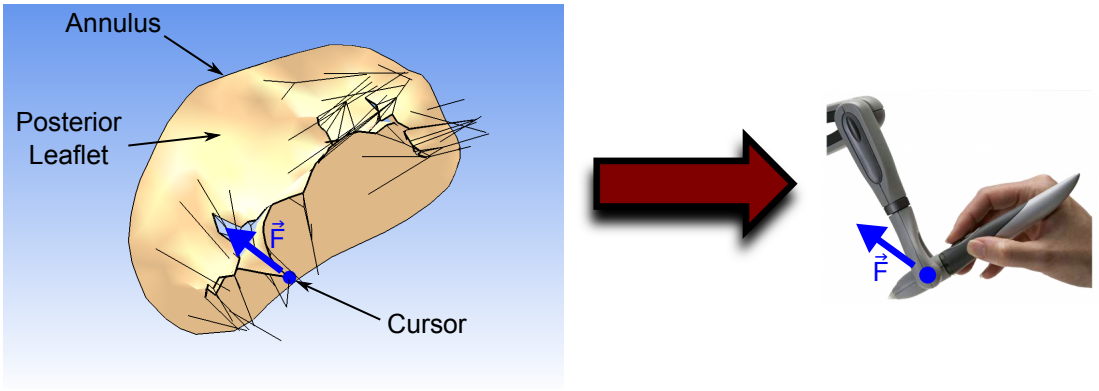

Figure 2.5: Using the haptic device, the surgeon can pull on leaflet tissue, enabling improved inspection of leaflet mobility and coaptation in systole.

a more involved, time-intensive procedure of ventricular insufflation with saline and subsequent "painting" of the leaflets with ink. By providing an intuitive, and at times simplified, means of interaction with the valve, the system encourages the surgeon to leverage previously developed skills thereby lessening the learning curve and facilitating system use.

However, utilizing haptics alone would not leverage the full potential of the virtual environment. The interactive platform also enables improved visualization and analysis of cardiac structures, far greater than that feasible intraoperatively. In addition to rotating, translating, and scaling the surgeon's view of the valve, cut planes can also be inserted to examine obscured regions of leaflet tissue, including the height of coaptation along the coaptated region (Figure 2.6). Further tools provided highlight leaflet prolapse through a rendered annular plane, identify regions of high chordal strain using color, compute key statistics detailing valve geometry, and measure dimensions selected by the user with the haptic stylus.

With the information gained from simulation as well as visual and haptic inspection, the surgeon can then perform virtual surgery. Supported surgical techniques include mitral annuloplasty and modification of the chordal apparatus, which consists of chordal length adjustments, synthetic chordal insertions, chordal excisions, and chordal transfers.

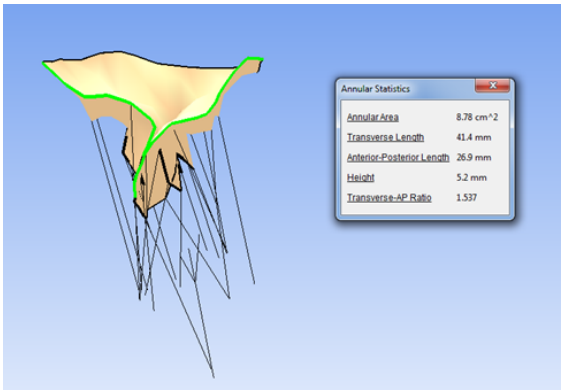

Figure 2.6: As opposed to physical models, virtual modeling enables improved visualization such as the insertion of cut planes to better observe and analyze leaflet coaptation. Quantitative measurements such as annular size can also be provided with ease.

Key anatomical landmarks defining the chosen technique are selected via the haptic device. Once completely specified, the valve model is updated and the results are instantly simulated and rendered to the user for confirmation. The action can then be accepted, upon which it is added to the surgical plan; revised; or rejected, with the changes to the valve discarded. At any time, previously accepted operations can also be modified or removed if desired. By providing immediate feedback in response to valve modifications and effortless alterations to the surgical plan, plans can be developed in a fast, iterative manner, thereby affording a simpler, more flexible planning process.

2.2.5 System Integration

Constructed with a modular design, the system is divided into three unique subsystems: a tissue modeling unit, a unit for haptic force computation, and a unit for the remaining non-haptic interactions, which consist of visual rendering and processing of user actions. These subsystems operate independently in three separate threads and are placed on separate processing cores to maximize concurrent execution. Such a design is preferred as the different subsystems execute at different rates and with different time constraints.

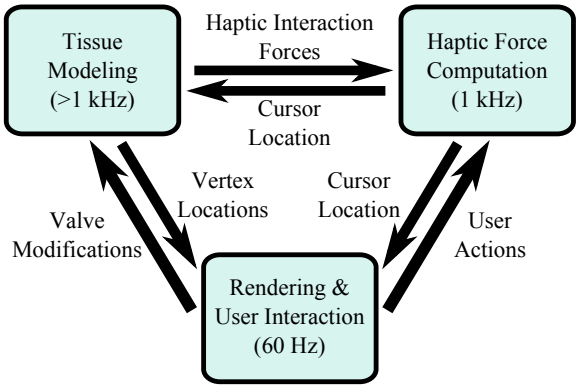

Figure 2.7: The interactive simulation platform is modularized to minimize the delay induced by costly operations on their faster, more time-sensitive counterparts. While this architecture improves computational efficiency, interthread communication must be handled with care due to the differing update rates.

For instance, while the haptic thread must run at 1 kHz for smooth, stable operation, valve rendering is too computationally expensive to achieve this rate and runs at only 60 Hz. By separating their activity, the slower units do not hinder the performance of the faster ones, an important concern given the haptic update rate that must be maintained. As a result, the various threads are required to pass data to each other asynchronously (Figure 2.7).

Information is exchanged via shared memory, rather than the the haptic device's programming interface, allowing for maximal flexibility. However, because of the concurrent access patterns, care must be taken to avoid data corruption; reading partially written data or simultaneously writing to the same memory address can have unexpected and unpredictable consequences. To prevent this, a variety of control mechanisms, differing in speed and flexibility, are implemented. For the most frequent and simplest operations, lightweight atomics and lock-free methods are used, whereas bulk data transfers are protected via read-write locks.

The compiler's optimization procedures can also present challenges. The transparent reordering of instructions to maximize computational efficiency, while safe in single-threaded code, can introduce deadlocks, race conditions and data corruption in a mul-

tithreaded environment. Therefore, memory fences are judiciously employed to regulate permissible reordering, minimizing the effects of memory and instruction latency. This enables aggressive optimization where possible while still preserving algorithmic integrity. Although the complexities introduced by multithreading are significant, the performance benefits it imparts are demanded by the computational requirements for haptic interaction.

2.2.6 Validation

With the interactive platform constructed, simulation accuracy was then assessed. A valve model, created using the previously described methods, is simulated to closure and compared with the closed shape of the pressurized, imaged valve. The model and image are aligned using the iterative closest point algorithm, and simulation error is evaluated on a node-by-node basis as the distance from the sparser, simulated valve to the higher resolution, imaged valve. This process was repeated for 5 unmodified valves excised from 25-40kg female Yorkshire pigs.

Various valve repair techniques were also validated. As performed in [49], one of the five valves was subsequently modified by shortening a chorda attached to the P2 scallop of the posterior leaflet until just before leakage. The valve was then pressurized and imaged, and the virtual valve model was updated with the new chordal length. The new, simulated model was then compared to the imaged result in a similar fashion.

Finally, an annuloplasty was performed on two of the valves. Custom-designed to mimic the Carpentier-Edwards Classic Annuloplasty Ring (Edwards Lifesciences Corp, Irvine, CA USA), the 3D-printed rings were fabricated in plastic to minimize imaging artifacts and carry a series of holes through which sutures can be passed (Figure 2.8). The rings were implanted into the porcine hearts by a trained cardiac surgeon, and the modified hearts were imaged (Figure 2.9). The virtual valves models were updated to reflect the new

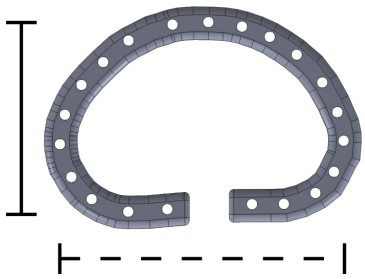

Figure 2.8: A custom annuloplasty ring was designed and fabricated using a 3D-printer to validate model accuracy post-surgical repair. The rings were constructed such that the ratio of the anterolateral-posteromedial dimension (dotted line) and the anterior-posterior dimension (solid line) is 4:3, the preferred physiological ratio.

annular geometry, and simulation error was computed. This procedure largely followed that found in [111] but with the addition of model anisotropy.

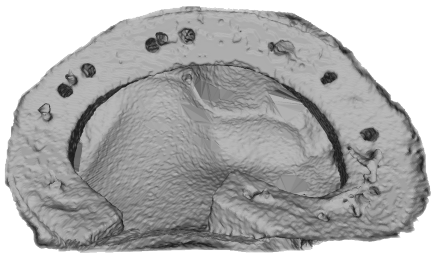

Figure 2.9: After ring implantation, the mitral valve is segmented and compared to the simulated model. The 3D-printed ring is clearly visible and has no adverse effect on image quality.

2.3 Results

2.3.1 Performance Characteristics

Simulations were run on a PC with a 2nd-Generation Core i5 2.5 GHz CPU and 8GB of RAM. To determine the optimal mesh resolution, i.e. the maximal resolution that would ensure the requisite 1 kHz update rates, simulations were run on meshes of identical geometry but varying coarseness. The lowest resolution was chosen to be roughly 650 faces,

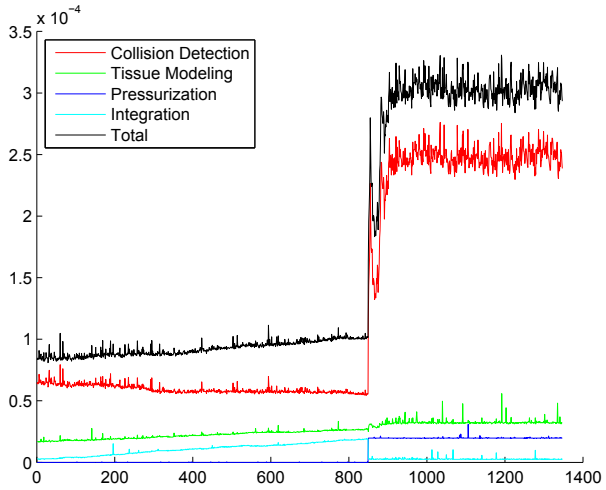

Figure 2.10: The performance of the tissue modeling thread is dependent upon valve state and depends largely time to compute collisions and impart collision forces.

that used by Hammer et al. in [50]. Additional meshes were constructed by dividing each face in four along edge midpoints, thus creating meshes of 4-times and 16-times resolution while preserving face quality. Computation time within the tissue modeling thread, dependent upon valve state, was logged across simulation of valve closure. Figure 2.10 shows the performance of the various mechanisms that comprise the modeling unit. Collision detection is by far the costliest operation.

As mesh resolution increased, the characteristic shape of Figure 2.10 remained constant. However, the scale of the y-axis increased due to the increasing computational burden imparted by the greater number of faces and vertices. Figure 2.11(a) highlights change in performance when the valve is fully closed and in steady state, the most computationally intensive period in the simulation. Superimposed is a power regression ($y = bx^a$) fit to the cummulative time data. Given the log-log scale of the plot, the slope of the regression, $a = 1.1$, approximates the simulation's algorithmic complexity in practice, $\mathcal{O}\left(N^{1.1}\right)$. Figure 2.11(b) shows that over this wide range of resolutions, the relative cost of each step of the simulation process remains nearly constant.

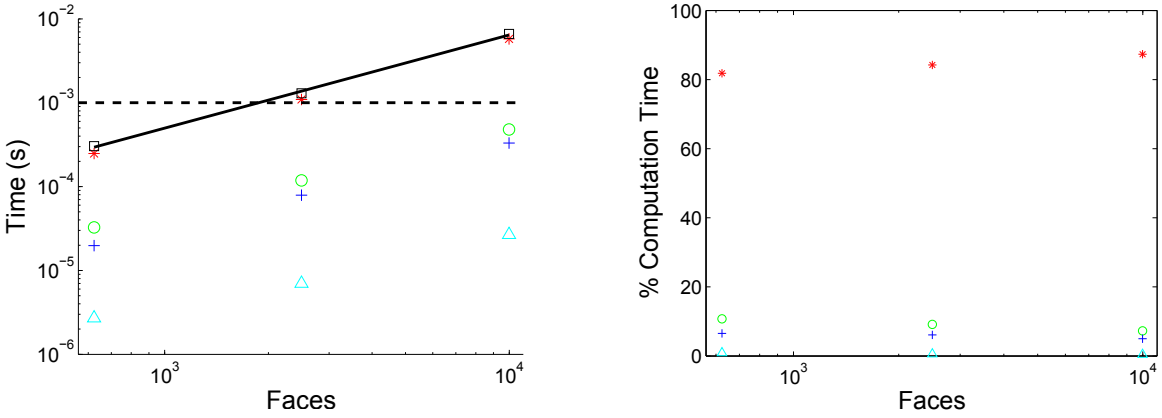

(a) (b)

Figure 2.11: Mesh resolution is strongly correlated with computational performance (time to execute a given simulation step). Cyan triangles correspond to numerical integration, blue plus markers to valve pressurization, green circles to tissue deformation, red stars to collision detection, and black squares to the total execution time, the sum of the previously mentioned components. In (a), a power law (black solid line) is fit to the total execution time, showing $\mathcal{O}\left(N^{1.1}\right)$ performance in the region of interest. A dashed line is added representing the 1 kHz update rate required for smooth haptic interaction. As shown in (b), collision detection dominates at all resolution scales.

2.3.2 Modeling Accuracy

After determining the resolution required to achieve haptic rates across all valve states, valve meshes were downsampled to the appropriate coarseness to evaluate accuracy at this resolution. While the first three specimens were similar in size, the fourth and fifth were excised from smaller animals and were thus smaller. Variations in chordal geometry were significant between the models, emphasizing the importance of this patient-specific approach. Sub-millimeter RMS error was observed across the simulations with the maximum error remaining below 2.5 mm. These results are summarized in Table 2.2 and Figures 2.12-2.14.

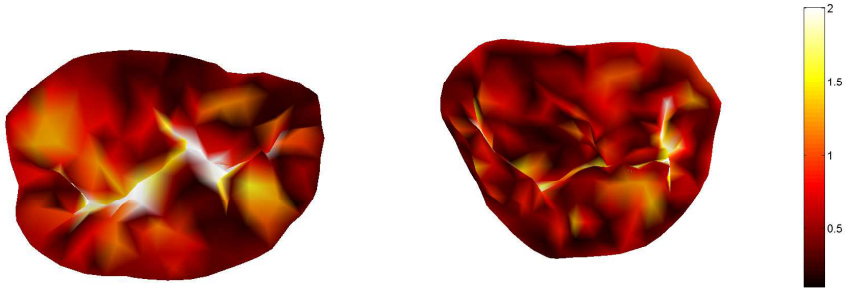

(a) Heart 1 (b) Heart 2

Figure 2.12: Two valve models are simulated to closure, and the error, computed as the distance from the simulated to imaged valve, is mapped using color. Both simulations produce root-mean-square error of less than 0.7 mm with a maximum error of approximately 2 mm.

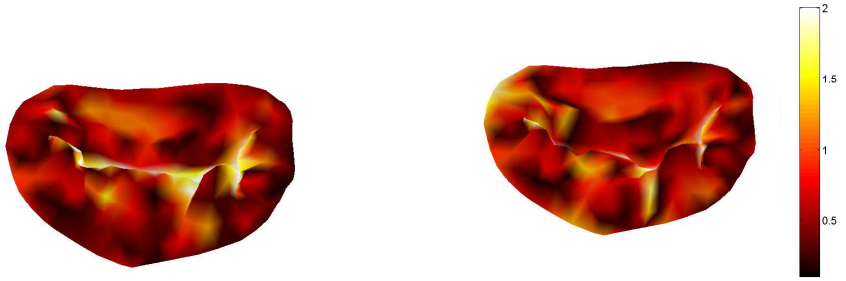

(a) Heart 3 - Before Shortening (b) Heart 3 - After Shortening

Figure 2.13: The predictive ability of the valve model is assessed by comparing the modeling error both before and after chordal shortening. The model is able to accurately predict changes in closed valve shape with only small increases in root-mean-square and maximum error.

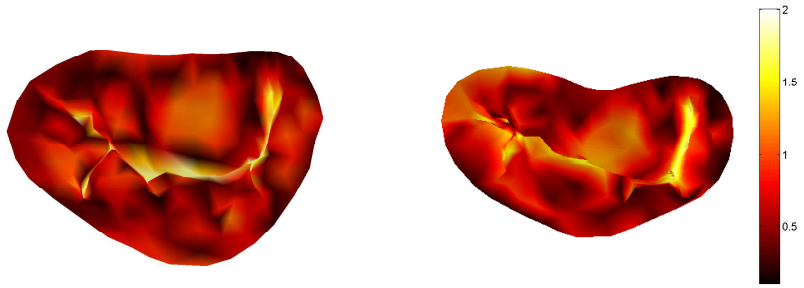

(a) Heart 4 - Before Annuloplasty

(b) Heart 4 - After Annuloplasty

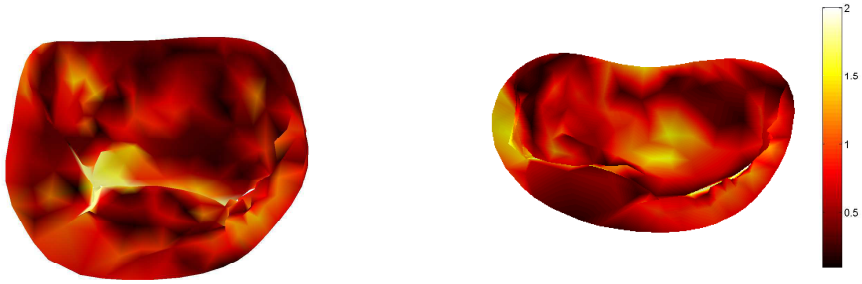

(c) Heart 5 - Before Annuloplasty

(d) Heart 5 - After Annuloplasty

Figure 2.14: Mitral annuloplasty is accurately simulated using the mass-spring model. Raw error values are smaller than those found in previously simulated valves due to the smaller size of the hearts used. Increased error is found along regions of the annulus due to the deformation of the incomplete ring.

2.4 Discussion

The goal of this work was to facilitate the planning of mitral valve repair. Therefore, usability and clinical relevance were of the utmost concern. By consulting cardiac surgeons possessing greater than 50 years combined experience, the system provides features that surgeons desire packaged in an intuitive, easy-to-use form.

2.4.1 System Design

While fast, visually rendered simulation by itself is an improvement over current methods of planning for valve repair, the inclusion of a haptic device makes the process easier, more intuitive, and more informative. The 3D input device facilitates navigation of the valve's complex 3D geometry. Additionally, the inclusion of force feedback allows the cardiac surgeon to apply their existing skillset to the virtual environment and augment

ID	# Tri.	# Vert.	AP (mm)	AL-PM (mm)	E_{RMS} (mm)	E_{max} (mm)
1	621	406	28.1	37.7	0.69	2.3
2	655	414	28.4	36.2	0.63	1.9
3	624	425	25.9	41.3	0.73	2.1
$3_{short.}$	624	425	26.3	40.1	0.82	2.4
4	611	366	18.4	27.1	0.58	1.6
$4_{ann.}$	611	366	14.2	21.7	0.68	1.9
5	736	442	18.3	21.4	0.56	1.7
$5_{ann.}$	736	442	12.8	19.6	0.72	1.7

Table 2.2: The results of the validation study are summarized in the table above. In addition to the RMS and maximum error, the triangle and vertex count of the simulated mesh as well as the anterior-posterior and anterolateral-posteromedial dimensions of the pressurized valve are provided for reference.

it with data and investigative techniques that would not be available intraoperatively. By emphasizing ease of use, surgeons are readily able to use this system after only minimal training, an important factor given their busy workload and desire to simplify, rather than further complicate, the procedure [112].

Such gains in usability are dependent upon a fast simulation, both the total simulation time as well as the update rate. While the former is certainly required for clinical viability, high-quality haptic feedback also rests upon a 1 kHz model update to obviate the need for haptic filtering, a technique which is commonly used in simulations that cannot achieve haptic rates. By smoothing the forces applied to the user, haptic filtering results in a phase delay, which although often imperceptible in soft tissue simulation, can be problematic in areas of stiffness. Given the chordae readily resist elongation at physiological loads, and the leaflets, when pulled, quickly enter their stiff, post-transitional region, a phase delay would be dangerous as it could quickly lead to model instability. With the surgeons lacking the technical expertise to understand the source of the instability, the system would become clinically unusable and would thus face the same issues confronting the more complex finite element models. However, by simulating at above haptic rates, these difficulties are avoided, and quality force feedback can be provided.

This need for a fast simulation informed much of the model design. The application of a static load to induce valve closure is one such instance. While computing fluid-structure interactions with a time-varying load would produce more physiologically accurate results, especially during valve closure, the computational cost is too great in a clinical setting and even more infeasible for an interactive simulation. Therefore, static loading is used as a proxy. Although not physiological and unable to predict valve shape during closure, such an approximation is still clinically relevant. Since peak systolic load is used, the conditions simulated represent the greatest mechanical load facing the valve and thus present

the greatest potential for regurgitation in the closed valve state. A valve preventing regurgitation under this load will likely prevent regurgitation in-vivo. Additionally, since the intraoperative "saline test" provides a similar approximation to that provided in this work, the same information is acquired prior to the procedure allowing for a more well-informed preoperative plan and potentially shorter operation times, thereby benefiting the patient.

However, static loading by itself is insufficient to achieve a fast, interactive simulation. Previously, many others have used a similar loading scheme coupled with a finite-element model but are unable to report interactive rates [122]. While finite-element models are the de factor standard with regard to simulation accuracy, they are also much more computationally expensive than their mass-spring approximations and tend to be much less stable, often requiring significantly smaller time steps. This combination of increased computational cost and decreased model stability motivated the implementation of an alternate tissue model. With the leaflets behaving much like an anisotropic cloth, inspiration was drawn from cloth simulation in the videogame community. Although they have recently shifted from mass-spring models to position-based dynamics for their ability to readily handle stiffness [88], such these new models are tuned for visual plausibility, not physical accuracy, making their application in this context infeasible. Thus, a mass-spring model combined with the physically realistic spring stiffnesses was used as it provided both speed and physical accuracy required. Furthermore, because the stiffnesses are computed offline, there is no performance cost for incorporating anisotropy, allowing arbitrary fiber patterns to be superimposed upon the leaflets.

Traditionally, the internal forces generated by these stiff mass-spring membranes are integrated using implicit integration schemes, such as the implicit Euler method, which demonstrate improved stability and permit larger time steps than explicit methods [9]. In interactive environments however, the cost of iteratively solving the implicit equations is

often too great. Additionally, the interactivity requirements prevent the use of variable time stepping as it would be disorienting to the user. This limits system performance as the computationally expensive integrator would be restricted to the time step that ensures stability across the entire simulation. With large impulses from user interaction, this could potentially be quite small and result in long simulation times. As a result, after much testing, a symplectic Euler integrator was chosen as it provided the best combination of speed and stability.

2.4.2 System Performance

Even with these algorithmic and modeling optimizations, achieving haptic rates is a challenge as the cost of computing each time step increases with mesh density, and unfiltered microCT images are of extremely high resolution. While the need for downsampling was clear, the precise amount was not. Therefore, the performance tradeoffs associated with mesh resolution were investigated. The minimum resolution was set to be roughly 650 faces as this is the coarsest resolution at which accuracy of mass-spring mitral valve simulations is preserved [50]. Below this level, modeling error increases due to quantization error and artificial bending stiffness induced by the planar nature of a triangular face, a source of error that is readily avoidable by subdividing a given triangle into smaller faces. Such stiffness can impede the natural folding of the leaflets observed in the loaded state, and therefore achieving the highest resolution feasible without adversely affecting system interactivity is of great importance.

As Figure 2.11 indicates, collision detection was the dominant factor limiting the simulation's update rate. Computing and resolving self-collisions is an inherently expensive task for cloth-like simulations, often requiring up to 90% of total simulation time [40]. Worsening the computational burden are the sharp folds that occur naturally in leaflet

tissue, leading to potential collisions between neighboring faces. While this can be partially mitigated by examining local curvature [121], collisions between neighboring faces remain feasible in areas of high curvature and must be considered. As a result, despite efforts to optimize the collision detection algorithms by maximizing cache coherency, collision detection still consumes approximately 85% of total computation with a 1:2 ratio between broadphase culling and collision resolution, highlighting the cost of large scale collision resolution.

The performance of the other components of the modeling unit highlight both the simplicity of the algorithms as well as the short time scale at which an individual update executes. With its inherent data parallelism, the symplectic Euler integrator, the fastest of the modeling units, is able to leverage the the SIMD instructions of the CPU, resulting in performance that scales extremely well with mesh resolution ($\frac{1}{2}\,\mu$s per 100 vertices). Even when compared to the next fastest unit, pressurization, which consists of the scaling and scattering of a face normal, the integrator is more than an order of magnitude faster. At these short time scales, the indirection associated with the scatter and non-contiguous memory access is costly. Of similar computational complexity yet 50% greater cost than the pressurization unit is the tissue deformation unit. A sizeable percentage of this performance decrease can be attributed to branching (both branch misprediction and inhibited code optimization) as half of the edges lie within 5% of the critical strain. With the simulation updating at over 3 kHz using the coarsest mesh, more than fifty times the rate of a typical videogame, the relative importance of hardware-level concerns highlight how this faster scale of computation brings a different series of challenges.

2.4.3 System Accuracy

While the model simplifications performed drew inspiration from the videogame community, the accuracy requirements differed greatly. In videogames, visual plausibility, not physical accuracy, is the standard developers strive to achieve, whereas in the context of surgical planning, physical accuracy must be maintained in order to provide meaningful information to the user. Therefore, after deviating from finite element models in lieu of these computationally simpler alternatives, validating the simulated model using observed physical data is essential to ensure the loss of accuracy is sufficiently small.

As the validation data indicates, the largest error lies along the leaflets' line of coaptation. This result, a function of mesh resolution and the method in which error is computed, is greater than the true modeling error and instead provides an upper bound on the greatest observable error. When imaging the pressurized valve, distinguishing between leaflets along the coaptation surface is infeasible because of the lack of spacing between them. As a result, to eliminate the possibility of registering the simulated anterior leaflet to the imaged posterior leaflet (or vice versa) and thereby underestimating our true modeling error, only the exposed atrial surface of the leaflets is considered in the error computation. The artificial bending stiffness, induced by the resolution of the mesh, exposes the coaptation surface where the imaged counterpart has been cropped and thus where the computed error is artificially high.

The largest errors found above the surface of coaptation tend to be located at the insertion sites of secondary chordae, which are designed to relieve leaflet tension in the pressurized state. These insertions into the ventricular surface of the leaflet splay to minimize the stress applied. As a result, not only does our point-insertion model lack this force distribution, it also becomes challenging to determine the precise length a chorda attached to the infinitely thin atrial leaflet surface model would possess. If desired, these

errors could be minimized using an inverse modeling procedure.

An additional source of error is the change in annular geometry, both after chordal shortening and a ring annuloplasty. Although the annulus is modeled as fixed due to its fibrous nature, the high annular stresses induced via the severe chordal shortening, stresses that are unopposed due to lack of annular contraction, result in an unmodeled change in behavior. In a beating heart, such changes would almost certainly have a lesser impact. Increased errors post-annuloplasty were also caused by unmodeled annular deformation. Because the rings were incomplete, narrow in cross-section, and constructed of plastic, they possessed an undesirable degree of flexibility, which could be bent when implanted and thus reduced accuracy along the annulus. In practice, the rigid rings that this work modeled typically possess a stiff titanium core, eliminating such issues.

While ideally this validation would have been performed in-vivo on human subjects, acquiring the necessary data would be challenging. Key to simulation accuracy is the structure of the chordae tendineae, which currently cannot be segmented using ultrasound-based methods. This often leads to unvalidated models or studies in which geometric modeling error from a generic chordal structure is confounded with mechanical modeling error, thus making it difficult to assess the accuracy of the physical model. Recently, Wang and Sun demonstrated the feasibility of using multi-slice cardiac CT to generate images of sufficient quality for full valve segmentation and modeling [126]. However, even when solely considering images of unmodified valves from an expansive patient database, they are only able to present a single segmented valve, highlighting the challenges of locating images of sufficient quality for segmentation. Validating repair techniques exacerbates this burden as both high quality pre- and post-operative images must be available. Additionally, since the modeler has no control over the procedure and multiple repair techniques are often performed in a given repair, confounded error is nearly unavoidable. Therefore, microCT was

used in this work as it both ensured an accurate valve segmentation and provided greater experimental flexibility, best isolating the mechanical modeling error of the various techniques. In the future, microCT can readily be substituted with a more clinically appropriate imaging modality as the simulation is indifferent to the source of the geometric valve model.

Nevertheless, the use of an excised porcine model and microCT introduced additional complications. The annuloplasty ring was originally modeled after a complete, i.e. continuous, ring as opposed to the split-ring design seen in Figure 2.8. While also mimicking a clinically successful design, the complete ring led to leakage along the commissures due to the non-physiological displacement of the papillary tips in the distended left ventricle. This regurgitation made the acquisition of a consistent image infeasible necessitating the updated, successful ring design.

Additionally, while chordal operations and mitral annuloplasty were virtually implemented and validated, leaflet resection, a common technique in repairing degenerative mitral valve disease, was not. This is also a direct result of the animal model used. As described in [33], porcine models are a poor proxy for human degenerative valve disease. Lacking the excess leaflet tissue observed in this pathology, it is extremely difficult, if not impossible, to remove leaflet tissue while still maintaining a surface of coaptation, especially with displaced papillary muscles. While others have suggested a canine model due to the relative prevalence of degenerative disease in the species [92], the time required for the animal to develop such a pathology is on the order of years, making it costly and largely impractical in this setting.

The fast, interactive, validated valve simulation platform described in this chapter serves as an enabling technology. By accurately simulating valve closure more than an order of magnitude faster than previous models, this system facilitates more expedient, comprehensive analysis that was previously infeasible due to computational cost. While

this chapter has demonstrated its viability as a surgical planning tool, Chapters 3 and 4 describe its application towards medical education and the controlled comparison of operative techniques.

Chapter 3

Training Valve Repair Using Surgical Simulation

3.1 Background

While one method of overcoming less experienced surgeons' inability to predict closed valve shape is to provide them with a quantitative prediction (as described in Chapter 2), another possibility is to improve their education to obviate or lessen such insufficiencies. Intraoperative valve analysis, aided by the surgeon's past experience, forms the basis for these predictions and thus provides an area for targeted training. While the motor skills required to perform valve analysis are minimal, the proprioceptive and tactile cues that must be recognized are subtle, making the predictive task challenging. With the heart arrested and evacuated of blood such that the valve can be exposed and directly visualized, a nerve hook is used to pull the valvular segments towards the annulus to determine their mobility as well as identify lesions in the subvalvular apparatus. Using P1, the anterolateral segment of the posterior leaflet, as a reference point unless contraindicated, the segments are examined in a clockwise manner, providing a consistent framework that can be repeated

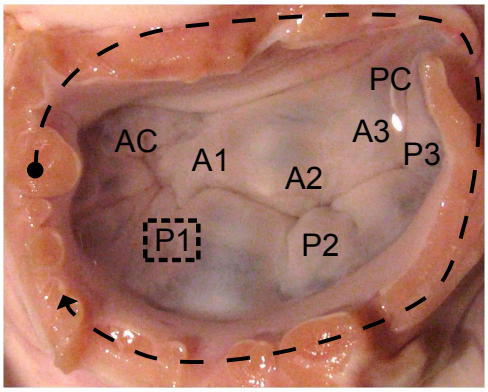

Figure 3.1: When performing valve analysis, P1 typically serves as a reference point as it is the segment least often affected by disease. The mobility of each segment is compared to that of the reference point in a deliberate manner, starting at the anterolateral commissure and proceeding in a clockwise manner.

case after case (Figure 3.1).

Traditionally, this technique, like most of medicine, is initially taught via non-interactive means such as readings and lectures followed by an apprenticeship model under the watchful eye of an attending surgeon, where the trainee is gradually given greater responsibility. Such instructional methodology limits the number of cases performed by the trainee, which is problematic as surgical volume is one of the largest predictors of a procedure's success [11]. Surgeons who have already completed their formal training but do not perform valve repair in considerable quantities are therefore also adversely affected, as continuing education credits are often satisfied by lectures and seminars. The inability to easily train in an interactive setting thereby decreases the quality of care for patients as simpler, but prognostically inferior, procedures are often performed instead [31].

While other medical specialties have adopted the use of simulation-based training to improve dexterous skills, decision-making, and team efficiency [25, 28, 29, 65, 76, 104], past efforts to improve surgeon training in valve repair have been more limited. Using plastic or porcine models, enhanced training for mitral valve repair has largely focused on *implementing* repair techniques rather than predicting closed valve shape and *formulat-*

ing an effective repair plan [59, 110], equally important tasks. Additionally, such efforts are expensive to scale, requiring a large investment in infrastructure, and would likely be challenging to deploy for a low-volume center [10]. Although virtual training would scale far more easily and at a lower cost, the slow speed and technical complexity of the prior generation of computer-based mitral valve models have prevented its adoption. However, the fast simulation techniques described in Chapter 2 eliminate these barriers, permitting real-time interaction with less technically advanced users.

In this chapter, the valve simulation platform detailed previously is used to instruct subjects on the execution of intraoperative valve analysis and improve predictive abilities. The subject is able to grasp chordal-leaflet attachment sites of a virtual model and feel a force response using the haptic device, thereby enabling valve analysis in the simulation environment. Leveraging this capability, the system is first used to highlight the differences in performance observed in users of differing skill levels, providing a metric upon which user skill can be assessed. Virtual instruction is then provided using the system, and improvements in subject performance are demonstrated. Finally, the effects of virtual training are assessed in an ex-vivo tissue model, establishing that the skills acquired transfer to real-world tasks.

3.2 Methods

3.2.1 Simulation Environment

The platform described in the previous chapter provides the ideal means to virtualize the valve analysis process. With the ability to grasp tissue using the haptic device, users can perform valve analysis on the virtual model and feel the force response (Figure 3.2). Further, with a 3 kHz update rate, far beyond what is necessary to convey stable

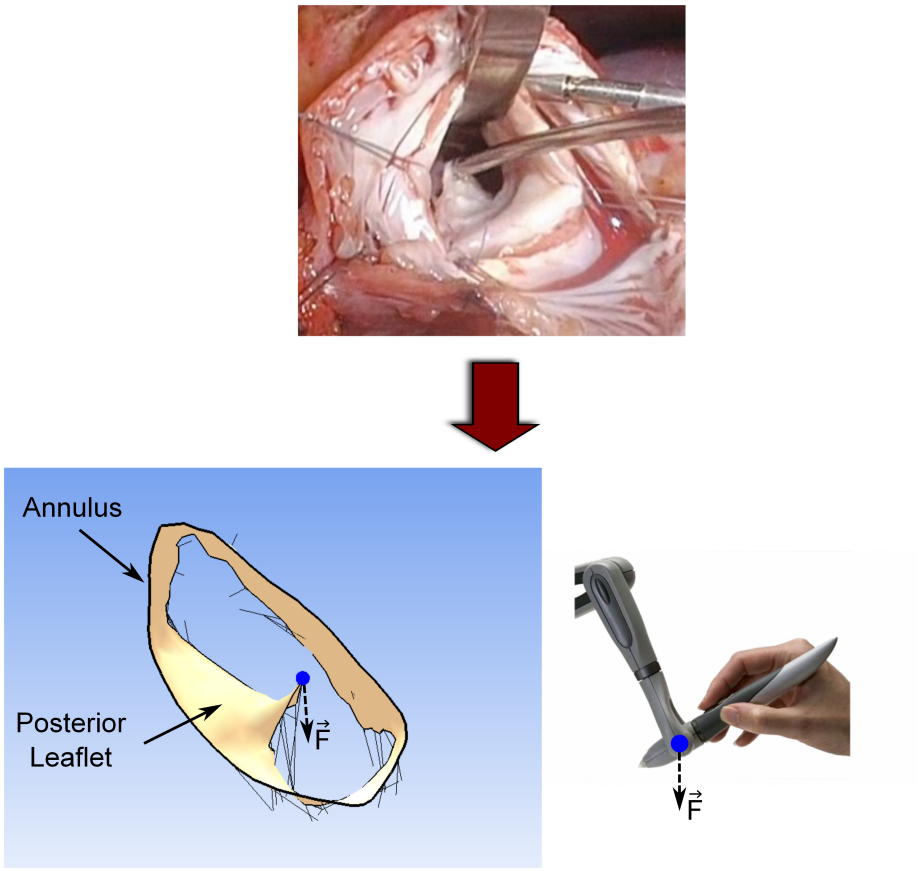

Figure 3.2: The valve simulation platform transfers the experience of intraoperative valve analysis into the virtual world. Using the haptic device, the user can perform virtual valve analysis, see the tissue response in real-time, and feel the forces exerted by the taut chordae in the virtual valve model. (Intraoperative image courtesy of Pedro del Nido, MD)

tactile feedback, the force applied to the user is limited only by the device itself, allowing the system to transmit the high stiffness taut chordae exert.

For meaningful analysis and instruction, realistic valve models are important. In the studies described in this chapter, virtual models, constructed via the process described in Chapter 2, are derived from microCT-imaged porcine valves, resulting in chordal geometry with the complex branching patterns observed in-vivo. While the valve modeling community often resorts to a simpler, generic chordal model when simulating valve closure [122], hiding this complexity from the user provides a virtual analysis experience that is less faithful to

its real-world counterpart. With the aim of assessing user ability and enhancing instruction, maximizing task realism is crucial to accurately measure and transfer skills.

3.2.2 Evaluative Protocol

Before using the system for instruction, discriminative measures of user skill must be developed and validated. Therefore, the system was used to evaluate the ability of users to predict closed valve shape from analysis of the open, flaccid valve. Subjects consisted of six third-year medical students, who have completed coursework in cardiac pathophysiology but have limited surgical experience, and three cardiac surgeons. It was hypothesized that the less skilled medical students would exhibit worse performance than the more skilled surgeons. Prior to testing, subjects were given unlimited time to familiarize themselves with the system.

Following an IRB approved protocol, examination took the form of ten four-alternative, forced-choice trials. For each trial, the subjects were first presented with visual-only renderings of four closed valves (Figure 3.3), which served as potential answers. All four renderings were generated from physical imaging of an unpresurized porcine valve. "Pathological" modifications of the valve in the form of changes in chord length and papillary position were made to produce differences in closed valve shape that were visually indetectable in the flaccid, open valve to be analyzed. The virtual valves were simulated to closure, and their final shapes were presented to the user. To best isolate the subject's ability to predict closed valve shape, lesions typically accompanying these etiologies such as changes in leaflet and annular geometry were omitted to prevent surgeons from applying pathology-specific knowledge. The focus was solely on haptically determining the effects of chordal length on closed valve shape. As a result, subjects were permitted to rotate and view from all angles the potential answer choices, i.e. closed valves renderings, to maximize

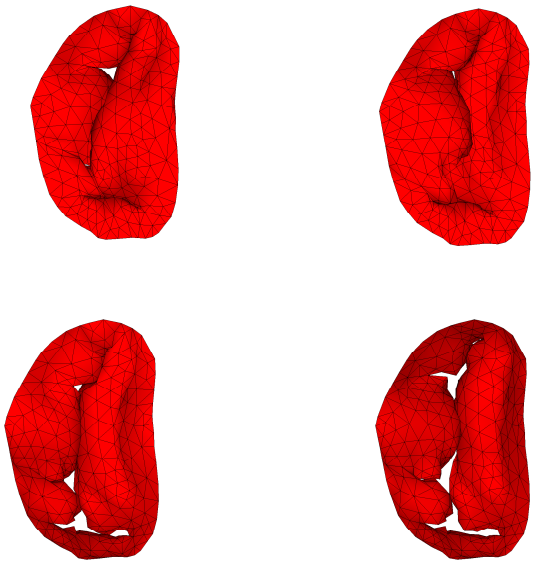

Figure 3.3: The subjects were provided with four choices for each trial. The valves are identical with the exception of changes to chordal lengths and papillary positions.

their understanding of their possible choices.

After examining the four closed valve choices, an atrial view of a single unpressurized valve was presented to the subject using the interactive valve simulation platform. They were allotted a maximum of three minutes to inspect the valve by pulling on various chordal attachment sites to determine areas of excessive or restricted leaflet mobility (Figure 3.2). However, subjects were not permitted to change the view of the valve, to best reproduce the limited visibility that is found intraoperatively.

Upon completion of virtual valve analysis, indicated either by the subject or the expiration of the three minutes allotted, the four valve choices were again presented. Subjects were given unlimited time to select the valve that he or she believed to correspond to the open valve analyzed. Answers, as well as time elapsed during valve analysis, were recorded. This process was repeated for a total of ten trials per subject. Trial order was randomized to minimize the effects of learning. In addition, only six unique trials were

presented, with four of the trials repeated to test for uncontrolled learning.

3.2.3 Instructional Protocol - Virtual Model

Upon validating the system's ability to discriminate user skill, it was posited that the system could be used for enhanced instruction. Since the evaluative protocol indicated that medical students performed no better than random chance when predicting closed valve shape (see Section 3.3.1), less experienced subjects would be expected to perform at a similar level and no worse. Thus, due to their increased availability, 12 graduate students familiar with valve anatomy and physiology were studied instead.

Similar to the evaluative protocol, each subject was presented with visual-only renderings of four closed valves, was asked to perform virtual valve analysis for a maximum of three minutes, and was then instructed to select the closed valve corresponding to the open valve analyzed. Three sets of five trials were given to each subject.

Prior to execution of the study, subjects were again given unlimited time to familiarize themselves with the system. They were then presented with a set of five baseline trials without formal instruction, just as in the evaluative protocol (Section 3.2.2). After the first set of trials, subjects were then provided with one of two forms of instruction regarding valve analysis: didactic instruction from *Carpentier's Reconstructive Valve Surgery* [21], a leading surgical text, or simulation-based training, which attempted to convert the written word into interactive tasks. Subjects were shown and then asked to perform proper valve analysis technique, were asked to feel the difference in the chordal support of a tethered and prolapsing leaflet, and were shown highlighted exemplars of valve dysfunction to assist in their identification (Figure 3.4).

Following initial instruction, a second set of five trials was conducted by each subject, after which the alternate form of instruction was provided. This was followed by

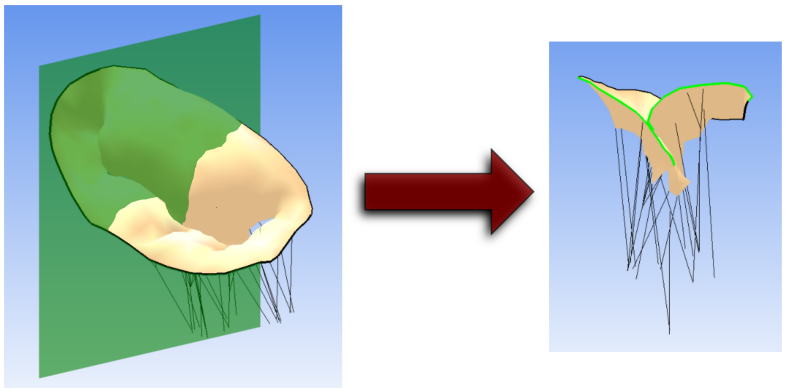

Figure 3.4: Simulation-based instruction included a tactile examination of prolapsing and tethered leaflet segments. It also visually highlighted and emphasized these segments by introducing an adjustable cut-plane, allowing for improved visualization of valve dysfunction.

a final set of five trials. Order of instruction as well as order of the trials within each set were randomized to best control for learning of the system rather than learning of the task. Again, correct answers and time elapsed during valve analysis were both recorded.

3.2.4 Instructional Protocol - Porcine Model

Finally, to ensure the skills learned and assessed in the previous protocol were not specific to the simulator and instead translated to real-world skills, a third study was conducted to evaluate subjects' predictive abilities on six explanted adult porcine hearts. In each heart, the mitral valve was surgically modified by a trained cardiac surgeon to introduce tethering, prolapse, and to preserve normal leaflet motion at various points around the leaflets (Figure 3.5(a)). The hearts were modified in such a manner that changes to the chordal apparatus and papillary muscles were visually indistuinguishable and therefore required the subjects to rely on tactile sensations. Additionally, the left atria were excised to increase valve accessibility for the non-expert subject population, and the hearts were refridgerated and stored in a phosphate-buffered saline solution containing antibacterials and antifungals to prolong tissue viability.

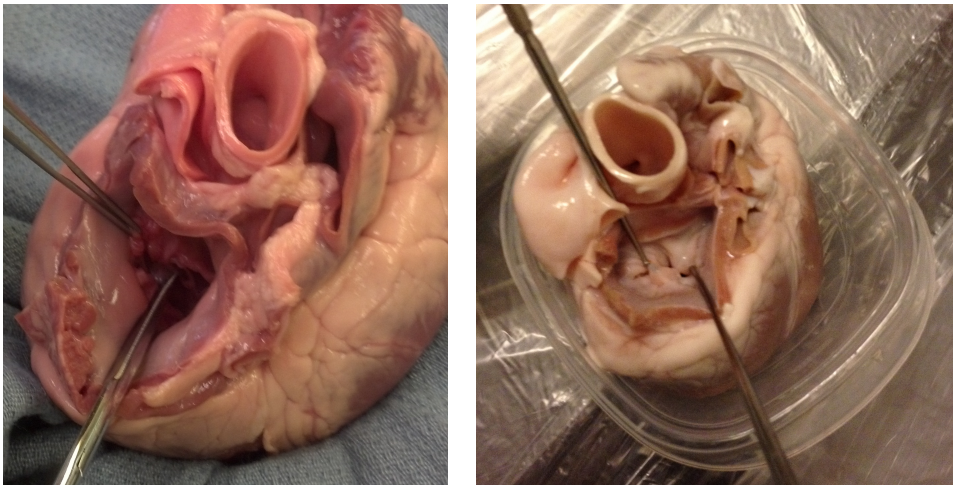

(a) (b)

Figure 3.5: (a) The porcine hearts were first modified by a trained cardiac surgeon to induce visually indetectable tethering and prolapse around the valve. In this instance, a chorda is excised from the anterior leaflet. (b) The subjects were then asked to identify the mobility of the 8 leaflet segments. Two nerve hooks, the same tools used in clinical practice, were used to manipulate the leaflet tissue.

Subjects, consisting of 17 medical students with coursework in cardiac pathophysiology, were randomly partitioned into two groups. Given the efficacy of didactic instruction in teaching proper valve analysis technique (see Section 3.3.2), both groups were provided with initial textbook training [21]. Using the same surgical tools used for intraoperative valve analysis, the subjects were asked to evaluate leaflet mobility (i.e. if the leaflet segment was tethered, prolapsing, or exhibited normal motion) at all eight segments of the mitral leaflets (Figure 3.5(b)). Subject responses, as well as time to complete valve analysis, were recorded for three different hearts.

After the first three trials, one group was provided additional simulation-based training while the other was not. Training was similar to that in previous studies. Subjects were first introduced to the simulator and then provided with both visual and tactile examples of normal leaflet motion, prolapse, and tethering. Differences were highlighted with

amplified forces, a translucent annular plane, and additionally the inclusion of orthogonal cut-planes. Subjects were then provided with a training case, which consisted of two virtual valve models - one of which exhibited tethering at the A2 region of the anterior leaflet while the other exhibited prolapse to reinforce the concepts.

Both groups were then presented with the remaining three hearts to evaluate. These trials were conducted in an identical manner to the previous set. The order of the six hearts presented to the subjects throughout the entirety of the study was randomized to control for individual difficulty.

3.3 Results

3.3.1 Evaluative Protocol

The time to complete valve analysis as well as predictive accuracy varied between the two subject populations (Figure 3.6). The average rate of correct responses among medical students and surgeons was 25% and 63% respectively ($p = 0.01$). In addition, while surgeons always used all of the allotted time (180 seconds), medical students used far less to complete the task ($p < 0.001$), averaging only 90 seconds to complete each trial. This decrease in time to completion was trial-dependent, with later trials requiring less time to complete.

3.3.2 Instructional Protocol - Virtual Model

Of the 12 subjects recruited, seven first received traditional, book-based instruction with the rest initially given interactive, simulation-based instruction. While first providing didactic instruction was shown to increase time to complete valve analysis in comparison to the control trials ($p = 0.01$), it did not result in improved predictive abilities. However, after receiving subsequent simulation-based training, subjects demonstrated improved predictive

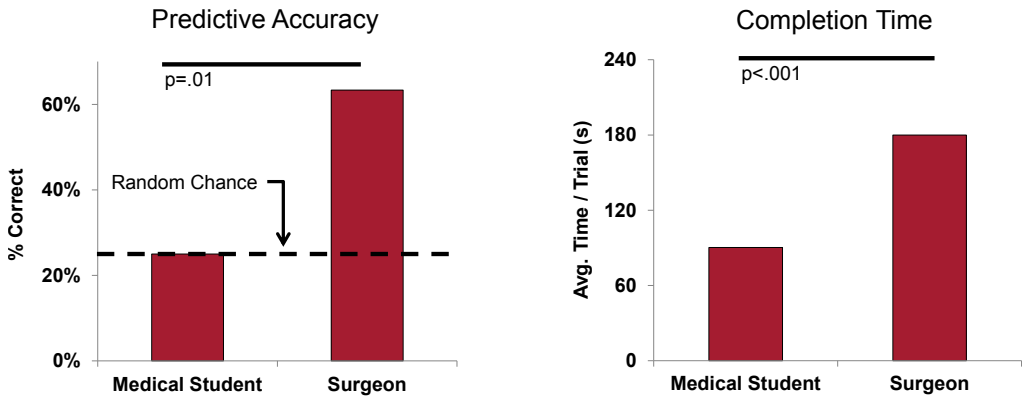

Figure 3.6: Medical students and surgeons exhibit notably different performance in the prediction task. Medical students demonstrate a predictive success rate of 25%, equivalent to random chance, while surgeons fare far better. However, surgeons spent more time on the task.

abilities ($p = 0.04$) with no increase in valve analysis time (Figures 3.7(a) and 3.7(b)). Conversely, those receiving simulation-based training first showed both increases in the time required for valve analysis ($p = 0.001$) and the rate of successful prediction (p = 0.04). Subsequent didactic instruction produced no improvement in valve analysis time nor prediction rates (Figures 3.7(c) and 3.7(d)).

3.3.3 Instructional Protocol - Porcine Model

Of the 17 subjects who participated in the study, nine received simulation-based training. Initially, both groups of subjects successfully predicted leaflet segment mobility at levels identical to random chance, i.e. 33% given the three choices for each segment. Without subsequent simulation-based training rates of successful prediction remained the same (Figure 3.3.3), whereas those receiving simulation-based training showed absolute improvements of 11% ($p = 0.02$). Independent of additional training were the decreases in time to complete valve analysis. While variable between subjects, both populations demonstrated faster valve analysis times with increased experience (Figure 3.3.3).

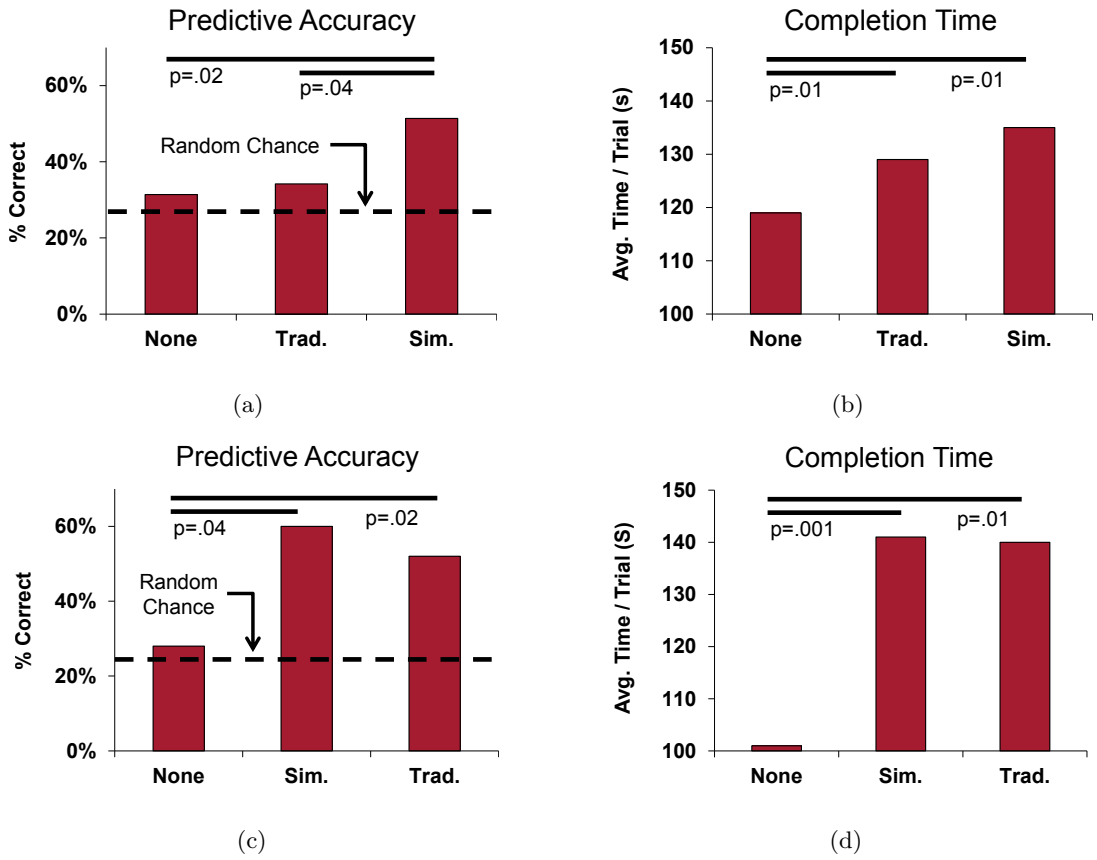

Figure 3.7: The training of subjects has a clear effect on their performance of valve analysis and insights gained from it. Plots (a) and (b) highlight the outcomes of training where initial instruction is provided by a leading surgical textbook [21]. Conversely, plots (c) and (d) show the effect of training where simulation-based instruction is provided first. While both forms of instruction result in increases in trial completion time, a proxy for analysis technique, only simulation-based training demonstrates improvements in predictive ability.

3.4 Discussion

The performance of the third-year medical students in the evaluative task highlights both the difficulty of valve analysis and the importance of training. Even after three years of post-graduate medical education (including time in anatomy laboratories and coursework in cardiac pathophysiology), the students performed no better than random chance in predicting closed valve shape. Their performance was so poor that, despite a limited sample size, surgeons exhibited improved predictive abilities at a statistically signifi-

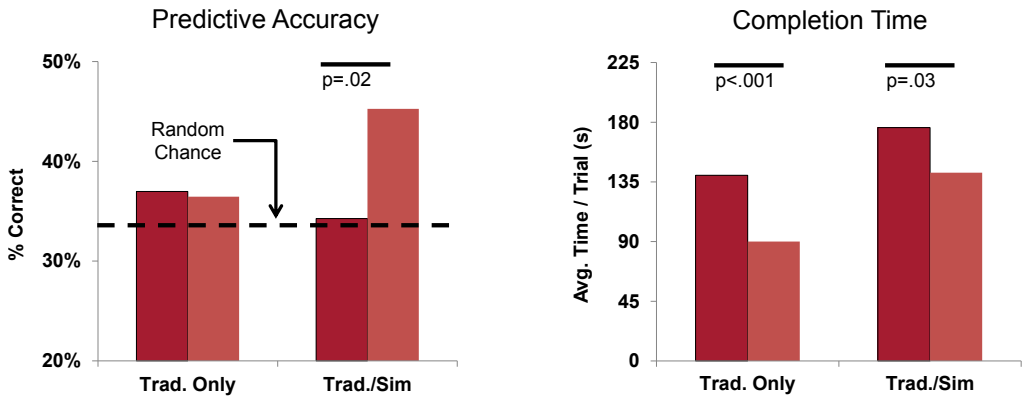

Figure 3.8: The benefits of simulation-based training on virtual models also translate to improved predictive skills with tissue models. Subject performance in the first set of three trials is shown in dark red, whereas the second set of trials is shown in light red. Subjects receiving simulation-based training showed an 11% increase in predictive rates, while the control group showed no discernible improvement. However, time to completion did decrease with additional experience as subjects became more familiar with the forces required to perform valve analysis.

cant level. While the difference can partially be attributed to a less thorough understanding of valve physiology, the contrasting manners in which the two populations perform valve analysis is easily discernible.

The cardiac surgeons were significantly more systematic in their analysis of the valve. The process was highly repeatable and consistent, always starting at the same location and proceeding around the valve in a predictable manner. Comparing different areas to the initially examined region, deviations from the norm only occurred when the surgeon felt compelled to examine the original region again or when areas were re-examined after analyzing the entire valve. While providing a consistent baseline for comparison, it was also more time-consuming explaining their increased valve analysis time. Conversely, the approach taken by the medical students was more haphazard, examining all areas of the valve but in a random and inconsistent ordering. This permitted them to finish in less time but also resulted in less information acquired. Therefore, it was not suprising to find greater predictive rates for cardiac surgeons, which occurred despite a lack of a preoperative

diagnosis or visible lesions that typically accompany these pathologies.

The poor performance of the medical students emphasized the need for training specific to valve analysis. While currently initial training consists of readings and lectures, the inefficiency of training an interactive task via passive learning techniques is obvious and results in unskilled trainees entering the operating room for hands-on instruction. If trainees were more skilled upon beginning apprenticeship, they could be given greater responsibility initially, leading to shorter training periods and/or greater time allotted to more advanced topics such as valve repair. Given the lengthy post-medical school education required for cardiac surgeons, the potential for a more efficient course of instruction is attractive.

Therefore, an active learning regimen was investigated with the aim of improving educational efficiency and efficacy. Rather than simply being told to analyze leaflet mobility, trainees were able to *feel* leaflet mobility, translating the written word into a combination of perceptual cues, tactile feedback, and motor skills. By assessing the subjects virtually, the trials were freed from the difficulties associated with the use of tissue specimens.

The results of the study were conclusive. While either instructional methodology was able to improve analysis technique, as observed qualitatively and measured quantitatively via time to completion, only simulation-based training resulted in improved predictive ability. However, even though the study controlled for learning due to repetition, subjects were evaluated and trained on the same system. As a result, any biases or inaccuracies inherent to the system and learned by the user would be indetectable, necessitating a final study to ensure the skills learned were applicable to a tissue model.

Again highlighting the difficulty of the task, the medical students in the study initially performed identically to random chance. In addition, those not receiving subsequent simulation-based training continued to operate at this level, thereby demonstrating that repetition alone would be insufficient to improve the subjects' skill level. Conversely, a

single session of simulation-based instruction resulted in an 11% increase in the subjects' rate of successful prediction. While they remained far less competent than a trained cardiac surgeon, the increase after only a single training session suggests that further interactive instruction would produce additional improvements.

When examining subject performance on a segment by segment basis, it was observed that the greatest improvement in predictive ability occurred at P1 ($p < 0.005$). This is notable as P1 typically serves as the reference point to which all other segments are compared, except when it exhibits abnormal mobility [21]. This improved recognition of proper P1 mobility not only demonstrates a more advanced understanding of leaflet function as it required a cognizant rejection of the reference point, it also likely assisted in lessening misclassification elsewhere in the valve. Unfortunately, unlike other leaflet segments, commissural assessment experienced no such gains in prediction accuracy. Given the commissures serve as a connection between the anterior and posterior leaflets, they tend to be far less mobile than other leaflet segments. With a limited time for instruction and thus no simulation-based instruction targeting the commissures, the subjects never learned to recognize this difference.

While repetition alone did not result in improved predictive abilities, it did provide increased comfort with the delicate leaflet tissue as indicated by the faster trial times in both groups. Initially, subjects were clearly hesitant and proceeded with caution, moving slowly in an attempt to avoid damaging the valve. Given the tissue's thin structure, this is unsurprising. By the end of the study however, subjects were significantly more efficient, making faster and more direct motions. Therefore, while repetition alone was unable to impart the ability to recognize the subtle differences in leaflet mobility, it did result in subjects gaining an understanding of the forces required to safely manipulate the valve tissue.

These findings were also reflected qualitatively in post-study discussions with the subjects. Despite the textbook providing clear instructions on performing valve analysis, subjects often expressed frustration at the difficulty of the task. Those receiving simulation-based training, while also acknowledging these difficulties, described having a better sense of the wrong answer and were often able to successfully eliminate one of the three choices, especially in cases of abnormal leaflet motion where the "most wrong" answer could be excluded.

Nevertheless, the precise mechanisms by which simulation-based training improves users' diagnostic ability have yet to be determined. When compared to the experimental training methodology provided to users, the didactic instruction was likely less effective in conveying complex three-dimensional spatial relationships, was non-interactive, and failed to provide haptic feedback. These confounding factors make it impossible to identify their relative importance in enhancing subject performance from the data collected. However, prior to widespread adoption, such a study should be conducted to optimize the system both for cost and efficiency of instruction.

It should be emphasized that, regardless of the adjustments made, this simulation platform is designed to complement, rather than replace, the hands-on training provided by the apprenticeship model. Despite the advantages of a simpler surgical approach and superior visualization of the valve than is afforded in surgery, subjects' performance after receiving simulation-based training would be deemed grossly inadequate for a trained cardiac surgeon. While further simulation-based training may lessen this deficit, it is unlikely to eliminate it entirely. Individualized instruction from a skilled attending surgeon, albeit expensive, is invaluable and irreplaceable. In addition to the individualized and specialized instruction the apprenticeship model provides, it also provides the opportunity to operate on living patients. Inevitably, computer-based simulation or explanted porcine models re-

sult in a valve analysis experience that is not entirely faithful to the conditions found in the operating room. This is impossible to eliminate entirely. Even if fresh cardiac specimens were safely accessible, the volume, limited viability, and therefore cost required would be infeasible for most centers. Simulation-based training avoids these issues by permitting indefinite model resuse at a negligible cost.

Therefore, while simulation-based training introduces modeling error and does not provide the expert guidance afforded by an attending surgeon, it is highly cost-effective and exceeds the educational value provided by traditional pre-apprenticeship pedagogy. By establishing an intermediate training regimen or using simulation-based training in lieu of readings and lectures, the training of cardiac surgeons would likely be improved.

Chapter 4

Evaluating the Robustness of Valve Repair for Ischemic Mitral Regurgitation

4.1 Background

While the previous two chapters detail methodologies for improving the performance of non-expert surgeons, the treatment of ischemic mitral regurgitation has proven challenging for even the most talented clinicians. As described in Chapter 1, ischemic mitral regurgitation is valve dysfunction resulting from coronary artery disease, in particular, myocardial infarction. After infarction, reduced ventricular contractility adversely alters the geometric relation between the valve and its subvalvular apparatus. The papillaries are displaced away from the valve, restricting leaflet motion (Figure 1.6). Additionally, non-uniform annular dilatation is often present, largely in the anteroposterior dimension with a lesser degree of annular flattening (Figure 4.1). The less mobile leaflets are therefore

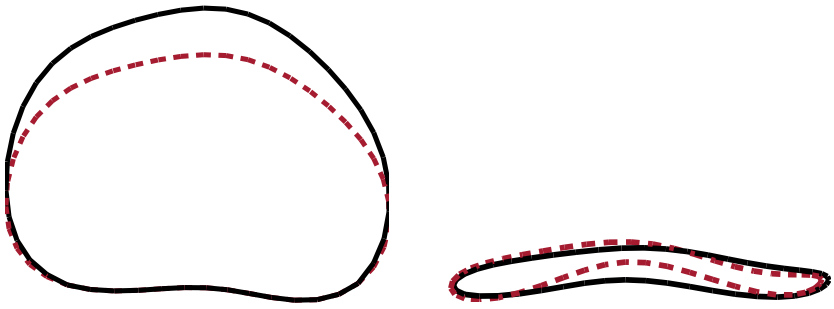

(a) Atrial View (b) Profile View

Figure 4.1: In a healthy mitral valve (dashed red), the anterolateral-posteromedial (ALPM) dimension of the annulus is roughly 33% larger than the anteroposterior (AP) dimension [21]. Additionally, the height of the three-dimensional annular profile is approximately 20% of the anterolateral-posteromedial dimension. However, the annulus of a pathological valve exhibiting ischemic mitral regurgitation (solid black) tends to dilate in the anteroposterior dimension and flatten.

unable to form a complete surface of coaptation, resulting in regurgitation. These effects of reduced ventricular function have been extensively documented in humans, as well as in porcine and ovine models [39, 42, 56, 90, 113, 114, 127].

The preferred method of treatment is valve repair. Currently, the majority of surgeons who repair these valves use a rigid annuloplasty ring to restore the physiological annular shape. To compensate for the tethering effects of the displaced papillaries, the ring is often undersized, facilitating valve closure [37]. While this technique largely eliminates regurgitation intraoperatively, post-operative recurrence is common and is attributed to continued ventricular remodeling, especially in those with a large left ventricular end diastolic diameter (LVEDD) [48, 51, 109]. As a result, survival for these patients is poor, with a 5-year mortality rate of greater than 50%, suggesting the need for an improved standard of care [46].

Motivated by the patients' poor long-term prognosis, clinicians have introduced complementary repair techniques to address leaflet tethering. Borger et al have proposed the excision of tethering secondary chordae [13]. While this technique has been demon-

strated to improve leaflet mobility, long-term stability remains uncertain as the importance of the secondary chordae in preserving left ventricular function is well established [26,27,97]. Messas et al attempted to address these concerns in [85] using an ovine model, but followed the sheep post-operatively for only eight weeks and did not perform a complementary annuloplasty as would be expected in a human patient.

However, cutting chordae, much like undersizing an annuloplasty ring, is symptomatic treatment and does not address the underlying cause of leaflet tethering, papillary displacement. Therefore, others have investigated the effect of repositioning the papillary muscles directly. Although possible through alternative means [52, 81], one method of approximation anchors the papillary head to the mitral annulus via a suture (Figure 4.2) [64, 75]. A recent retrospective study, comparing restrictive annuloplasty to a properly sized annuloplasty complemented by this technique, has shown papillary approximation results in fewer five-year post-operative cardiac-related events and a decreased recurrence of regurgitation [32]. Currently, this technique is performed by only a few select surgeons worldwide. To better predict its efficacy and robustness in a larger patient population and in the hands of potentially lesser skilled surgeons, sensitivity to a wide range of papillary displacements and surgical variation must be assessed.

Ex-vivo and in-silico models therefore provide an attractive means of evaluating these techniques in a safe, controlled environment. With their largely physiologic tissue properties, valves suffering from ischemic mitral regurgitation have been studied in depth using such models. In [79] and [124], the authors use a finite element model to compare the impact of various annular prostheses in restoring valve function. Similarly, Cochran and Kunzelman examined the effect of papillary displacement on valve function [23]. These models employ idealized valve geometry and only consider uniaxial papillary displacement, simplifying the three-dimensional displacements observed in-vivo [56, 114]. Wang and Sun

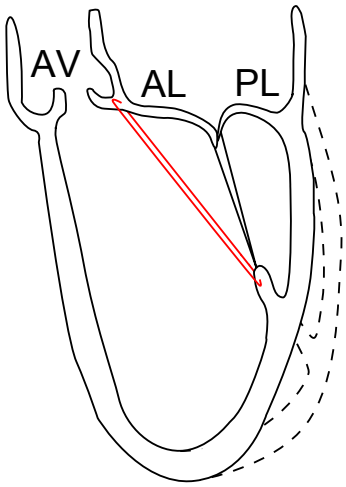

Figure 4.2: Papillary displacement techniques are growing in prominence to address the ventricular dilatation (dashed outline) associated with ischemic mitral regurgitation. In one form of papillary approximation, the papillary muscles are displaced by using suture (red curve) to anchor them to the mitral annulus.

improved upon these methods using patient-specific valve geometry, but again only considered uniaxial apical papillary displacement and also modeled annular dilatation in a uniform, non-physiological manner [125]. This one-dimensional assessment of papillary displacement, likely influenced by the heavy computational requirements of multi-dimensional analysis, potentially obscures the possibility of interactions between the axes of displacement, making an accurate investigation of procedural robustness infeasible.

Rather than use a computational model, Siefert et al placed excised ovine valves in a flow simulator to investigate the effects of uniform annular dilatation, annular flattening, and uniaxial papillary displacement [105]. However, due to the need for human intervention and challenges of maintaining tissue viability, testing was again performed uniaxially at a coarse resolution, and the coupling between annular deformation and papillary displacement was not considered. Yamauchi et al also adopted an ex-vivo approach when studying an alternate form of papillary approximation in the right ventricle of excised porcine hearts [130]. Much like in [105] though, this work was bound by the physical limitations of ex-vivo

experimentation.

Throughout these studies, both in simulation and ex-vivo, the fundamental hindrance to fine-grained, multi-dimensional analysis of robustness has been the cost of acquiring data. However, fast simuation eliminates the barriers to data acquisition, making previously intractable problems tractable. This chapter details application of the simulation methodology described in Chapter 2 to the analysis of ischemic mitral regurgitation. First, the coupled effects of annular dilatation, annular flattening, and papillary displacement are investigated, providing insights into the effects of disease progression. Then, a restrictive annuloplasty is performed, and the valve's sensitivity to continued ventricular remodeling is assessed. Finally, the efficacy of papillary approximation and its robustness to ventricular remodeling and surgical variation is examined.

4.2 Methods

4.2.1 Computation of Total Regurgitant Orifice Area

To assess the effects of annular remodeling, papillary displacement, and surgical treatment, a competent valve model, generated from an excised porcine heart as described in Chapter 2, was perturbed from its initial state using custom scripts written in Matlab (Mathworks, Natick, MA). Perturbed models were then simulated to closure using the previously developed simulation methodology. To facilitate batch processing of simulations and minimize the need for human intervention, the interactive platform was removed and simulations used a command-line interface.

The competency of the closed valves was assessed using a simple ray casting technique. From an atrial view, each valve was rendered black on a white background and saved as a binary image with a resolution of 800x600 pixels (Figure 4.3). Therefore, white

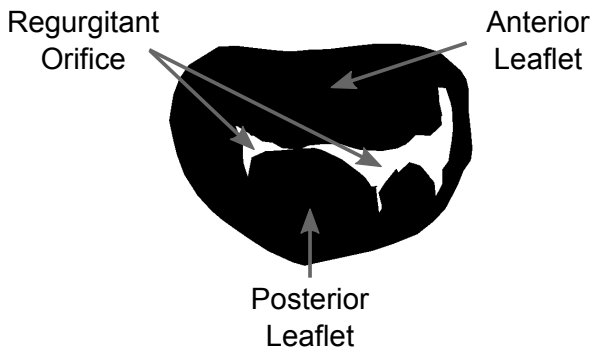

Figure 4.3: By rendering the closed valve from an atrial view, a connected component detection algorithm allows for the measurement of regurgitant orifice area. White regions within the rendered valve are regurgitant jets, which are scaled from pixels to mm^2 using the area bounded by the annulus and its known size.

regions within the mitral annulus signified regurgitant orifices. The area of these orifices, as measured in pixels, were individually computed using a connected component detection algorithm. The size of each pixel in square millimeters was then calculated using the annulus as a reference. The regurgitant orifices were first filled, and the area, in pixels, of the region bounded by the mitral annulus was determined. Next, using coordinate geometry and the projection of the annular vertices onto the annular plane (as determined via principal component analysis), the true projected annular area in square millimeters was computed (Equation 4.1). The ratio of these two values was then used to convert regurgitant orifice sizes from pixels to square millimeters (Equation 4.2). Finally, the orifice areas were summed to provide a total regurgitant orifice size.

$$A_{Ann,mm^2} = \frac{1}{2}\left(\begin{vmatrix} x_1 & x_2 \\ y_1 & y_2 \end{vmatrix} + \begin{vmatrix} x_2 & x_3 \\ y_2 & y_3 \end{vmatrix} + \ldots + \begin{vmatrix} x_N & x_1 \\ y_N & y_1 \end{vmatrix}\right) \tag{4.1}$$

$$A_{RO,mm^2} = A_{RO,px} \cdot \frac{A_{Ann,mm^2}}{A_{Ann,px}} \tag{4.2}$$

To minimize the effect of transient motion in a malcoapted valve, five simulations, each with small variations in simulation time, were executed for a given configuration, .

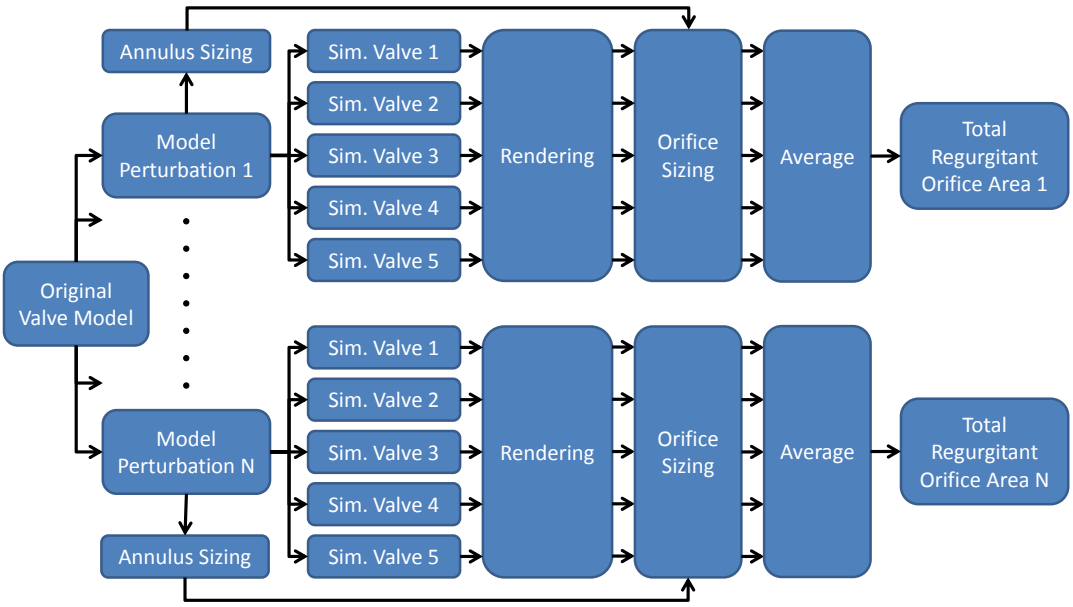

Figure 4.4: The workflow to quantify valve competency is a multi-step process. The valve model is first perturbed to generate the desired boundary conditions and then simulated to closure. The resultant closed valve is projected into a two-dimension image to detect regurgitant orifices. The image is then processed to determine the size of the individual orifices, which are then summed. This process is repeated five times with varying simulation times for each perturbed valve to minimize the effect of transients due to malcoaptation.

The results were then processed using the methods described above, and the resulting total regurgitant orifice areas were averaged to provide a robust estimate of valve coaptation. This pipeline is depicted in Figure 4.4.

4.2.2 Sensitivity to Perturbations in Valvular Geometry

With a workflow in place for the high-throughput simulation of valve closure and evaluation of regurgitant orifice size, the tools required for the in-depth analysis of restrictive annuloplasty and papillary approximation were present. However, to best predict and interpret the robustness of a given surgical technique, a more thorough understanding of the imapct of annular dilatation and papillary position on valve competency was required. These factors were therefore studied, both individually and in a coupled manner, to better

inform the subsequent analysis.

Non-uniform annular dilatation was examined first. With the papillary muscles and trigones held fixed, the annulus was first dilated in the anteroposterior dimension up to 30% in 1% increments. Simultaneously, the height of the annulus was reduced in 25% increments to represent the flattening that has been observed in-vivo [113, 127]. During this process, the anterolateral-posteromedial (transverse) dimension remained constant. As shown in [42], dilatation in this dimension is present in ovine models with induced myocardial infarctions exhibiting no signs of regurgitation. Additionally, Tibayan has shown that there is no significant difference in the transverse dilatation observed in non-regurgitant and regurgitant valves post-myocardial infarction [114]. Given the loading conditions in which the valve model was generated, namely insufflation of the left ventricle, the unperturbed valve model was assumed to be of this non-regurgitant, pathological type.

Following the modeling of annular dilatation, the effect of isolated papillary displacement was then considered. Similar to Siefert's work with a flow simulator [105], three classes of displacement were considered: asymmetric anterolateral papillary displacement, asymmetric posteromedial papillary displacement, and symmetric displacement of both the anterolateral and posteromedial papillary muscles. However, unlike this previous work which only considered oblique uniaxial displacements made simultaneously along the apical, transverse, and anteroposterior dimensions, the use of fast simulation allowed for multi-dimensional analysis where each dimension could be independently controlled, and the interactions between them could be evaluated. In each of the three classes studied, the papillaries were independently shifted laterally, posteriorly, and apically at one millimeter increments for a total of six millimeters in any direction. This resulted is a total of 343 configurations for each of the three classes considered.

4.2.3 Modeling Restrictive Annuloplasty and Papillary Approximation

To investigate the cause of recurrent regurgitation after a restrictive annuloplasty, undersized rings, varying from one to three sizes smaller than that prescribed by valvular geometry (one size corresponds to a two millimeter decrease in the transverse dimension and proportional decreases along the others), were applied to the virtual valve model. The papillary muscles were then shifted, similar to the previous assessment, independently and simultaneously up to six millimeters along each axis. To reduce the number of configurations to be examined, perturbations were made at two millimeter increments. The reguritant orifice area was then computed using the methodology described above.

With the data generated from the papillary displacement studies, the effects of papillary approximation were then examined. Given Fattouch's promising results with a properly sized annuloplasty ring [32], annular geometry was held fixed in the undilated state. Potential anchoring sites for the displacing suture included the peak of the annular saddle [75] or the ipsilateral fibrous trigone [32, 64]. Approximation was simulated by translating the displaced papillary in the direction of the anchor. Using the computed orifice area associated with each potential papillary displacement, translation continued until a new position corresponding to a regurgitant orifice of less than 5 mm^2 was found. This process was repeated for each displaced location with a corresponding regurgitant orifice larger than the threshold.

For each approximated configuration, two types of variation were then considered: further displacement of the papillary head and variation in suture length. While continued ventricular remodeling would not increase the distance betwen the papillary and the anchor site given the assumed lack of suture distensibility, the position of the papillary could move along the surface of a sphere defined by the anchor site and length of suture used. Therefore, variations along this surface were considered (up to five degrees in one degree increments

along both rotational axes). Simultaneously, deviations from the intended suture length were also investigated. The length was varied in quarter millimeter increments up to one millimeter in either direction, simulating uncertainty in the surgical environment. This produced a region of interest in the form of a shell-like spherical cap. The mean and standard deviation of orifice size in this region was then computed.

4.3 Results

A total of 3,723 valve configurations were simulated to closure in this study. While large in number, the fast speed of simulation and command-line interface allowed for each configuration to be processed, from simulation to mean total orifice area computation, with no human intervention in less than ten seconds on a standard laptop PC. This corresponds to a cummulative simulation and data processing period of approximately ten hours.

4.3.1 Effects of Changes in Valvular Geometry

Changes in annular geometry resulted in responses that are both nonlinear and non-uniform in dimension (Figure 4.5). When first dilating the annulus in the anteroposterior dimension from its inital state, growth in the regurgitant orifice area was neglibile. However, this growth increased dramatically with increasing levels of dilatation. While a 10% enlargement from its initial configuration resulted in 6.7 mm^2 of total regurgitant orifice area, subsequent increases from 10% to 20% and 20% to 30% produced an additional 25.3 mm^2 and 54.9 mm^2 respectively. Conversely, the effect of annular flattening was far less pronounced, with large changes in annular height having a minimal impact on orifice area. Even when coupled with large anteroposterior dilations, a 25% reduction in annular height resulted in only a 5% - 10% reduction in regurgitant orifice size.

Displacement of the anterolateral papillary muscle also resulted in superlinear

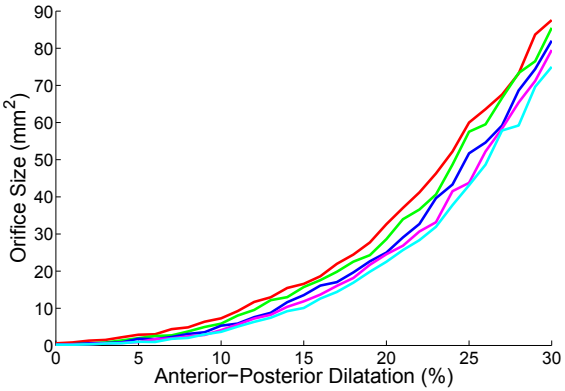

Figure 4.5: Changes in annular geometry can have a profound impact on regurgitant orifice size. While dilation in the anteroposterior dimension increases regurgitation at a continuously growing rate, reductions from 100% (red) of the original annular height to 75% (green), 50% (blue), 25% (magenta), or 0% (cyan) have a lesser effect on orifice size.

growth of the regurgitant orifice (Figure 4.6(a)). However, sensitivity was non-uniform and a function of the axis of perturbation. As shown in Figure 4.6(b), orifice size is most sensitive to apical displacements. Additionally, lateral displacements, while less impactful than those in apical direction, demonstrate a greater effect than posterior papillary motion.

Similar results were obtained when examining the response of orifice size to displacements of the posteromedial papillary muscle. Growth remained superlinear (Figure 4.7(a)), and the apical axis remained the most sensitive to perturbation, followed by the transverse and then anteroposterior axes (Figure 4.7(b)). Valvular response to posteromedial papillary displacements were more sensitive than those of the anterolateral papillary muscle, with a greater regurgitant orifice observed in more than 90% of the configurations.

When simultaneously displacing both the anterolateral and posteromedial papillary muscles, synergistic enlargement of the regurgitant orifice was observed (Figure 4.8(a)). In greater than 81% of the simulated configurations, the size of the orifice from simultaneous papillary displacement was greater than the sum of the areas previously computed from individual perturbations. This increased to 92% for displacements of one millimeter or greater along each axis and 100% for displacements of two millimeters or greater, indicative

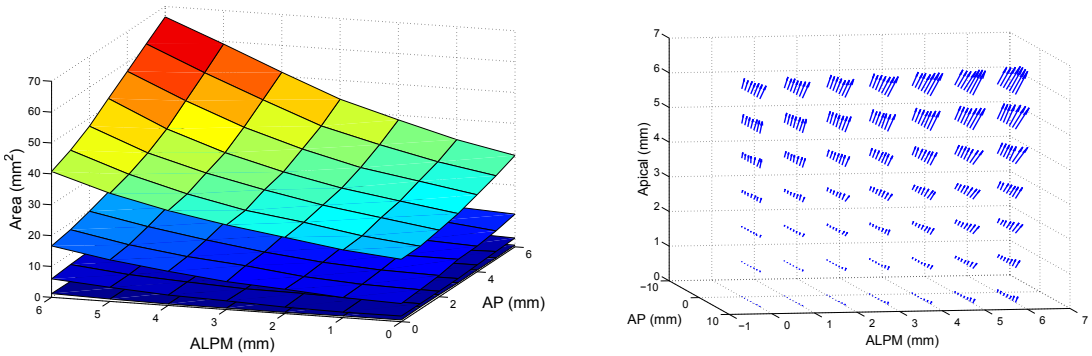

(a) (b)

Figure 4.6: The displacement of the anterolateral papillary produces non-uniform, superlinear growth of the regurgitant orifice. (a) The five surfaces shown in (a) illustrate the effect of posterior (AP) and transverse (ALPM) displacement of the papillary muscle with varying amounts of concurrent apical displacement. The bottommost surface shows the response to no apical displacement, whereas each superior surface corresponds to an additional two millimeter shift apically. (b) For each simulated displacement, the gradient of orifice area is shown. Pointing in the direction of maximum increase, the magnitude of the arrow highlights the size of the increase. The nearly vertical orientation is therefore indicative of a strong sensitivity to apical displacement in all of the evaluated configurations.

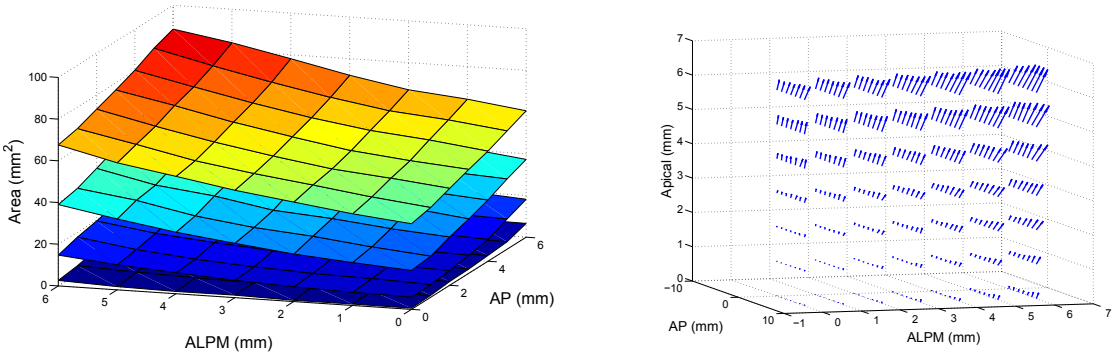

(a) (b)

Figure 4.7: Displacements of the posteromedial papillary muscle result in the growth of regurgitant orifices similar to that observed in the anterolateral papillary muscle but with greater sensitivity, hence the difference in scales between (a) and (a).

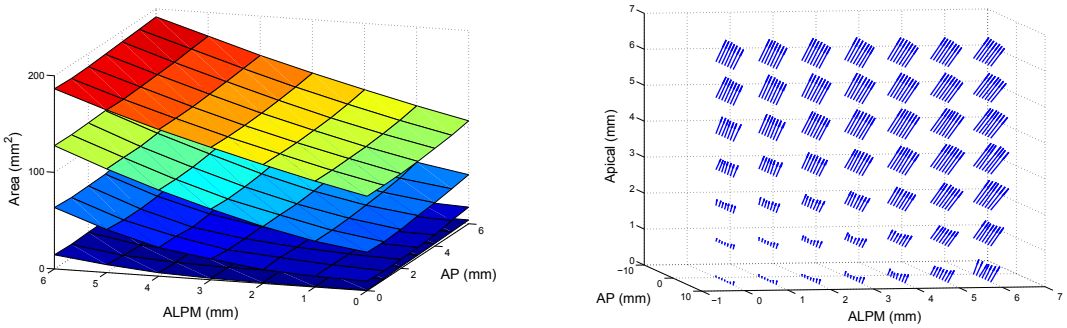

(a) (b)

Figure 4.8: (a) Simultaneous displacement of both the anterolateral and posteromedial papillary muscles results in greater orifice area than the summed area of individual displacements. Increased sensitivity to lateral displacements, as observed in (b), is likely a contributing factor.

of an interaction between the two axes. The result is a 37% average increase in orifice area across all simulations. While the valve remained most sensitive to apical displacements and least sensitive to posterior displacements, sensitivity to simultaneous lateral displacements increased dramatically when compared to individual papillary disturbances (Figure 4.8(b)). The maximum orifice area associated with each axis of displacement and their interactions is shown below in Table 4.1.

	T	P	A	T + P	T + A	P + A	All
AL PM Only	1.2	0.5	20.2	4.1	40.8	29.6	66.6
PM PM Only	2.6	6.6	41.1	17.5	67.6	60.6	88.6
Symmetric	14.6	4.0	97.7	26.0	186.5	106.6	191.7

Table 4.1: This maximum orifice size (in mm^2) varies greatly with the mode (AL PM = anterolateral papillary muscle, PM PM = posteromedial papillary muscle) and direction (T = Transverse, P = Posterior, A = Apical) of papillary displacement. While apical displacements produce the largest orifices, simulation also illustrated valve sensitivity to simultaneous lateral papillary motion.

	U1	U2	U3
AL PM Only	54.5%	27.3%	13.0%
PM PM Only	75.4%	52.8%	32.4%
Symmetric	81.9%	64.1%	47.3%

Table 4.2: A restrictive annuloplasty reduced reguritant orifice size in all configurations. The ratio of orifice area between valves with reduced and properly sized anuluses is a function of the size of the displacement, the papillary muscle displaced (AL PM = anterolateral papillary muscle, PM PM = posteromedial papillary muscle), and the extent to which the ring is undersized (U1, U2, and U3 represent a ring undersized by one, two, and three sizes respectively). The maximum ratios observed across all displacements are presented in this table.

4.3.2 Robustness of Surgical Repair

Regardless of the ring size selected, when performing a restrictive annuloplasty the area of the regurgitant orifice was reduced in all configurations. However, its efficacy greatly diminished for large papillary displacements, especially along the apical axis. As the displacements grew, the size of the orifice increased relative to that found in a valve with a properly sized annulus and identical papillary locations (i.e., the ratio of the orifice areas increased towards unity, implying a faster rate of orifice growth in the undersized valve). Simultaneous lateral displacements of both papillary muscles further reduced the efficacy of the undersized ring, with the sensitivity approaching that of apical displacements (Figures 4.9(a) and 4.9(b)). The maximum observed ratio of orifice areas in each configuration is presented in Table 4.2.

Conversely, papillary approximation was effective in robustly reducing the regurgitant orifice area, regardless of the initial papillary position and choice of anchor site. Upon approximation, orifice area exhibited greater sensitivity to suture length than angle of variation due to the greater degree of apical motion it afforded. When comparing the two anchoring sites, the fibrous trigones provided greater reliability, with a smaller standard

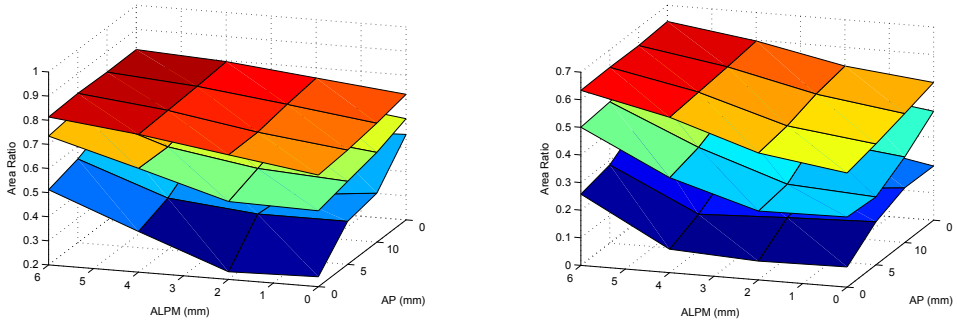

(a) (b)

Figure 4.9: For small displacements of both the anterolateral and posteromedial papillaries, a restrictive annuloplasty greatly reduces the size of the regurgitant orifice relative to a valve with properly sized annulus. However, further ventricular remodeling creates an orifice that grows faster, resulting in an area ratio that approaches unity. More aggressive downsizing from (a) one size to (b) two sizes increased this rate of growth, especially along the transverse axis. In these figures, the bottommost surface represents two millimeter apical displacement, with each superior surface presenting a further two millimeter displacement.

deviation within each region of interest, a smaller mean orifice area within the region of interest, and a smaller standard deviation across these mean orifice areas (Figure 4.10).

4.4 Discussion

The mitral valve is an adaptable cardiac structure that is readily able to compensate for small deviations from its physiologic geometry. Much of this robustness stems from the behavior and anatomy of the anterior leaflet. When afforded sufficient freedom of motion by the chordae, its excess height allows it to compensate for abnormal motion elsewhere in the valve.

This compensatory behavior was readily observed in simulation. When independently displacing the anterolateral or posteromedial papillary muscle laterally by six millimeters, the entire anterior leaflet shifted both laterally and apically, sliding under the posterior leaflet, to lessen the regurgitant orifice. This was quantified by tracking three

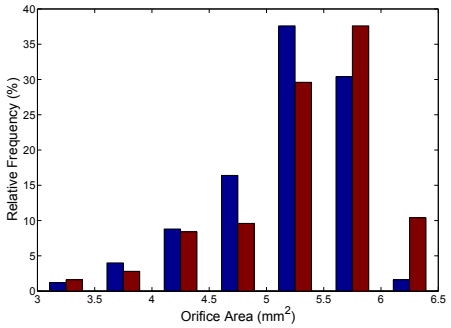

(a) Anterolateral Papillary Approximation

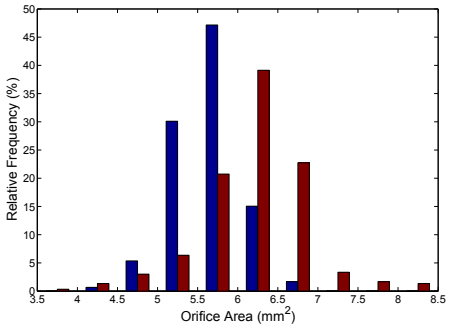

(b) Posteromedial Papillary Approximation

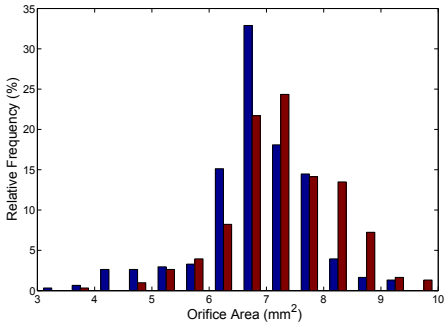

(c) Symmetric Papillary Approximation

Figure 4.10: Anchoring to the fibrous trigones (blue), rather than the peak of the annular saddle (red), provides improved robustness to variation. Each entry accumuluated by the histogram corresponds to the mean orifice size in the post-repair region of interest for a single papillary configuration. In cases of (a) anterolateral, (b) posteromedial, and (c) symmetric papillary displacement, the location of the trigones relative to the papillary muscles results in a more advantageous suture angle that reduces orifice size and variability in reponse to variation in suture length and continued ventricular remodeling.

mesh vertices (mid-leaflet on A1, A2, and A3 respectively) and comparing their location in the perturbed and unperturbed models. All three moved approximately one millimeter in the direction of tethering, with the greatest motion exhibited by the nearby vertex, and apically to a lesser extent to enable this motion.

4.4.1 The Positive Feedback Loop of Disease Progression

However, the geometric deformations observed in ischemic mitral regurgitation overwhelm the valve's compensatory mechanisms. Posterior dilatation of the mitral annulus, while well supported initially by the excess leaflet tissue, eventually results in an anteroposterior dimension that is too large for the anterior leaflet to span. Once this occurs, the sensitivity of the regurgitant orifice to posterior dilatation rapidly grows, and any subsequent orifice growth leads to further increases in sensitivity. Although simulation results suggest annular flattening can nominally shrink the regurgitant orifice, such distortions are highly undesirable as the annular saddle is known to reduce stresses in the anterior leaflet, preserving its long-term viability [101]. Therefore, regardless of the other repair techniques performed, dilatation along the anteroposterior dimension must be reduced to a level supported by the anterior leaflet to ensure a robust repair.

The response of the valve to papillary displacement was also highly directionally dependent. While the valve was largely able to compensate for significant asymmetric, lateral and posterior uniaxial displacements via the shifting of the anterior leaflet, moving the papillary muscles apically inhibited the natural upward motion of the leaflets, thereby preventing coaptation. Once displaced apically, the addition of lateral or posterior perturbations worsened leaflet tethering as the anterior leaflet was no longer free to compensate, resulting in the synergistic increases in orifice size. Such interactions were also present in symmetric papillary displacements. Lateral motion of the papillaries tautened the anterior leaflet, much like tightening an inflated sail, restricting the motion of the medial anterior leaflet scallop and producing a central jet.

Interestingly, the posteromedial papillary exhibited greater sensitivity than the anterolateral papillary to identical, isolated displacements. Whether this contributes to the increased prevalence of tethering at the medial and posterior segments of the posterior

leaflet or is merely an artifact of the loading conditions or porcine valve model requires further study.

Superlinear growth of the regurgitant orifice area, both in response to posterior annular dilatation and papillary displacement, highlights the importance of early treatment. Chronic ventricular remodeling is common in patients with a low ejection fraction [35]. When these geometric changes are combined with the increasing sensitivity to orifice growth demonstrated in this work, the effect on orifice size is amplified, resulting in an unstable positive feedback loop and an ever-growing regurgitant orifice. Even in asymptomatic patients, the dangers of a large regurgitant orifice are well documented, and the increased sensitivity of orifice size to further geometric change may potentially be a contributing factor [30].

4.4.2 Developing a Robust Repair Strategy

To prevent this downward spiral and ensure the robustness of valve repair, these results suggest that the surgeon should not only minimize post-operative regurgitation, but also restore the valve to a geometry that is less senstive to small perturbations. While this implies the need for an annuloplasty in cases of posterior annular dilatation, it also highlights the issues associated with a restrictive annuloplasty. If performed in a patient with a highly enlarged left ventricle, an undersized annuloplasty ring will acutely improve valve function. However, as illustrated by simulation, the patient's valvular and subvalvular geometry will remain highly sensitive to continued remodeling, more so than a valve with properly sized annulus, larger regurgitant orifice, and identical papillary positions.

The tethering effects induced by the restrictive annuloplasty are one contributing factor. The cinching of the annulus towards its center increases the distance between the papillaries and the posterior annulus. As a result, the posterior leaflet is tethered, and the anterior leaflet becomes almost solely responsible for ensuring valve competence. Further

decreasing the size of the annuloplasty ring only exacerbates posterior leaflet tethering. In this quasi-unicuspid valve, any increased restriction on anterior leaflet mobility greatly increases the size of the regurgitant orifice, thus explaining the increased sensitivity. While this tethering has previously been observed in humans and animal models [43,51], the use of simulation allowed for the controlled variation in cardiac geometry, enabling the observation and characterization of this more severe rate of orifice growth.

To prevent such issues, ensuring proper leaflet mobility is crucial. Papillary approximation aids in this process by repositioning the papillary muscles towards the anchor site. The large vertical component of the displacement opposes the computed orifice gradient, resulting in a large decrease in orifice size per millimeter translation. This also makes the technique more sensitive to variation in suture length than angular perturbances, which for the most part are largely uncontrollable. Placing the greatest sensitivity under the direct control of an expert surgeon, rather than cardiac geometry, likely increases the probability of procedural success. However, with less precise surgeons, this may prove to be problematic. One compromise is to select an anchor site with lesser sensitivity to variations in suture length.

As shown in Figure 4.10, this corresponds to the fibrous trigones rather than the peak of the annular saddle. The sensitivity to variations in asymmetric approximation anchored to the trigones is less than 2 mm^2, making the procedure highly robust. This sensitivity increases when anchoring to the peak of the annular saddle, as the angle of the suture better aligns with the gradients of orifice area. While this computed sensitivity widens for both anchoring sites in the case of symmetric approximation, this increase can be partly attributed to modeling error. Since the valve and subvalvular apparatus do not exhibit perfect symmetry unlike the simulated displacements, a mean papillary-to-anchor vector had to be constructed and applied to both papillary heads. Moving forward, if

the sensitivities computed in this study prove to be too great for non-expert surgeons, alternate papillary displacement techniques such as the papillary sling [53] or transverse approximation [81], which displace the papillaries along a less sensitive axis at the cost of larger required displacements and more poorly controlled vertical motion, may prove to be a better fit.

4.4.3 Final Considerations

It should be emphasized that the sensitivity analysis performed in this work is not intended to serve as a model of disease progression. Unlike in [128], the left ventricle remains unmodeled, and as a result, changes in annular and papillary geometry cannot be predicted. Instead, using prescribed geometric perturbations, the effect on valve function can be estimated. Such analysis complements [51, 56, 60, 113, 113], which characterize in-vivo the changes in valvular geometry associated with ischemic mitral regurgitation and restrictive annuloplasty.

The results of this senstivity study can also be employed to inform the design of novel procedures and surgical techinques. As considered in the case of anchor site selection for papillary approximation, orifice sensitivity can be used to minimize cardiac deformations, lessen the impact of naturally occurring variation, facilitate surgical implementation, or a weighted combination of the three. The ability to prospectively analyze the effect of key parameters on procedural efficacy and robustness would allow for decreased development costs and an expedited path to clinical use.

Nevetheless, care should be taken in generalizing these results to other valve geometries. While qualitatively similar patterns will likely emerge in other patients, quantitatively the magnitude of such effects will likely vary on a case by case basis. To better understand this variation, a larger number of valve geometries would have to be considered. This could

either be achieved by generating multiple patient-specific models or by parameterizing the valve and adapting it to best fit a patient's cardiac geometry.

The computational methods applied in this work, while sufficiently fast to make tractable the thousands of simulations performed, do present their own drawbacks. The valve model was generated from an explanted, insufflated heart. Although simliar to what the surgeon observes in the operating room, the model is not entirely faithful to systolic valve geometry. Additionally, the quasti-static analysis performed inhibits the assessment of hemodynamics, an important factor in evaluating valve function. Other key metrics of valve competency, including coaptation height, tenting height, and tenting area, are also not considered. Given the single projection used to measure orifice size, eccentric regurgitant jets may also be underestimated; however, this could be mitigated by considering multiple projections from varying angles. With key sensitivity parameters identified, a second, more thorough analysis using a more realistic valve model, improved metrics of valve function, and enhanced regurgitant orifice detection could be performed over a reduced configuration space to accomodate the increased computational demands. Nevertheless, despite all of the benefits that fast simulation provides, validation in a tissue model, either via an ex-vivo flow simulator or an in-vivo animal study, would be required before these results can be applied clinically.

In summary, this work presents the most thorough investigation of the mitral valve's complex, nonlinear, coupled response to changes in valve geometry. By using fast simulation, geometric perturbations can be precisely controlled in a low-cost manner, enabling the identification and evaluation of nonlinear anatomic interactions. These relations can then be leveraged to assess existing surgical procedures and optimize novel surgical techinques.

Chapter 5

Conclusions and Future Work

5.1 Conclusions

This thesis investigated the use of fast, approximate simulation as a tool to improve the treatment of mitral regurgitation, more specifically, its applications in patient-specific surgical planning and rehearsal, the training and evaluation of surgeons, and procedure development and sensitivity assessment. Recognizing the challenges of predicting closed valve shape in the operating room, this work first aimed to facilitate this task. Chapter 2 described the construction and validation of an interactive surgical planning system, which leveraged the fast computational model to enable the iterative development and evaluation of a proposed surgical plan. This was complemented by the work in Chapter 3, which improved users' predictive abilities through simulation-based training. Finally, Chapter 4 addressed the difficulties of treating ischemic mitral regurgitation, analyzing the sensitivty to geometric variation in the current standard of care and optimizing a novel surgical technique to enhance the robustness of valve repair in these patients. This chapter considers the implications of these results and explores potential avenues of continued work.

5.1.1 Use of Approximate Models to Enable Interactivity

Simulation accuracy and speed often present a design tradeoff, where the modeler must weigh the relative importance of each. In much of the research community, accuracy is of the utmost concern, which results in involved, computationally expensive models that simulate complex phenomena. Conversely, the video game industry largely eschews accuracy in lieu of visual plausability, enabling the development of dense, interactive virtual environments. Surgical simulators typically lie somewhere between the two, using linear finite element models to predict the behavior of soft tissue. While providing accuracy surpassing most video games at the expense of decreased speed, surgical simulators maintain update rates sufficient for real-time user interaction.

In this work, video game simulation techniques were modified to achieve submillimeter accuracy. Modeling the physics of the mitral valve, the sparse virtual environment updated at a rate of greater than two kilohertz, exceeding nearly all video games and surgical simulators. This enabled the integration of a haptic device without the need for haptic filtering, which can induce instability in response to large perturbances. This contrasts most surgical simulators, which because of their underlying finite element model, are unable to achieve haptic update rates. As a result, when using the simulation platform developed in this work, users were able to safely and stably pull on the stiff leaflet tissue and feel the immediate force response.

Despite the simplifying assumptions made, the mass-spring model implemented in this work accurately simulated valve closure to within the resolution of clinical imaging modalities and of the same order as human dexterity. Therefore, rather than attempt to increase the speed of highly accurate models, perhaps, as in this work, greater gains in interactive simulation can be achieved by improving the accuracy of faster, approximate methods.

5.1.2 Benefits of Low-Cost Virtual Instruction

Although amplified forces and a simplified graphical rendering were used, virtual instruction was able to improve the users' ability to assess leaflet mobility and predict closed valve shape. A likely contributing factor is the initial skill level of the population studied. Despite having completed coursework in cardiac pathophysiology and being provided with additional material regarding the valve analysis, the medical students were unable to assess leaflet mobility and predict closed valve shape, highlighting the importance of teaching interactive tasks via interactive means.

However, high-fidelity simulation-based instruction can be costly when compared to traditional pedagogy and potentially unnecessary depending on the user's skill level. Initially, novice users are merely learning gross skills and motions and are unable to assimilate the finer details presented. Therefore, during this stage, the benefits of realism are diminished, making justifying the increased costs more challenging. In these instances, as demonstrated by this work, lower fidelity, low-cost simulation can be used to successfully provide initial instruction. Upon the plateauing of user performance, higher fidelity models, in the form of more complex virtual simulators or tissue specimens, can be employed. By treating training as a multi-step process, the use of higher-cost, and potentially more challenging to maintain, models can be lessened.

The use of virtual training also frees up clinicians. Instead of instructing basic tasks that could easily be taught virtually, they would be able to focus more more challenging techniques and procedures. This could allow for more in-depth instruction or a greater volume of residents per instructor, a key motivator given the growing demand for cardiac procedures and growing shortage of cardiac surgeons [47].

5.1.3 Sensitivity Analysis Through Repeated Simulation

By using an approximate model, the resulting gains in speed enabled batch simulation over a wide range of variations. This allowed for the sensitivity of valve function to various geometric distortions to be evaluated, the benefit of which was multifactorial. By highlighting the valve's increasing sensitivity to further displacements, the seriousness of disease progression and importance of early treatment are emphasized. Additionally, the idea of robustness to variation as a metric for surgical success is also demonstrated.

Restoring valve competency does not always imply a successful repair. As is the case in a restrictive annuloplasty with displaced papillaries, a repair that will fail following even minimal ventricular remodeling, while providing acute relief, does not improve the patient's long-term prognosis, severely limiting the procedure's positive impact and lessening the realized benefit relative to the surgical risk. Therefore, robustness to geometric disturbances should be a key consideration in any procedure. However, such robustness is typically challenging to quantify. Repeated simulation thus solves this issue and allows for an improved quantitative estimate of post-operatove risk as well as the ability to optimize procedures to minimize this newly available risk factor.

5.2 Future Directions

5.2.1 Generation of Patient-Specific Valve Models

The inability to robustly generate a patient-specific geometric valve model in an automated manner using clinical imaging modalities is the primary factor preventing a comprehensive pipeline from acquired image to simulated closed valve shape. The closest that has been achieved to date is presented in [125, 126]. Although the authors generate a patient-specific model from multi-slice CT, the process is highly manual and likely infeasible

in many patients. Conversely, automated ultrasound-based methods have shown promise in extracting leaflet and annular geometry, but image resolution has precluded the acquisition of the chordae tendineae [102, 103]. Given the physics of ultrasound, this will likely require the mosaicing of multiple images, with the subvalvular apparatus imaged via transcardiac or intracardiac echocardiography thereby enabling the use of higher frequencies and providing improved resolution.

5.2.2 Complications of Degenerative Valve Disease

The modeling of pathological leaflet tissue also presents a challenge to the simulation community. Despite degenerative valve disease being the most common cause of mitral regurgitation, there has been little work in characterizing the mechanical properties of diseased tissue. Such efforts are required to understand the changes in tissue behavior, which likely span a continuum depending on the disease and its progression. The simplest means of characterization would be mechanical testing. However, this could prove to be costly and resource-intensive given the large number of tissue samples that would need to be examined. Inverse modeling could provide an alternate, more automated means of testing but would require the automated generation of a patient-specific geometric valve model. Regardless of the method used, until the characterization of pathological leaflet tissue has been completed, modeling degenerative pathologies will remain a challenge.

5.2.3 Improved Instruction in the Visualization of Closed Valve Shape

Chapter 3 largely focused on the use of valve analysis to determine leaflet mobility and predict closed valve shape. However, the surgical workflow is far more complex and nuanced. Surgeons must also integrate preoperative echocardiography into their mental model when generating a surgical plan. Ideally, a second generation simulation-based

training platform would include this task. Synthetic ultrasound would be used to generate preoperative imaging, whose quality could be varied to present changes in difficulty. By providing both the visual information from preoperative imaging and the tactile cues associated with valve analysis, users would be required to perform the same multi-source fusion that cardiac surgeons regularly carry out. The cognitive challenges associated with this task would likely increase substantially and therefore should only be added once competency in valve analysis is achieved.

5.2.4 Automated Assessment of User Skill

Improved methods of gauging user competency could also be developed. Currently, the simulation system is unable to differentiate between a correct guess and a well-informed decision. However, by incorporating alternate sources of information, such as efficiency of user motion, maximum force exerted, question difficulty, and time requird for analysis, a more educated evaluation of user ability would be feasible. These variables, and their correlation to user skill, could be determined via machine learning techniques, such as a support vector machine or neural network, with an initial calibration performed using expert assessment. Such a system could then be leveraged to automatically adapt question difficulty to the user's skill level.

5.2.5 Automating the Planning of Valve Repair

In Chapter 4, valve models were generated combinatorially in batch across a desired range of configuations for simulation and assessment of valve competency. While executed by a custom-written script, this process could also be automated and controlled by an intelligent algorithm, which could explore combinations of repair techniques in search of a high quality repair plan.

Repair quality would be assessed by a repair metric to evaluate valve competency and limit the search space to physically viable solutions. While one method of generating such a metric would be to codify the physiological ratios described in literature, an indirect, and perhaps more robust, approach would be to use machine learning techniques to learn a suitable metric. By presenting expert surgeons with a diseased valve and prompting them to select the better of two potential repair strategies from the simulated results, a metric could be developed that implicitly incorporates surgeon knowledge. This would not only include well-documented and widely taught physiological ratios, but also the collective intuition of expert surgeons.

Because the space of potential repairs is large and the evaluated repair quality would be derived from the results of simulation, the gradient would likely be complex and poorly defined. As a result, black-box optimization techniques such as genetic algorithms or Bayesian optimization would be required to find a satisfactory minima. The corresponding repair strategy could then be provided to the non-expert surgeon for execution. By eliminating the need to develop a repair plan, the burden on these less-skilled surgeon would be dramatically reduced, potentially increasing the frequency and durability of repairs performed.

5.2.6 Optimizing the Design of Novel Medical Devices

Rather than optimize a single surgical technique or valve repair plan, high-volume simulation could also be used to optimize the design of medical devices in an analagous process. Variations in device design would first be enumerated or, to potentially improve the efficiency of assessment, parameterized. Given a metric to minimize which could encompass device efficacy, durability, robustness to geometric perturbations, and other desired considerations, potential designs would then be evaluated. For a standardized device, further

variations in patient geometry could be considered to ensure efficacy across the population. However, given recent improvements in rapid prototyping technologies, the device could also be optimzed to the patient's anatomy, providing a customized solution that could then be fabricated to best address his or her needs.

Bibliography

[1] Christophe Acar, Michael Tolan, Alain Berrebi, Jullien Gaer, Roger Gouezo, Thierry Marchix, Jean Gerota, Sylvain Chauvaud, Jean-Noel Fabiani, Alain Deloche, et al. Homograft replacement of the mitral valve: graft selection, technique of implantation, and results in forty-three patients. *The Journal of Thoracic and Cardiovascular Surgery*, 111(2):367–380, 1996.

[2] D.H. Adams and A.C. Anyanwu. The cardiologist's role in increasing the rate of mitral valve repair in degenerative disease. *Current Opinion in Cardiology*, 23(2):105, 2008.

[3] Cary W Akins, Alan D Hilgenberg, Mortimer J Buckley, Gus J Vlahakes, David F Torchiana, Willard M Daggett, and W Gerald Austen. Mitral valve reconstruction versus replacement for degenerative or ischemic mitral regurgitation. *The Annals of thoracic surgery*, 58(3):668–676, 1994.

[4] Anelechi C Anyanwu, Benjamin Bridgewater, and David H Adams. The lottery of mitral valve repair surgery. *Heart*, 96(24):1964–1967, 2010.

[5] Ani C Anyanwu and David H Adams. Etiologic classification of degenerative mitral valve disease: Barlows disease and fibroelastic deficiency. In *Seminars in thoracic and cardiovascular surgery*, volume 19, pages 90–96. Elsevier, 2007.

[6] Ani C Anyanwu and David H Adams. The intraoperative ink test: a novel assessment tool in mitral valve repair. *The Journal of Thoracic and Cardiovascular Surgery*, 133(6):1635–1636, 2007.

[7] A Arnoldi, A Invernizzi, Raffaele Ponzini, E Votta, Enrico G Caiani, and Alberto Redaelli. Mitral valve models reconstructor: a python based gui software in a hpc environment for patient-specific fem structural analysis. In *Innovations and Advances in Computer Sciences and Engineering*, pages 215–219. Springer, 2010.

[8] D. Baraff. *Dynamic Simulation of Non-Penetrating Rigid Bodies*. PhD thesis, Cornell University, 1992.

[9] D. Baraff and A. Witkin. Large steps in cloth simulation. In *Proceedings of the 25th Annual Conference on Computer Graphics and Interactive Techniques*, pages 43–54. ACM, 1998.

[10] Gilberto Venossi Barbosa, Carlos Manuel de Almeida Brandão, and Vinicius José da Silva Nina. Hands on as educational process in cardiovascular surgery. In *Cardiac Surgery - A Commitment to Science, Technology and Creativity*. InTech, 2014.

[11] Steven F Bolling, Shuang Li, Sean M O'Brien, J Matthew Brennan, Richard L Prager, and James S Gammie. Predictors of mitral valve repair: clinical and surgeon factors. *The Annals of thoracic surgery*, 90(6):1904–1912, 2010.

[12] Robert O. Bonow, Blase A. Carabello, Kanu Chatterjee, Antonio C. de Leon Jr, David P. Faxon, Michael D. Freed, William H. Gaasch, Bruch Whitney Lytle, Rick A. Nishimura, Patrick T. O'Gara, Robert A. O'Rourke, Catherine M. Otto, Pravin M. Shah, and Jack S. Shanewise. ACC/AHA 2006 guidelines for the management of patients with valvular heart disease. *Journal of the American College of Cardiology*, 48:e1–e148, 2006.

[13] Michael A Borger, Patricia M Murphy, Asim Alam, Shafie Fazel, Manjula Maganti, Susan Armstrong, Vivek Rao, and Tirone E David. Initial results of the chordal-cutting operation for ischemic mitral regurgitation. *The Journal of thoracic and cardiovascular surgery*, 133(6):1483–1492, 2007.

[14] William R Brown, Dixon M Moody, Venkata R Challa, David A Stump, and John W Hammon. Longer duration of cardiopulmonary bypass is associated with greater numbers of cerebral microemboli. *Stroke*, 31(3):707–713, 2000.

[15] P Burlina, R Mukherjee, and C Sprouse. A personalized mitral valve closure simulator. In *Engineering in Medicine and Biology Society (EMBC), 2012 Annual International Conference of the IEEE*, pages 6636–6640. IEEE, 2012.

[16] P. Burlina, C. Sprouse, D. DeMenthon, A. Jorstad, R. Juang, F. Contijoch, T. Abraham, D. Yuh, and E. McVeigh. Patient-specific modeling and analysis of the mitral valve using 3D-TEE. *Information Processing in Computer-Assisted Interventions*, pages 135–146, 2010.

[17] Philippe Burlina, Chad Sprouse, Ryan Mukherjee, Daniel DeMenthon, and Theodore Abraham. Patient-specific mitral valve closure prediction using 3d echocardiography. *Ultrasound in medicine & biology*, 39(5):769–783, 2013.

[18] Francesca Bursi, Maurice Enriquez-Sarano, Vuyisile T Nkomo, Steven J Jacobsen, Susan A Weston, Ryan A Meverden, and Véronique L Roger. Heart failure and death after myocardial infarction in the community the emerging role of mitral regurgitation. *Circulation*, 111(3):295–301, 2005.

[19] Blase A Carabello. The current therapy for mitral regurgitation. *Journal of the American College of Cardiology*, 52(5):319–326, 2008.

[20] Alain Carpentier. Cardiac valve surgery–the" french correction". *The Journal of thoracic and cardiovascular surgery*, 86(3):323, 1983.

[21] Alan Carpentier, David H Adams, and Farzan Filsoufi. *Carpentier's Reconstructive Valve Surgery*. Saunders Elsevier, 2010.

[22] Javier G Castillo, Anelechi C Anyanwu, Valentin Fuster, and David H Adams. A near 100% repair rate for mitral valve prolapse is achievable in a reference center: Implications for future guidelines. *The Journal of Thoracic and Cardiovascular Surgery*, 144(2):308–312, 2012.

[23] Richard P Cochran and Karyn S Kunzelman. Effect of papillary muscle position on mitral valve function: relationship to homografts. *The Annals of thoracic surgery*, 66(6):S155–S161, 1998.

[24] J.E. Colgate, M.C. Stanley, and J.M. Brown. Issues in the haptic display of tool use. In *IROS*, page 3140. Published by the IEEE Computer Society, 1995.

[25] Julie Damp, Ryan Anthony, Mario A Davidson, and Lisa Mendes. Effects of transesophageal echocardiography simulator training on learning and performance in cardiovascular medicine fellows. *Journal of the American Society of Echocardiography*, 26(12):1450–1456, 2013.

[26] TE David, DE Uden, and HD Strauss. The importance of the mitral apparatus in left ventricular function after correction of mitral regurgitation. *Circulation*, 68(3 Pt 2):II76–82, 1983.

[27] Tirone E David. Ischemic mitral regurgitation: Chordal-sparing mitral valve replacement. *Operative Techniques in Thoracic and Cardiovascular Surgery*, 17:194–203, 2012.

[28] Jennifer Davies, Manaf Khatib, and Fernando Bello. Open surgical simulationa review. *Journal of Surgical Education*, 2013.

[29] B Dunkin, GL Adrales, K Apelgren, and JD Mellinger. Surgical simulation: a current review. *Surgical endoscopy*, 21(3):357–366, 2007.

[30] Maurice Enriquez-Sarano, Jean-François Avierinos, David Messika-Zeitoun, Delphine Detaint, Maryann Capps, Vuyisile Nkomo, Christopher Scott, Hartzell V Schaff, and A Jamil Tajik. Quantitative determinants of the outcome of asymptomatic mitral regurgitation. *New England Journal of Medicine*, 352(9):875–883, 2005.

[31] Maurice Enriquez-Sarano, Hartzell V Schaff, Thomas A Orszulak, A Jamil Tajik, Kent R Bailey, and Robert L Frye. Valve repair improves the outcome of surgery for mitral regurgitation a multivariate analysis. *Circulation*, 91(4):1022–1028, 1995.

[32] Khalil Fattouch, Patrizio Lancellotti, Sebastiano Castrovinci, Giacomo Murana, Roberta Sampognaro, Egle Corrado, Marco Caruso, Giuseppe Speziale, Salvatore Novo, and Giovanni Ruvolo. Papillary muscle relocation in conjunction with valve annuloplasty improve repair results in severe ischemic mitral regurgitation. *The Journal of thoracic and cardiovascular surgery*, 143(6):1352–1355, 2012.

[33] Eric N Feins, Haruo Yamauchi, Gerald R Marx, Franz P Freudenthal, Hua Liu, Pedro J del Nido, and Nikolay V Vasilyev. Repair of posterior mitral valve prolapse with a novel leaflet plication clip in an animal model. *The Journal of thoracic and cardiovascular surgery*, 2013.

[34] Ted Feldman, Elyse Foster, Donald D Glower, Saibal Kar, Michael J Rinaldi, Peter S Fail, Richard W Smalling, Robert Siegel, Geoffrey A Rose, Eric Engeron, et al. Percutaneous repair or surgery for mitral regurgitation. *New England Journal of Medicine*, 364(15):1395–1406, 2011.

[35] William H Gaasch and Theo E Meyer. Left ventricular response to mitral regurgitation implications for management. *Circulation*, 118(22):2298–2303, 2008.

[36] James S. Gammie, Shubin Sheng, Bartley P. Griffith, Eric D. Peterson, J. Scott Rankin, Sean M. O'Brien, and James M. Brown. Trends in mitral valve surgery in the united states: Results from the society of thoracic surgeons adult cardiac database. *Annals of Thoracic Surgery*, 87:1431–1439, 2009.

[37] A Marc Gillinov, Per Nils Wierup, Eugene H Blackstone, Ehab S Bishay, Delos M Cosgrove, Jennifer White, Bruce W Lytle, and Patrick M McCarthy. Is repair preferable to replacement for ischemic mitral regurgitation? *The Journal of Thoracic and Cardiovascular Surgery*, 122(6):1125–1141, 2001.

[38] Wolfgang A Goetz, Hou-Sen Lim, Emmanuel Lansac, Hashim A Saber, Filip Pekar, Patricia A Weber, and CM Duran. Anterior mitral basal staychords are essential for left ventricular geometry and function. *J Heart Valve Disease*, 14(2):195–202, 2005.

[39] Joseph H Gorman III, Robert C Gorman, Benjamin M Jackson, Yoshiharu Enomoto, Martin G St John-Sutton, and L Henry Edmunds Jr. Annuloplasty ring selection for chronic ischemic mitral regurgitation: lessons from the ovine model. *The Annals of thoracic surgery*, 76(5):1556–1563, 2003.

[40] Naga K Govindaraju, David Knott, Nitin Jain, Ilknur Kabul, Rasmus Tamstorf, Russell Gayle, Ming C Lin, and Dinesh Manocha. Interactive collision detection between deformable models using chromatic decomposition. In *ACM Transactions on Graphics (TOG)*, volume 24, pages 991–999. ACM, 2005.

[41] Jonathan S Grashow, Ajit P Yoganathan, and Michael S Sacks. Biaixal stress–stretch behavior of the mitral valve anterior leaflet at physiologic strain rates. *Annals of biomedical engineering*, 34(2):315–325, 2006.

[42] G Randall Green, Paul Dagum, Julie R Glasson, George T Daughters, Ann F Bolger, Linda E Foppiano, Gerald J Berry, Neil B Ingels, and D Craig Miller. Mitral annular dilatation and papillary muscle dislocation without mitral regurgitation in sheep. *Circulation*, 100(suppl 2):II–95, 1999.

[43] G Randall Green, Paul Dagum, Julie R Glasson, J Nistal, George T Daughters II, Neil B Ingels Jr, and D Craig Miller. Restricted posterior leaflet motion after mitral ring annuloplasty. *The Annals of thoracic surgery*, 68(6):2100–2106, 1999.

[44] Boyce E Griffith, Richard D Hornung, David M McQueen, and Charles S Peskin. Parallel and adaptive simulation of cardiac fluid dynamics. *Advanced computational infrastructures for parallel and distributed adaptive applications*, page 105, 2010.

[45] Boyce E Griffith, Xiaoyu Luo, David M McQueen, and Charles S Peskin. Simulating the fluid dynamics of natural and prosthetic heart valves using the immersed boundary method. *International Journal of Applied Mechanics*, 1(01):137–177, 2009.

[46] Francesco Grigioni, Maurice Enriquez-Sarano, Kenton J Zehr, Kent R Bailey, and A Jamil Tajik. Ischemic mitral regurgitation long-term outcome and prognostic implications with quantitative doppler assessment. *Circulation*, 103(13):1759–1764, 2001.

[47] Atul Grover, Karyn Gorman, Timothy M Dall, Richard Jonas, Bruce Lytle, Richard Shemin, Douglas Wood, and Irving Kron. Shortage of cardiothoracic surgeons is likely by 2020. *Circulation*, 120(6):488–494, 2009.

[48] T Sloane Guy, Sina L Moainie, Joseph H Gorman, Benjamin M Jackson, Theodore Plappert, Yoshiharu Enomoto, Martin G St John-Sutton, L Henry Edmunds, and Robert C Gorman. Prevention of ischemic mitral regurgitation does not influence the outcome of remodeling after posterolateral myocardial infarction. *Journal of the American College of Cardiology*, 43(3):377–383, 2004.

[49] P.E. Hammer, P.J. del Nido, and R.D. Howe. Anisotropic mass-spring method accurately simulates mitral valve closure from image-based models. In *Functional Imaging and Modeling of the Heart*, pages 233–240, 2011.

[50] P.E. Hammer, M.S. Sacks, P.J. del Nido, and R.D. Howe. Mass-spring model for simulation of heart valve tissue for mechanical behavior. *Annals of Biomedical Engineering*, 39:1668–1679, 2011.

[51] Judy Hung, Lampros Papakostas, Stephen A Tahta, Bruce G Hardy, Bruce A Bollen, Carlos M Duran, and Robert A Levine. Mechanism of recurrent ischemic mitral regurgitation after annuloplasty continued lv remodeling as a moving target. *Circulation*, 110(11 suppl 1):II–85, 2004.

[52] Ulrik Hvass and Thomas Joudinaud. The papillary muscle sling for ischemic mitral regurgitation. *The Journal of thoracic and cardiovascular surgery*, 139(2):418–423, 2010.

[53] Ulrik Hvass, Michel Tapia, Frank Baron, Bruno Pouzet, and Abdel Shafy. Papillary muscle sling: a new functional approach to mitral repair in patients with ischemic left ventricular dysfunction and functional mitral regurgitation. *The Annals of thoracic surgery*, 75(3):809–811, 2003.

[54] Razvan Ioan Ionasec, Ingmar Voigt, Bogdan Georgescu, Yang Wang, Helene Houle, Fernando Vega-Higuera, Nassir Navab, and Dorin Comaniciu. Patient-specific modeling and quantification of the aortic and mitral valves from 4-d cardiac ct and tee. *Medical Imaging, IEEE Transactions on*, 29(9):1636–1651, 2010.

[55] Bernard Iung, Gabriel Baron, Eric G Butchart, François Delahaye, Christa Gohlke-Bärwolf, Olaf W Levang, Pilar Tornos, Jean-Louis Vanoverschelde, Frank Vermeer, Eric Boersma, et al. A prospective survey of patients with valvular heart disease in

europe: The euro heart survey on valvular heart disease. *European heart journal*, 24(13):1231–1243, 2003.

[56] Henrik Jensen, Morten O Jensen, Morten H Smerup, Steffen Ringgaard, Thomas S Sørensen, Niels T Andersen, Per Wierup, J Michael Hasenkam, and Sten L Nielsen. Three-dimensional assessment of papillary muscle displacement in a porcine model of ischemic mitral regurgitation. *The Journal of thoracic and cardiovascular surgery*, 140(6):1312–1318, 2010.

[57] Janne J Jokinen, Mikko J Hippeläinen, Otto A Pitkänen, and Juha EK Hartikainen. Mitral valve replacement versus repair: propensity-adjusted survival and quality-of-life analysis. *The Annals of thoracic surgery*, 84(2):451–458, 2007.

[58] Erica C Jones, Richard B Devereux, Mary J Roman, Jennifer E Liu, Dawn Fishman, Elisa T Lee, Thomas K Welty, Richard R Fabsitz, and Barbara V Howard. Prevalence and correlates of mitral regurgitation in a population-based sample (the strong heart study). *The American journal of cardiology*, 87(3):298–304, 2001.

[59] David L Joyce, Tanvir S Dhillon, Anthony D Caffarelli, Daniel D Joyce, Dimitrios N Tsirigotis, Thomas A Burdon, and James I Fann. Simulation and skills training in mitral valve surgery. *The Journal of Thoracic and Cardiovascular Surgery*, 141(1):107–112, 2011.

[60] Shuichiro Kaji, Michihiro Nasu, Atsushi Yamamuro, Kazuaki Tanabe, Kunihiko Nagai, Tomoko Tani, Koichi Tamita, Kenichi Shiratori, Makoto Kinoshita, Michio Senda, et al. Annular geometry in patients with chronic ischemic mitral regurgitation three-dimensional magnetic resonance imaging study. *Circulation*, 112(9 suppl):I–409, 2005.

[61] Jingjing Kanik, Tommaso Mansi, Ingmar Voigt, Puneet Sharma, Razvan Ioan Ionasec, Dorin Comaniciu, and James Duncan. Estimation of patient-specific material properties of the mitral valve using 4d transesophageal echocardiography. In *Biomedical Imaging (ISBI), 2013 IEEE 10th International Symposium on*, pages 1178–1181. IEEE, 2013.

[62] Jingjing Kanik, Tommaso Mansi, Ingmar Voigt, Puneet Sharma, Razvan Ioan Ionasec, Dorin Comaniciu, and James Duncan. Automatic personalization of the mitral valve biomechanical model based on 4d transesophageal echocardiography. In *Statistical Atlases and Computational Models of the Heart. Imaging and Modelling Challenges*, pages 162–170. Springer, 2014.

[63] Mary E. Klingensmith, Abdulhameed Aziz, Ankit Bharat, Amy C. Fox, and Matthew R. Porembka. *The Washington Manual of Surgery*. Lippincott Williams & Wilkins, 2011.

[64] Irving L Kron, G Randall Green, and Jeffrey T Cope. Surgical relocation of the posterior papillary muscle in chronic ischemic mitral regurgitation. *The Annals of thoracic surgery*, 74(2):600–601, 2002.

[65] Kevin Kunkler. The role of medical simulation: an overview. *The International Journal of Medical Robotics and Computer Assisted Surgery*, 2(3):203–210, 2006.

[66] Karyn Kunzelman, Matthew S Reimink, Edward D Verrier, and Richard P Cochran. Replacement of mitral valve posterior chordae tendineae with expanded polytetrafluoroethylene suture: a finite element study. *Journal of cardiac surgery*, 11(2):136–145, 1996.

[67] Karyn S Kunzelman, David W Quick, and Richard P Cochran. Altered collagen concentration in mitral valve leaflets: biochemical and finite element analysis. *The Annals of thoracic surgery*, 66(6):S198–S205, 1998.

[68] KS Kunzelman and RP Cochran. Mechanical properties of basal and marginal mitral valve chordae tendineae. *Transactions of the American Society of Artificial Internal Organs*, 36(3):M405–407, 1990.

[69] KS Kunzelman, RP Cochran, C. Chuong, WS Ring, ED Verrier, and RD Eberhart. Finite element analysis of the mitral valve. *The Journal of Heart Valve Disease*, 2(3):326, 1993.

[70] KS Kunzelman, RP Cochran, ED Verrier, and RC Eberhart. Anatomic basis for mitral valve modelling. *The Journal of heart valve disease*, 3(5):491, 1994.

[71] KS Kunzelman, Daniel R Einstein, and RP Cochran. Fluid–structure interaction models of the mitral valve: function in normal and pathological states. *Philosophical Transactions of the Royal Society B: Biological Sciences*, 362(1484):1393–1406, 2007.

[72] K.S. Kunzelman, D.R. Einstein, and R.P. Cochran. Fluid-structure interaction models of the mitral valve: Function in normal and pathological states. *Philosophical Transactions of the Royal Society of London B Biological Sciences*, 362:1393–1406, 2007.

[73] K.S. Kunzelman, M.S. Reimink, , and R.P. Cochran. Flexible versus rigid ring annuloplasty for mitral valve annular dilation: A finite element analysis. *Journal of Heart Valve Disease*, 7:108–116, 1998.

[74] KS Kunzelman, MS Reimink, and RP Cochran. Annular dilatation increases stress in the mitral valve and delays coaptation: a finite element computer model. *Vascular*, 5(4):427–434, 1997.

[75] Frank Langer, Takashi Kunihara, Klaus Hell, Rene Schramm, Kathrin I Schmidt, Diana Aicher, Michael Kindermann, and Hans-Joachim Schäfers. Ring+ string successful repair technique for ischemic mitral regurgitation with severe leaflet tethering. *Circulation*, 120(11 suppl 1):S85–S91, 2009.

[76] Chang Ha Lee, Alan Liu, Sofia Del Castillo, Mark Bowyer, Dale Alverson, Gilbert Muniz, and Thomas P Caudell. Towards an immersive virtual environment for medical team training. *Studies in health technology and informatics*, 125:274, 2006.

[77] Lieng H Ling, Maurice Enriquez-Sarano, James B Seward, A Jamil Tajik, Hartzell V Schaff, Kent R Bailey, and Robert L Frye. Clinical outcome of mitral regurgitation due to flail leaflet. *New England Journal of Medicine*, 335(19):1417–1423, 1996.

[78] X.S. Ma, H. Gao, N. Qi, C. Berry, B.E. Griffith, and X.Y. Luo. Image-based immersed boundary/finite element model of the human mitral valve. In *Proceedings of the Third International Conference on Computational & Mathematical Biomedical Engineering*, 2013.

[79] Francesco Maisano, Alberto Redaelli, Monica Soncini, Emiliano Votta, Lorenzo Arcobasso, and Ottavio Alfieri. An annular prosthesis for the treatment of functional mitral regurgitation: finite element model analysis of a dog bone–shaped ring prosthesis. *The Annals of thoracic surgery*, 79(4):1268–1275, 2005.

[80] Tommaso Mansi, Ingmar Voigt, Bogdan Georgescu, Xudong Zheng, Etienne Assoumou Mengue, Michael Hackl, Razvan I Ionasec, Thilo Noack, Joerg Seeburger, and Dorin Comaniciu. An integrated framework for finite-element modeling of mitral valve biomechanics from medical images: Application to mitralclip intervention planning. *Medical Image Analysis*, 16(7):1330–1346, 2012.

[81] Yoshiro Matsui, Yukio Suto, Shinichiro Shimura, Yasuhisa Fukada, Yuji Naito, Keishu Yasuda, and Shigeyuki Sasaki. Impact of papillary muscles approximation on the adequacy of mitral coaptation in functional mitral regurgitation due to dilated cardiomyopathy. *Annals of thoracic and cardiovascular surgery*, 11(3):164, 2005.

[82] Laura Mauri, Elyse Foster, Donald D Glower, Patricia Apruzzese, Joseph M Massaro, Howard C Herrmann, James Hermiller, William Gray, Andrew Wang, Wesley R Pedersen, et al. Four-year results of a randomized controlled trial of percutaneous repair versus surgery for mitral regurgitation. *Journal of the American College of Cardiology*, 2013.

[83] K. May-Newman and FC Yin. Biaxial mechanical behavior of excised porcine mitral valve leaflets. *American Journal of Physiology-Heart and Circulatory Physiology*, 269(4):H1319, 1995.

[84] Karen P McCarthy, Liam Ring, and Bushra S Rana. Anatomy of the mitral valve: understanding the mitral valve complex in mitral regurgitation. *European Journal of Echocardiography*, 11(10):i3–i9, 2010.

[85] Emmanuel Messas, Chaim Yosefy, Miguel Chaput, J Luis Guerrero, Suzanne Sullivan, Philippe Menasché, Alain Carpentier, Michel Desnos, Albert A Hagege, Gus J Vlahakes, et al. Chordal cutting does not adversely affect left ventricle contractile function. *Circulation*, 114(1 suppl):I–524, 2006.

[86] Laura Millard, Daniel M Espino, Duncan ET Shepherd, David WL Hukins, and Keith G Buchan. Mechanical properties of chordae tendineae of the mitral heart valve: Young's modulus, structural stiffness, and effects of aging. *Journal of Mechanics in Medicine and Biology*, 11(01):221–230, 2011.

[87] R.R. Moss, K.H. Humphries, M. Gao, C.R. Thompson, J.G. Abel, G. Fradet, and B.I. Munt. Outcome of mitral valve repair or replacement: a comparison by propensity score analysis. *Circulation*, 108(90101):II–90, 2003.

[88] Matthias Müller, Bruno Heidelberger, Marcus Hennix, and John Ratcliff. Position based dynamics. *Journal of Visual Communication and Image Representation*, 18(2):109–118, 2007.

[89] Juha Nissinen, Fausto Biancari, Jan-Ola Wistbacka, Timo Peltola, Pertti Loponen, Pekka Tarkiainen, Markku Virkkilä, and Matti Tarkka. Safe time limits of aortic cross-clamping and cardiopulmonary bypass in adult cardiac surgery. *Perfusion*, 24(5):297–305, 2009.

[90] Michele Oppizzi, Francesco Maisano, Michele De Bonis, Arend FL Schinkel, Lucia Torracca, Alberto Margonato, Giulio Melisurgo, Ottavio Alfieri, et al. Echocardiographic classification of chronic ischemic mitral regurgitation caused by restricted motion according to tethering pattern. *European Journal of Echocardiography*, 5(5):326–334, 2004.

[91] John A Ormiston, Pravin M Shah, Chuwa Tei, and Maylene Wong. Size and motion of the mitral valve annulus in man. i. a two-dimensional echocardiographic method and findings in normal subjects. *Circulation*, 64(1):113–120, 1981.

[92] Henrik D Pedersen and Jens Häggström. Mitral valve prolapse in the dog: a model of mitral valve prolapse in man. *Cardiovascular research*, 47(2):234–243, 2000.

[93] P.O. Persson and G. Strang. A simple mesh generator in MATLAB. *SIAM review*, 46(2):329–345, 2004.

[94] Charles S Peskin. Flow patterns around heart valves: a numerical method. *Journal of computational physics*, 10(2):252–271, 1972.

[95] Charles S Peskin and David M McQueen. A three-dimensional computational method for blood flow in the heart i. immersed elastic fibers in a viscous incompressible fluid. *Journal of Computational Physics*, 81(2):372–405, 1989.

[96] MS Reimink, KS Kunzelman, and RP Cochran. The effect of chordal replacement suture length on function and stresses in repaired mitral valves: a finite element study. *The Journal of heart valve disease*, 5(4):365–375, 1996.

[97] Filiberto Rodriguez, Frank Langer, Katherine B Harrington, Frederick A Tibayan, Mary K Zasio, Allen Cheng, David Liang, George T Daughters, James W Covell, John C Criscione, et al. Importance of mitral valve second-order chordae for left ventricular geometry, wall thickening mechanics, and global systolic function. *Circulation*, 110(11 suppl 1):II–115, 2004.

[98] Jhon D Rozich, Blase A Carabello, Bruce W Usher, John M Kratz, Adelle E Bell, and Michael R Zile. Mitral valve replacement with and without chordal preservation in patients with chronic mitral regurgitation. mechanisms for differences in postoperative ejection performance. *Circulation*, 86(6):1718–1726, 1992.

[99] Michael S Sacks and Ajit P Yoganathan. Heart valve function: a biomechanical perspective. *Philosophical Transactions of the Royal Society B: Biological Sciences*, 362(1484):1369–1391, 2007.

[100] Yongyuth Sahasakul, William D Edwards, James M Naessens, and A Jamil Tajik. Age-related changes in aortic and mitral valve thickness: implications for two-dimensional echocardiography based on an autopsy study of 200 normal human hearts. *The American journal of cardiology*, 62(7):424–430, 1988.

[101] Ivan S Salgo, Joseph H Gorman, Robert C Gorman, Benjamin M Jackson, Frank W Bowen, Theodore Plappert, Martin G St John Sutton, and L Henry Edmunds. Effect of annular shape on leaflet curvature in reducing mitral leaflet stress. *Circulation*, 106(6):711–717, 2002.

[102] Robert J. Schneider, Douglas P. Perrin, Nikolay V. Vasilyev, Gerald R. Marx, Pedro J. del Nido, and Robert D. Howe. Mitral annulus segmentation from four-dimensional ultrasound using a valve state predictor and constrained optical flow. *Medical Image Analysis*, 16:497–504, 2012.

[103] Robert J. Schneider, Neil A. Tenenholtz, Douglas P. Perrin, Gerald R. Marx, Pedro J. del Nido, and Robert D. Howe. Patient-specific mitral leaflet segmentation from 4d ultrasound. In *14th International Conference on Medical Image Computing and Computer-Assisted Intervention*, 2011.

[104] Howard A Schwid, G Alec Rooke, Jan Carline, Randolph H Steadman, W Bosseau Murray, Michael Olympio, Stephen Tarver, Karen Steckner, Susan Wetstone, et al. Evaluation of anesthesia residents using mannequin-based simulation: a multiinstitutional study. *Anesthesiology*, 97(6):1434–1444, 2002.

[105] Andrew William Siefert, Jean-Pierre Michel Rabbah, Neelakantan Saikrishnan, Karyn Susanne Kunzelman, and Ajit Prithivaraj Yoganathan. Isolated effect of geometry on mitral valve function for in silico model development. *Computer methods in biomechanics and biomedical engineering*, In Press.

[106] C. Sprouse, R. Mukherjee, and P. Burlina. Mitral valve closure prediction with 3-d personalized anatomical models and anisotropic hyperelastic tissue assumptions. *Biomedical Engineering, IEEE Transactions on*, 60(11):3238–3247, 2013.

[107] Marco Stevanella, Francesco Maffessanti, Carlo A Conti, Emiliano Votta, Alice Arnoldi, Massimo Lombardi, Oberdan Parodi, Enrico G Caiani, and Alberto Redaelli. Mitral valve patient-specific finite element modeling from cardiac mri: application to an annuloplasty procedure. *Cardiovascular Engineering and Technology*, 2(2):66–76, 2011.

[108] David A Stump, Anne T Rogers, John W Hammon, and Stanton P Newman. Cerebral emboli and cognitive outcome after cardiac surgery. *Journal of cardiothoracic and vascular anesthesia*, 10(1):113–119, 1996.

[109] SA Tahta, JH Oury, JM Maxwell, SP Hiro, and CM Duran. Outcome after mitral valve repair for functional ischemic mitral regurgitation. *The Journal of heart valve disease*, 11(1):11–8, 2002.

[110] Murat Tavlasoglu, Ahmet Baris Durukan, Zekeriya Arslan, Mustafa Kurkluoglu, Anar Amrahov, and Artan Jahollari. Evaluation of skill-acquisition process in mitral valve repair techniques: A simulation-based study. *Journal of surgical education*, 70(3):318–325, 2013.

[111] Neil A. Tenenholtz, Peter E Hammer, Assunta Fabozzo, Eric N. Feins, Pedro J. del Nido, and Robert D. Howe. Fast simulation of mitral annuloplasty for surgical planning. In *Proceedings of the 7th International Conference on Functional Imaging and Modeling of the Heart*, 2013.

[112] Neil A Tenenholtz, Peter E Hammer, Robert J Schneider, Nikolay V Vasilyev, and Robert D Howe. On the design of an interactive, patient-specific surgical simulator for mitral valve repair. In *Intelligent Robots and Systems (IROS), 2011 IEEE/RSJ International Conference on*, pages 1327–1332. IEEE, 2011.

[113] Frederick A Tibayan, Filiberto Rodriguez, Frank Langer, Mary K Zasio, Lynn Bailey, David Liang, George T Daughters, Neil B Ingels Jr, and D Craig Miller. Annular remodeling in chronic ischemic mitral regurgitation: ring selection implications. *The Annals of thoracic surgery*, 76(5):1549–1555, 2003.

[114] Frederick A Tibayan, Filiberto Rodriguez, Mary K Zasio, Lynn Bailey, David Liang, George T Daughters, Frank Langer, Neil B Ingels, and D Craig Miller. Geometric distortions of the mitral valvular-ventricular complex in chronic ischemic mitral regurgitation. *Circulation*, 108(10 suppl 1):II–116, 2003.

[115] Zoltan G. Turi. Mitral valve disease. *Circulation*, 109(6):38–41, 2004.

[116] AlexanderG G Turpie, Jack Hirsh, John Gunstensen, Harvey Nelson, and Michael Gent. Randomised comparison of two intensities of oral anticoagulant therapy after tissue heart valve replacement. *The Lancet*, 331(8597):1242–1245, 1988.

[117] Alec Vahanian, Ottavio Alfieri, Felicita Andreotti, Manuel J Antunes, Gonzalo Barón-Esquivias, Helmut Baumgartner, Michael Andrew Borger, Thierry P Carrel, Michele De Bonis, Arturo Evangelista, et al. Guidelines on the management of valvular heart disease (version 2012) the joint task force on the management of valvular heart disease of the european society of cardiology (esc) and the european association for cardio-thoracic surgery (eacts). *European heart journal*, 33(19):2451–2496, 2012.

[118] A. Van Gelder. Approximate simulation of elastic membranes by triangulated spring meshes. *Journal of Graphics Tools*, 3(2):21–42, 1998.

[119] Christina M Vassileva, Theresa Boley, Stephen Markwell, and Stephen Hazelrigg. Meta-analysis of short-term and long-term survival following repair versus replacement for ischemic mitral regurgitation. *European Journal of Cardio-Thoracic Surgery*, 39(3):295–303, 2011.

[120] Ingmar Voigt, Tommaso Mansi, Razvan Ioan Ionasec, Etienne Assoumou Mengue, Helene Houle, Bogdan Georgescu, Joachim Hornegger, and Dorin Comaniciu. Robust physically-constrained modeling of the mitral valve and subvalvular apparatus. In *Medical Image Computing and Computer-Assisted Intervention–MICCAI 2011*, pages 504–511. Springer, 2011.

[121] Pascal Volino and Nadia Magnenat Thalmann. Efficient self-collision detection on smoothly discretized surface animations using geometrical shape regularity. In *Computer Graphics Forum*, volume 13, pages 155–166. Wiley Online Library, 1994.

[122] E. Votta, Trung Bao Le, Marco Stevanella, Laura Fusini, Enrico G Caiani, Alberto Redaelli, and Fotis Sotiropoulos. Toward patient-specific simulation of cardiac valves: State-of-the-art and future directions. *Journal of Biomechanics*, 46:217–228, 2013.

[123] E Votta, F Maisano, M Soncini, A Redaelli, FM Montevecchi, and O Alfieri. 3-d computational analysis of the stress distribution on the leaflets after edge-to-edge repair of mitral regurgitation. *The Journal of heart valve disease*, 11(6):810–822, 2002.

[124] Emiliano Votta, Francesco Maisano, Steven F. Bolling, Ottavio Alfieri, Franco M. Montevecchi, and Alberto Redaelli. The geoform disease-specific annuloplasty system: A finite element study. *Annals of Thoracic Surgery*, 84:92–102, 2007.

[125] Qian Wang, Charles Primiano, and Wei Sun. Can isolated annular dilation cause significant ischemic mitral regurgitation? another look at the causative mechanisms. *Journal of Biomechanics*, In Press.

[126] Qian Wang and Wei Sun. Finite element modeling of mitral valve dynamic deformation using patient-specific multi-slices computed tomography scans. *Annals of biomedical engineering*, 41(1):142–153, 2013.

[127] Nozomi Watanabe, Yasuo Ogasawara, Yasuko Yamaura, Nozomi Wada, Takahiro Kawamoto, Eiji Toyota, Takashi Akasaka, and Kiyoshi Yoshida. Mitral annulus flattens in ischemic mitral regurgitation: Geometric differences between inferior and anterior myocardial infarction a real-time 3-dimensional echocardiographic study. *Circulation*, 112(9 suppl):I–458, 2005.

[128] J.F. Wenk, Z. Zhang, G. Cheng, D. Malhotra, G. Acevedo-Bolton, M. Burger, T. Suzuki, D.A. Saloner, A.W. Wallace, and J.M. Guccione. First Finite Element Model of the Left Ventricle With Mitral Valve: Insights Into Ischemic Mitral Regurgitation. *The Annals of Thoracic Surgery*, 89(5):1546–1553, 2010.

[129] Jonathan F Wenk, Liang Ge, Zhihong Zhang, Dimitri Mojsejenko, D Dean Potter, Elaine E Tseng, Julius M Guccione, and Mark B Ratcliffe. Biventricular finite element modeling of the acorn corcap cardiac support device on a failing heart. *The Annals of thoracic surgery*, 95(6):2022–2027, 2013.

[130] Haruo Yamauchi, Nikolay V Vasilyev, Gerald R Marx, Hugo Loyola, Muralidhar Padala, Ajit P Yoganathan, and Pedro J del Nido. Right ventricular papillary muscle

approximation as a novel technique of valve repair for functional tricuspid regurgitation in an ex vivo porcine model. *The Journal of thoracic and cardiovascular surgery*, 144(1):235–242, 2012.